

Thin Film Point of Care Diagnostic and the Potential Mitigation of Antimicrobial Resistance

by

Ciaran James Terry

A thesis submitted in partial fulfillment of the requirements for the degree of

Master of Science

Department of Biomedical Engineering

University of Alberta

© Ciaran James Terry, 2021

## **Abstract**

Antimicrobial resistance is an emerging worldwide threat that endangers the effectiveness of many of the gains of modern medicine. Therapies are becoming less effective through their overuse even while antimicrobial stewardship programs have been developed to measure and improve how antibiotics are prescribed by clinicians and used by patients. Bacterial and viral infections have many overlapping symptoms, but the use of antibiotics for viral infections are ineffective and can lead to the development of drug-resistant microbes. There are biomarker distinctions between viral and bacterial infections. Procalcitonin is a biomarker whose circulating levels are only detectable during a bacterial infection. Therefore, a rapid point-of-care procalcitonin diagnostic could diagnose bacterial infections, guide antibiotic therapy, improve patient outcomes and promote antimicrobial stewardship.

This thesis investigates the development of a qualitative procalcitonin diagnostic that uses a solid-state version of the same thin film colour generating phenomena as seen from an oil slick on wet tarmac. A test strip would have a layer of procalcitonin antibody adsorbed to the aluminum oxide surface—this would produce a colour. Any procalcitonin in a 20–100 $\mu$ l sample of patient blood would bind to the antiprocalcitonin and the formation of this immunocomplex would produce a different colour and signify a bacterial infection. Light's optical path length can be altered by changing two parameters: the physical distance the light travels through a medium and the refractive index of that medium. A matrix was designed to test 10nm increment changes in an aluminum oxide layer on tantalum pentoxide between 80–130nm and 2V increments in the voltage at which the thin films were anodized between 2-10V. An increase in anodization voltage increases the refractive index. Additionally, four different procalcitonin antibodies were engineered so they would orient perpendicular to the alumina surface exposing the binding sites and minimizing the variability in the physical distance light would travel through the system. Two different combinations were standouts: 2V/120nm/Antibody C and 10V/90nm/Antibody C. The former produced the most substantial colour shift without amplification, while the latter

produced a significant colour shift following a second application of antibody C. These optimal combinations were used in following studies.

In buffer, clinically relevant picomolar procalcitonin sensitivity was shown, in addition to an experiment designed to show procalcitonin's specificity to antiprocacitonin. A blinded validation experiment was designed for an independent observer to distinguish between procalcitonin-spiked blood, but there were significant issues with non-specific binding of different blood proteins to the alumina surface.

A 3D-printed procalcitonin kit prototype was developed that included everything necessary to conduct a point-of-care test that could diagnose bacterial infections and guide antibiotic therapy at a tenth of the cost of a procalcitonin lab test.

This device shows promise as a visually qualitative point-of-care procalcitonin test, but a solution to the blood's non-specific binding on the device's aluminum oxide surface is necessary.

## **Preface**

This thesis is an original work by Ciaran Terry. No part of this thesis has been previously published.

## **Dedication**

To my amazing, wonderful children Nova and Ronan. Never stop learning.

## **Acknowledgements**

I would like to thank my supervisors Dr. Robert Burrell, Dr. Todd McMullen and Dr. Anthony Yeung for their advice and guidance.

I would also like to thank Ana Lopez-Campistrous for her aid in the lab. I would like to thank Khally Bhan and Jacob Damant, two engineering students who helped with anodizing and 3D printing.

This work was funded by a grant from the Canadian Institute of Health Research (CIHR).

Lastly, I would like to thank my parents, Tim and Joan and my partner Suzanne for their unwavering support and belief in me.

## Table of Contents

Ch 1 Introduction .....	1
1.1 Problem Statement .....	1
1.2 Research Objectives .....	2
1.3 Thesis Overview .....	2
Ch 2 Background.....	3
2.1 Antimicrobial Resistance.....	3
2.2 Procalcitonin .....	5
2.2.1 Procalcitonin Algorithms .....	8
2.3 Point-of-care Testing and Devices .....	11
2.4 Thin Film Diagnostics .....	13
2.4.1 Substrate .....	15
2.4.2 Tantalum and Tantalum Oxide .....	15
2.4.3 Aluminum and Aluminum Oxide .....	17
2.5 Anodization .....	18
2.6 Optical Path Length .....	18
2.6.1 Film Thickness .....	20
2.6.2 Refractive Index .....	20
2.6.3 Amplification .....	21
2.6.4 Tunability .....	23
2.7 Colour Interference .....	23
2.7.1 Colour Interference Charts .....	24
2.7.2 MacAdam Ellipse.....	25
2.8 Protein Immobilization.....	26
2.8.1 Antibody Structure .....	26
2.8.2 Procalcitonin IgG/GLA Fusions .....	27
Chapter 3 Methodology .....	29
3.1 Introduction.....	29
3.2 Sputter Deposition .....	29
3.2.1 Tantalum Deposition .....	30
3.2.2 Aluminum Deposition .....	31
3.2.3 Establishing Deposition Rate .....	32
3.3 Anodization .....	33

3.4 Scanning Electron Microscopy.....	36
3.4.1 Results.....	36
3.5 X-ray Powder Diffraction .....	39
3.5.1 Results.....	39
3.6 Matrix 1: Anodization Voltage and Aluminum Oxide Thickness Combinations .....	40
3.6.1 Results.....	45
3.7 Matrix 2: Procalcitonin Sensitivity of Optimal Condition Slides .....	48
3.7.1 Results .....	48
3.8 Procalcitonin Specificity.....	49
3.8.1 Results.....	50
Chapter 4 ProvLab.....	50
4.1 Blinded Validation of Optimal Conditions.....	50
4.1.1 Results.....	51
Chapter 5 Device Manufacturing .....	52
5.1 Procalcitonin Point of Care Device Benefits .....	52
5.2 Device Requirements .....	52
5.3 Device Design.....	53
Chapter 6 Conclusions .....	54
6.1 Future Directions .....	55
References.....	56
Appendix 1 Pictures .....	59
Appendix 2 University of Alberta nanoFAB SOPs.....	67
Bob Sputtering System SOP .....	67
Floyd Sputtering System SOP .....	71
Rigaku Ultima IV XRD SOP .....	77

## List of Tables

Table 1. The differences in needs for resource-limited point-of-care (POC) diagnosis and conventional diagnosis based on World Health Organization (WHO) standards. ....	12
Table 2. List of the IgG/GLA fusions produced by Dr. Sidhu's Toronto Recombinant Antibody Centre. ....	28
Table 3. Spot breakdown of a particular slide of voltage/thickness combination.....	44
Table 4. Matrix 1: Voltage/Thickness Combinations.....	45
Table 5. The four different procalcitonin IgG's and their concentrations .....	45
Table 6. Completed Matrix 2 with ratings .....	46
Table 7. Procalcitonin Sensitivity of Optimal Condition Slides.....	48
Table 8. PCT Immunocomplex specificity spot breakdown .....	49

## List of Figures or Illustrations

Figure 1. Procalcitonin specificity and sensitivity along with other inflammatory biomarkers. The graph demonstrates that the levels of procalcitonin remain negligible until a bacterial infection occurs. Ref Meisner .....	6
Figure 2. Kinetics of Procalcitonin (PCT) compared to other inflammatory markers upon infection. Procalcitonin levels surge drastically upon infection while levels do not remain high. Upon the infection's resolution, procalcitonin would also be an ideal biomarker to determine the duration of antibiotic treatment because of its relatively short half-life. [ref Thermofisher].....	7
Figure 3. A visual representation of PCT levels is seen in the figure above and how it could be used to guide antibiotic treatment based on follow-up PCT plasma concentration. [ref thermofisher] ....	7
Figure 4. A single stage procalcitonin algorithm to guide appropriate antibiotic therapy. [ref corti] .....	8
Figure 5. A two stage procalcitonin algorithm requires reassessment to determine the most prudent antibiotic therapy. [ref Shaddock] .....	9
Figure 6. Sepsis Initial Antibiotic Use Algorithm. Advises blanket use of antibiotics in all patients with the suspicion of infection. [ref nebraskamed.com] .....	10
Figure 7. Sepsis PCT Follow Up Algorithm.....	10
Figure 8. Interference colours generated by changing optical path length of light passing through oil on wet tarmac. The oil is thicker in the center of the slick and thins as gravity pulls it outward. [ref hyperphysics] .....	14
Figure 9. This figure shows two types of thin film interference. A) is an example of constructive interference where the rays A and B recombine in phase and the resultant ray is superposed. B) demonstrates two rays A and B recombining destructively. [Figure Credit By Jhbdel - using inkscape Previously published: unpublished, CC BY-SA 3.0, <a href="https://commons.wikimedia.org/w/index.php?curid=25234684">https://commons.wikimedia.org/w/index.php?curid=25234684</a> ].....	16
Figure 10. An illustration of the highly ordered porous nanostructure that develops during the anodization of aluminum. The introduction of pores introduces air into the channels that lowers the system's effective refractive index. ....	18
Figure 11. Demonstrates how an antigen/antibody pair produces different interference colours by increasing the distance light travels in between layers before recombining. (Credit: Nickel, M, 2018) .....	19
Figure 12. Light striking a thin film is partially reflected and partially refracted at the top surface. The refracted ray is partially reflected at the bottom surface and emerges as ray 2. These rays interfere in a way that depends on the thickness of the film and the indices of refraction of the various media. In this	

case,  $\eta_1 < \eta_2 < \eta_3$ . Rays A and B both experience a  $180^\circ$ , so there is no colour change due to phase shift. Image taken from work by Nicoguara ..... 20

Figure 13. Four different binding scenarios and the likelihood of a significant colour shift from the base colour and the immunocomplex..... 22

Figure 14. Order of interference colours generated with increasing thin film thickness from left to right. .... 24

Figure 15. CIE 1931 Colour Chart. The CIE XYZ color space encompasses all color sensations that are visible to a person with average eyesight. The chart is a 2D representation of a 3D model. Attributed to: Paulschou at English Wikipedia / CC BY-SA (<https://creativecommons.org/licenses/by-sa/3.0>)25

Figure 16. Ellipses within a CIE Colour Chart. The colours inside the MacAdam ellipses are areas inside the chart that are indistinguishable by eye..... 26

Figure 17. Antibody structure Human antibodies are composed of four polypeptide chains: two heavy chains (dark blue) and two light chains (light red). Antigen binding sites are each formed by the variable regions of a light chain and a heavy chain (Fab regions). The constant regions of the heavy chains form the trunk of the Y (Fc region). The two Fab regions and Fc region are linked by a flexible hinge region that improves the ability of the Ab to bind antigen. <https://www.myeloma.org/types-of-myeloma> Accessed: Mar 19, 2021.....27

Figure 18. Graphical Representations of the IgG/GLA Fusions. Antibodies A, B, C have the GLA linked to the C-terminus of both heavy chain polypeptides. Sample D links the GLA to the C-terminus of both light chains. Credit to Blazer, L. TRAC ..... 29

Figure 19. Graphical representation of a magnetron sputtering system. The magnetic field generated behind the target increases plasma density by confining charged plasma particles close to the target surface. <https://www.polifab.polimi.it/equipments/orion-8/> accessed: Mar22, 2021..... 30

Figure 20. a) The University of Alberta nanoFAB’s manually operated planar sputter system Bob used for tantalum deposition. b) Wafers are affixed to the underside of the platen with spring hooks with the side to be deposited on facing toward the target. ....31

Figure 21. a) University of Alberta’s nanoFAB Floyd Sputter system is a load-locked, computer-controlled, planar magnetron sputter system. b) Floyd’s wafer holder with six wafer capacity .. 32

Figure 22. The Princeton Applied Research Potentiostat used for all anodizations. .... 34

Figure 23. An illustration of the different current/time plot features based on type of oxide film being generated by anodization..... 35

Figure 24. A typical anodization plot that demonstrates three distinct zones. An aluminum oxide barrier layer forming in Zone A, pore formation in the alumina layer in Zone B and a tantala barrier layer forming in Zone C. .... 36

Figure 25. A topographic image of the porous nanostructure generated at 2V. .... 37

Figure 26. A topographic image of aluminum oxide pores anodized at 10V.....	38
Figure 27. A cross-sectional image and measurement of the aluminum oxide layer. Target thickness was 90nm.....	38
Figure 28. A cross-sectional image of the tantalum layer. Target thickness was 225nm.....	39
Figure 29. XRD scan of wafer segment demonstrates tantalum peaks for alpha and beta tantalum. The absence of an aluminum peak confirms the complete anodic consumption of aluminum. ....	40
Figure 30. The reflectance spectra of silver, gold, copper and aluminum is represented. Aluminum has over 90% reflectance within the visible spectrum. www.eng.libret.....	41
Figure 31. The 3D printed wafer template that was used to cleave the wafer into six long rectangles. ....	43
Figure 32. Wafer segment with six 1cm circles drawn with an ultra fine tip marker. ....	43
Figure 33. Examples of Voltage/Thickness Combinations and their ratings. ....	47
Figure 34. Optimal Combinations of Voltage/Thickness. ....	47
Figure 35. PCT sensitivity assay prior to amplification. ....	48
Figure 36. PCT sensitivity assay post amplification. ....	49
Figure 37. 2V/120nm APCTC slide used to test PCT immunocomplex specificity. ....	50
Figure 38. An example of the randomized series for a Voltage/Thickness combination Ex: 2V/120nm/C and 0.5ng/ml. ....	51
Figure 39. Randomized PCT-spiked blood for 2V/120nm/C. * denotes PCT-spiked sample.....	51
Figure 40. Randomized PCT-spiked blood for 10V/90nm/C. * denotes PCT-spiked sample. ....	51
Figure 41. Non-specific binding onto tow different wafer combination surfaces. ....	52
Figure 42. The 3D printed PCT blood testing kit. A) The lid removed and placed on box edge. The X denotes the testing area. B) The interior of the box with compartments for a 23-gauge lancet, an EDTA blood collection tube and a collection tube holder. C) The size of the box in relation to a pen. ..	54

## List of Symbols and Abbreviations

Abbreviation	Definition
AMR	antimicrobial resistance
APCT	antiproliferative agent
BSA	bovine serum albumin
CDC	Center for Disease Control Prevention
CIE	International Commission on Illumination or Commission Internationale de l'Éclairage
CRP	C-reactive protein
d	physical path length of light
Da	Dalton
EDTA	ethylenediaminetetraacetic acid
EMA	effective medium approximation
FAb	antigen binding fragment
Fc	crystallized fragment
FDA	U.S. Food and Drug Administration
GLA	Vitamin K-dependent carboxylation/gamma-carboxyglutamic domain
IgG	immunoglobulin G
kDa	kilodalton
LFA	lateral flow assay
M	molar, moles per liter
m	mass
nanoFAB	nano fabrication and characterization facility
OPL	optical path length
PBS	phosphate buffered saline
PCT	procalcitonin
POC	point-of-care
POCD	point-of-care diagnostics
POCT	point-of-care testing
ProvLab	Public Health Laboratory Alberta Health Services

PVD	physical vapour deposition
RGB	red, green, blue
SEM	scanning electron microscopy
TRAC	Toronto Recombinant Antibody Centre
XRD	X-ray diffraction
$\eta$	refractive index
$\lambda$	wavelength

## Ch 1 Introduction

This chapter details the general overview of the thesis. The research problem is defined, and the research objectives presented. The reader will also find an overview of the thesis with defined research objectives and chapter breakdown.

### 1.1 Problem Statement

Antimicrobial Resistance (AMR) is a rapidly emerging worldwide threat that endangers the effectiveness of many of the gains of modern medicine. AMR is the ability of microorganisms to resist the effects of medication that once could successfully treat the microbe.

AMR arises from the exposure of microorganisms to antimicrobial therapies under a variety of conditions. These can include the blanket use of antibiotics to farmed animals or fish and the misuse or overuse of antibiotics in humans. This can occur, most often, when individuals suffering from viral infections—which present analogous symptoms to bacterial infections—are prescribed ineffective antibiotics. AMR organisms pose a significant threat to patient health but can dramatically increase healthcare costs by necessitating additional AMR treatments and prolonged hospital stays.

Some strategies to minimize the prevalence of AMR include limiting the duration of antibiotic use and instituting programs that limit the overuse of antibiotics which has become the primary cause of rising levels of antibiotic resistance. Essential to limiting the misuse/overuse of antibiotics is differentiating viral infections from bacterial infections. One biomarker, procalcitonin (PCT) has proven to be useful in distinguishing between viral and bacterial infection. Only in a bacterial infection can PCT levels be detected; otherwise circulating PCT levels are negligible. A point-of-care (POC) device will be developed that can rapidly and confidently diagnose bacterial infections so that antibiotics may be prescribed appropriately. An ideal POC device is rapid, precise, and accurate. It should also be portable, with the ability to diagnose bacterial infection on-site, and relatively low cost to manufacture.

The World Health Organization has a list of criteria, an anagram known as ASSURED, for an ideal point-of-care test<sup>1</sup> **A**ffordable; **S**ensitive (few false-negatives); **S**pecific (few false-positives); **U**ser-friendly; **R**apid; **E**quipment-free; and **D**eliverable (to those in need).

Some POC devices currently on the market include lateral flow assays (LFA) and microfluidics, but both have deterrents. LFA's are inexpensive, but lack sensitivity and can require extensive sample preparation<sup>2</sup>. Microfluidic devices achieve acceptable sensitivities with specific outputs, but they are not affordable, user-friendly nor equipment-free.

## 1.2 Research Objectives

The overall focus of the research was the development and optimization of a thin film, point-of-care-device for procalcitonin—an important biomarker for diagnosing bacterial infections. The specific objectives of this study were as follows:

1. Establish optimal combinations of deposited aluminum oxide thickness and anodization voltage based on colour shift produced by the difference in the optical path length of the procalcitonin antigen/antibody complex.
2. Determine procalcitonin sensitivity of the optimal thickness/voltage slides.
3. Characterize the thin film surface.
4. Verify results through blinded validation with blood samples from ProvLab.
5. Develop a point-of-care prototype for on-site procalcitonin testing.

## 1.3 Thesis Overview

Antimicrobial resistance has been described as the “slow” pandemic. It is not disruptive like Covid-19, but it is forecast to have a greater global impact than cancer by 2050. The goal of the thesis was to determine the optimal conditions for a thin film diagnostic that could determine the difference between a viral and bacterial infection. The test would be performed at the point of care, improve patient outcome and promote appropriate antimicrobial stewardship.

Chapter 2 provided background on antimicrobial resistance and how it is increasing through the misuse of antibiotics. A point of care, thin film diagnostic for a bacterial infection-specific biomarker called procalcitonin was offered. The benefits of point of care testing were described and how it might benefit patient outcomes.

An overview of thin films was described and how changes in optical path length can produce colour shifts that can denote a qualitative test. Chapter 3 described the methods used throughout the thesis. Four different procalcitonin antibodies were engineered and tested to determine optimal conditions in conjunction with two matrices. The first matrix was designed to assess the best anodization parameters. By manipulating anodization conditions with different aluminum thicknesses, we were able to determine visually optimal conditions that produced the most significant colour shifts. The second matrix would test procalcitonin’s sensitivity. The optimal conditions, from matrix 1, would be assessed

with different concentrations of procalcitonin in buffer. A third test was designed to serve as a negative control and test procalcitonin's specificity.

Blind validation would take place in Chapter 4. An experiment was designed so that any colour shifts due to an immunocomplex could be read by an impartial observer. Optimal combination of voltage/oxide thickness/base layer antiprocalcitonin would be tested with procalcitonin-spiked blood.

A point of care kit was designed in Chapter 5 to be delivered to end users. The kit would include everything needed to perform a qualitative test for bacterial infection. This kit included a 3D printed box, a test piece, a lancet and an EDTA blood collection tube.

Optimal conditions were determined as well as procalcitonin's sensitivity and specificity in buffer. Blood proved to be a difficult to use as the test solution. Future research should focus on fine tuning the optimal conditions of the thin film device and try and solve the non-specific binding of blood proteins to the surface. Lastly, smartphone camera software could be developed to make the test quantitative—not just qualitative.

## Ch 2 Background

### 2.1 Antimicrobial Resistance

The US Centers for Disease Control and Prevention (CDC) states that antimicrobial resistance (AMR) occurs when bacteria and fungi develop the ability to defeat the drugs that could previously kill them<sup>3</sup>. Standard treatments become ineffective and infections persist. These microbes are more difficult to treat often requiring additional courses of medication and/or hospital stays.

Jim O'Neill, in his review on AMR, estimates that 700,000 deaths occur every year and that by 2050 that number could grow to 10 million—1.2 million more than cancer. Additionally, O'Neill, an economist, estimates that the cost in terms of lost global production between now and 2050 would be a mind-boggling 100 trillion USD<sup>4</sup>. According to the CDC, approximately 30% of antibiotic prescriptions written in outpatient settings are unnecessary<sup>5</sup>.

AMR occurs naturally over time through genetic mutations; however, the misuse and overuse of antibiotics in humans and animals is accelerating this process. In Alexander Fleming's 1945 Nobel Prize acceptance speech he warned about the misuse of antibiotics, "...But I would like to sound one note of warning. Penicillin is to all intents and purposes non-poisonous so there is no need to worry about giving an overdose and poisoning the patient. There may be a danger, though, in underdosage. It is not difficult to make microbes resistant to penicillin in the laboratory by exposing them to concentrations not sufficient to kill them, and the same thing has occasionally happened in the body. The time may

come when penicillin can be bought by anyone in the shops. Then there is the danger that the ignorant man may easily underdose himself and by exposing his microbes to non-lethal quantities of the drug make them resistant. Here is a hypothetical illustration. Mr. X. has a sore throat. He buys some penicillin and gives himself, not enough to kill the streptococci but enough to educate them to resist penicillin. He then infects his wife. Mrs. X gets pneumonia and is treated with penicillin. As the streptococci are now resistant to penicillin the treatment fails. Mrs. X dies. Who is primarily responsible for Mrs. X's death? Why Mr. X whose negligent use of penicillin changed the nature of the microbe. Moral: If you use penicillin, use enough..."<sup>6</sup>. Misuse occurs when antibiotics are blanket prescribed for people with viral infections, like colds and flu. Similarly, individuals misuse antibiotics when they fail to follow their healthcare professional's advice and a pharmacist's directions. For example, failing to complete a full cycle of antibiotics, sharing or using leftover antibiotics. Amoxicillin (a penicillin-type drug) can be used to treat a bacterial strep throat but will not work for some common pneumonias or bladder infections. While the person sharing might mean well, the bacteria causing the sick person's infection may not be susceptible to the prescribed antibiotic. In turn, those bacteria may not die and the infection could worsen. Additionally, the person receiving the antibiotic may experience side effects or serious allergic reactions from the antibiotic.

Food producers have contributed to the misuse of antibiotics by giving their animals antibiotics for growth promotion, trying to prevent disease in healthy animals or giving animals antibiotics while not under veterinary supervision<sup>7</sup>.

There are several multi-tiered initiatives that aim to promote proper antimicrobial stewardship to minimize AMR<sup>1</sup>. These involve simple, healthy habits for individuals such as hand washing, keeping wounds clean and getting recommended vaccines. These programs aim to reduce the unnecessary use of antimicrobials in agriculture and their propagation into the environment. They seek new rapid diagnostics to eliminate unnecessary prescription of antibiotics. They encourage increased research, global funding and better incentives for the creation of new antibiotics. Additionally, they also hope to improve the global surveillance of AMR in humans and animals.

Clinically, there are many more antimicrobial stewardship programs. A quick Google search, from 2010 to present day, found approximately 898,000 results (accessed April 1, 2021). While some threshold levels of infection may differ between health authorities, these programs all follow the same structure. Is a bacterial infection present, yes/no? If yes, prescribe a course of antibiotics, monitor and re-evaluate.

Effective antimicrobial stewardship are practices that use antibiotics for the shortest duration necessary to minimize the development of antimicrobial resistance. In turn, this minimizes secondary infections and reduces healthcare costs.

The goal of this research is to develop a rapid, point-of-care device that could aid healthcare givers diagnose bacterial infections, support clinical decision making and guide the correct use of antimicrobial therapies.

## 2.2 Procalcitonin

Sepsis is an immune response to the body fighting infection. There is a massive release of chemicals into the bloodstream that causes widespread inflammation. Bacterial infections are often the cause, but sepsis or septicemia can occur from any other type of infection. Symptoms may include fever; general malaise; rapid pulse; shallow breathing; nausea and vomiting etc. In extreme cases, sepsis can be life-threatening. Feeling unwell generally necessitates a visit to the physician. Appropriate treatment requires identifying the source of infection. Bacterial and viral infections can present similar symptoms. For example, runny nose, cough, headache, and fatigue can occur with the common cold (virus) and with a sinus infection (bacteria). As noted in 2.1, the overuse of antibiotics has led to the proliferation of AMR.

Diagnosing a bacterial infection in a clinical setting can be an arduous process. Currently, there is no rapid test for healthcare professionals to differentiate between viral and bacterial infections. To confirm a bacterial infection, blood samples are sent to a centralized lab for testing. Historically, the consensus wait time for results has been 48 to 72 hours<sup>8</sup>. Traditional diagnostic methods simply cannot identify in real-time a bacterial infection.

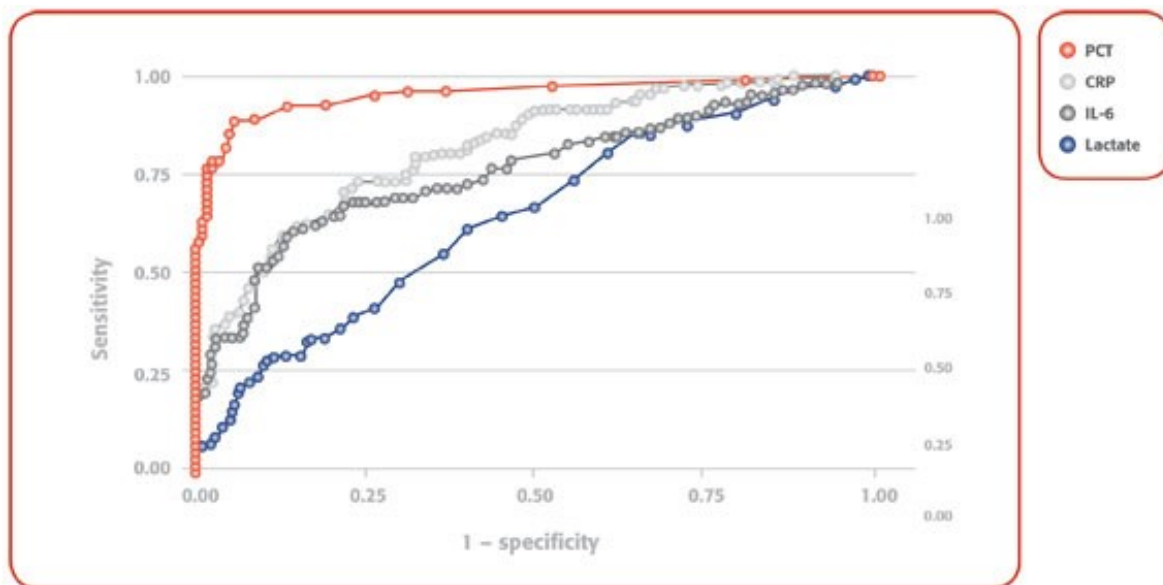
In a busy doctor's office, it may be easier to prescribe a course of antibiotics to give the patient a sense of relief or to ward off the possibility of secondary infection<sup>9</sup>. Secondary infections occur when someone is in a weakened or compromised state due to an existing illness. Microbes can cause acute infections, which are short-lived or chronic infections, which can last for weeks, months, or a lifetime. Studies have shown that disease severity can prompt physicians to prescribe antibiotics, but also to increase the duration of treatment<sup>10</sup>. Some factors that influence a physician's decision-making are patient and disease characteristics like severity as well as the physician's experience.

The broth culture method is the gold standard for the diagnosis of bacterial infection<sup>11</sup>. There are several inflammatory biomarkers that are used to diagnose inflammation and infection. These include leukocyte cell count, C-reactive protein (CRP), and cytokines (TNF- $\alpha$ , IL-1 $\beta$  or IL-6), but these lack specificity—meaning they present in an infection whether caused by virus, bacteria or fungi etc.

A different biomarker, procalcitonin (PCT), has shown promise in diagnosing bacterial infection. PCT is a peptide precursor of the hormone calcitonin. It consists of 116 amino acids and has a molecular weight of 14.5 kDa<sup>12</sup>. Comparatively, C-reactive protein consists of 224 amino acids with a molecular weight of

25kDa<sup>13</sup>. Only a bacterial infection can produce detectable PCT levels; otherwise, circulating PCT levels are nearly undetectable. This specificity to bacteria makes PCT an interesting biomarker for diagnosis and treatment.

Levels of PCT are highest in acute bacterial infections and sepsis, but do not elevate in autoimmune inflammation of localized infections such as abscesses<sup>14</sup>. PCT levels were demonstrated to be more sensitive and specific than other biomarkers that makes it a superior in monitoring the therapeutic response to antibacterial therapy and reduce antibiotic exposure, see Figure 1 and Figure 2<sup>15</sup>. PCT also provides value as a diagnostic biomarker for chronic obstructive pulmonary disease (COPD), congestive heart failure (CHF), meningitis, urinary tract infections, bone and joint infections, septic arthritis and others<sup>16</sup>.



**PCT has demonstrated diagnostic performance superior to that of other markers for sepsis.<sup>2</sup>**

*Figure 1. Procalcitonin specificity and sensitivity along with other inflammatory biomarkers. The graph demonstrates that the levels of procalcitonin remain negligible until a bacterial infection occurs. Ref Meisner<sup>15</sup>*

Procalcitonin's kinetics, shown in Figure 2 below, demonstrate why it is such a good biomarker for diagnosing sepsis. In response to a bacterial infection, Covington notes that PCT levels begin to rise within 3–4 hours and peak after 12–24 hours<sup>16</sup>. There are no enzymes that breakdown PCT, so once PCT enters the bloodstream, it remains unchanged. With a half life of 30 hours, PCT levels will noticeably fall with successful treatment within a day illustrated in Figure 3<sup>17</sup>. This makes it ideal to monitor treatment and minimize the duration of antibiotic exposure. For example, a 14-day course of antibiotics could be reduced to 9 or 10 days, provided a follow up test indicates no further bacterial infection.

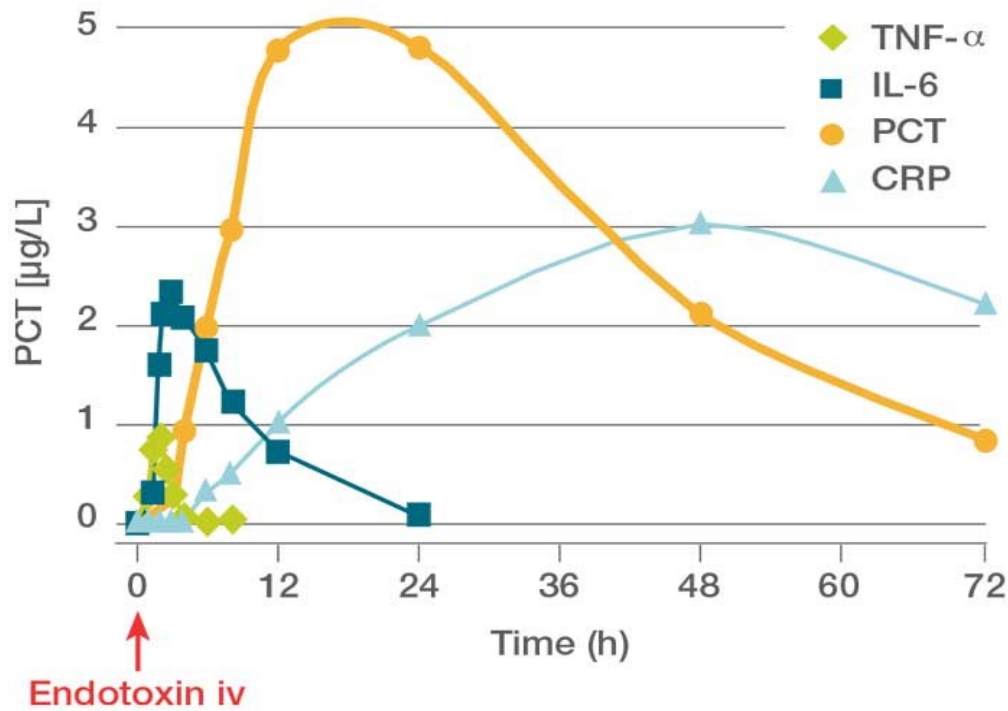


Figure 2. Kinetics of Procalcitonin (PCT) compared to other inflammatory markers upon infection. Procalcitonin levels surge drastically upon infection while levels do not remain high. Upon the infection's resolution, procalcitonin would also be an ideal biomarker to determine the duration of antibiotic treatment because of its relatively short half-life. [<https://www.procalcitonin.com/clinical-utilities/#Ref-1>. accessed: April 1, 2021]

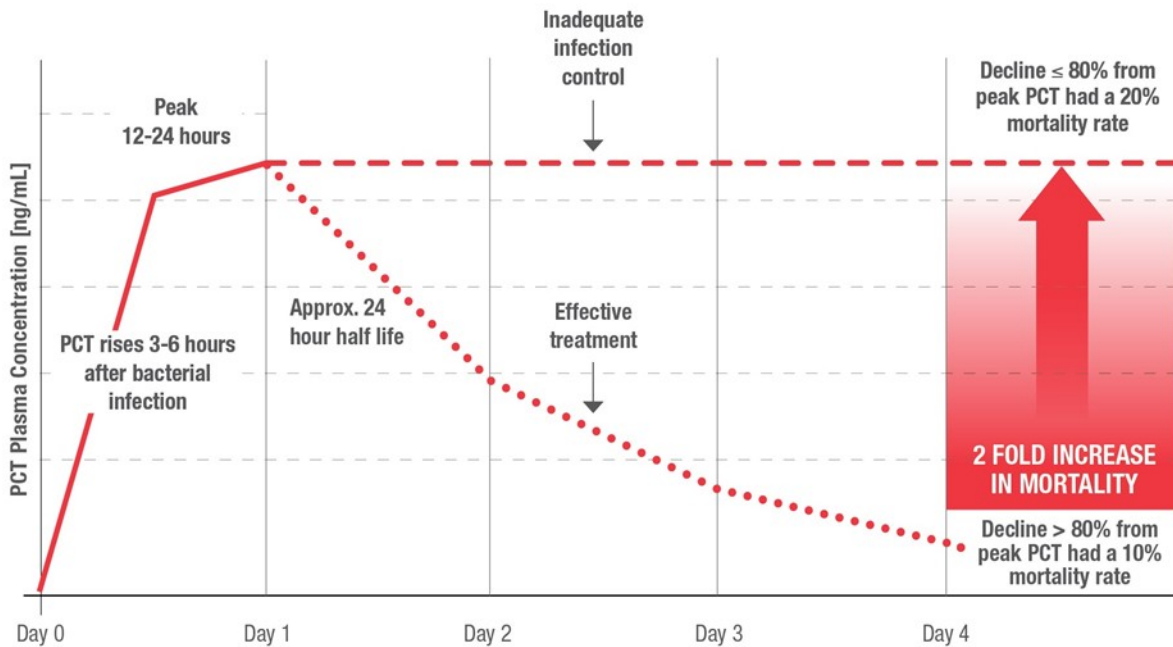


Figure 3. A visual representation of PCT levels is seen in the figure above and how it could be used to guide antibiotic treatment based on follow-up PCT plasma concentration. [<https://www.procalcitonin.com/clinical-utilities/#Ref-1>. Accessed: April 1, 2021]

At the point of care, a single-serum, qualitative, PCT-sensitive, point-of-care device could diagnose a bacterial infection within a patient’s visit and guide clinical reasoning and proper treatment. This would help limit the overuse of antibiotics and mitigate the AMR problem.

### 2.2.1 Procalcitonin Algorithms

There are several antimicrobial stewardship algorithms that use PCT as a biomarker to guide antibiotic therapy along with clinically tested serum levels. Some examples include: Figures # and #

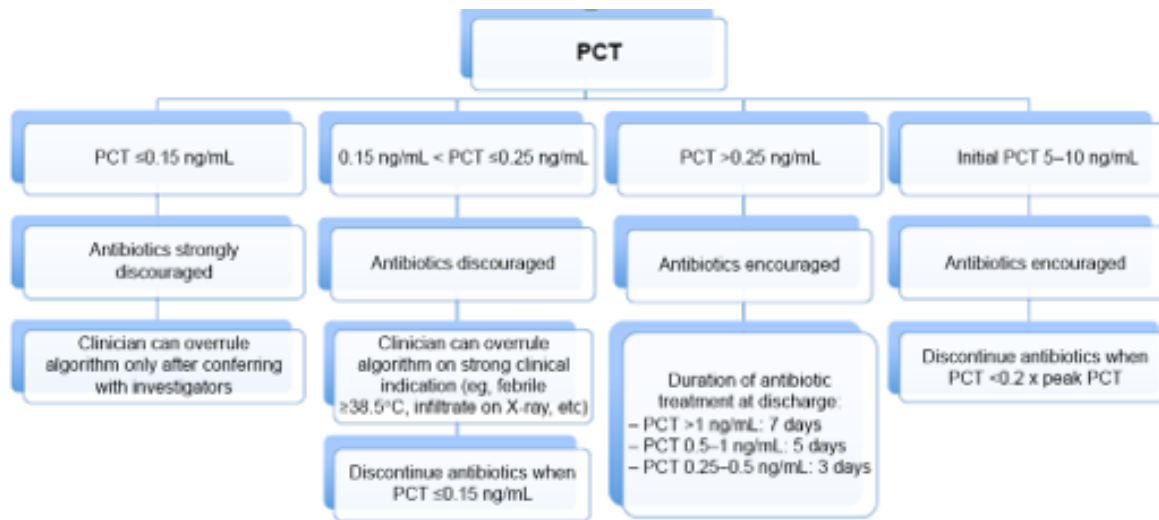


Figure 4. A single stage procalcitonin algorithm to guide appropriate antibiotic therapy<sup>18</sup>.

A single stage algorithm might be most appropriate when a patient is evaluated once. There are also two stage algorithms that some health regions employ. These two stage algorithms require reassessment to determine appropriate courses of action and would be ideal for a patient under constant monitoring like in the hospital.

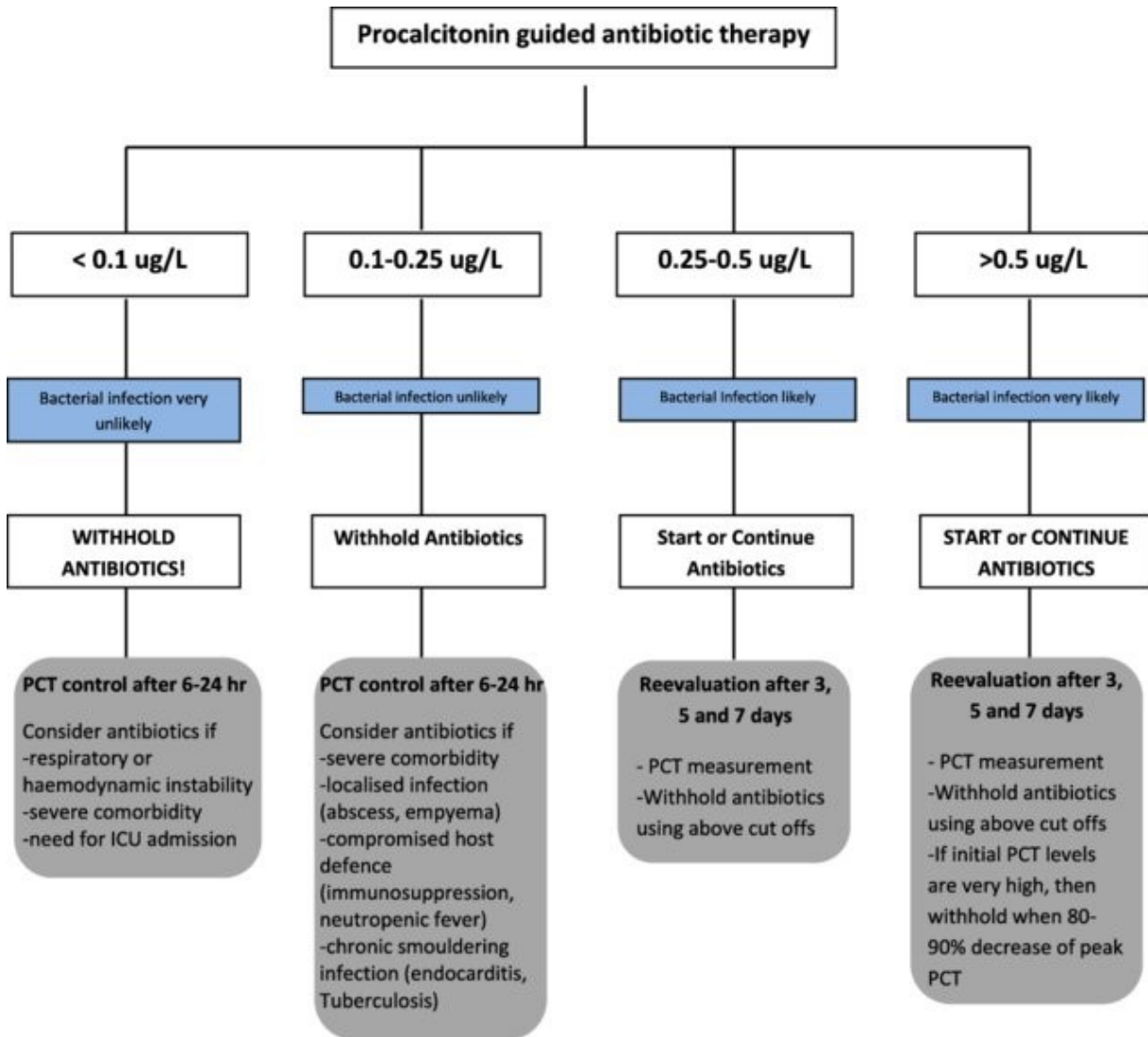


Figure 5. A two stage procalcitonin algorithm requires reassessment to determine the most prudent antibiotic therapy.<sup>19</sup>

# Sepsis Initial Antibiotic Use Algorithm

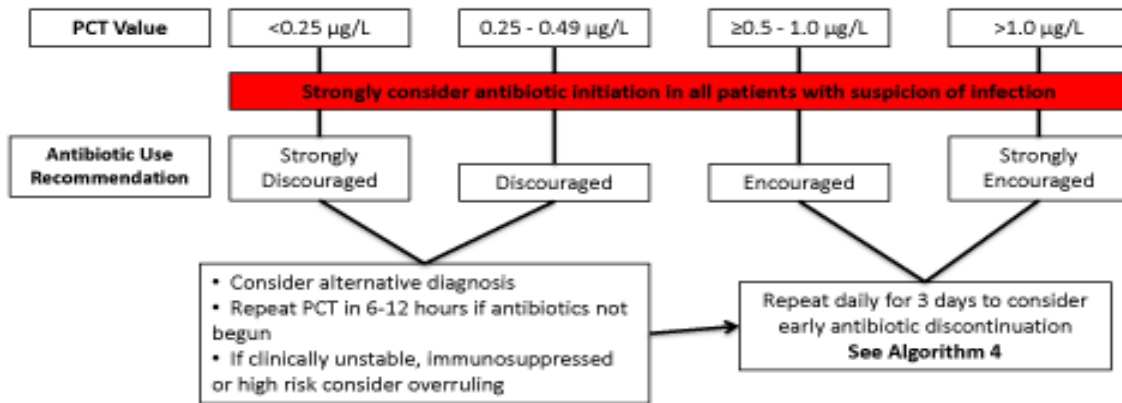


Figure 6. Sepsis Initial Antibiotic Use Algorithm. Advises blanket use of antibiotics in all patients with the suspicion of infection.<sup>20</sup>

A second Follow Up PCT algorithm (fig 7) is used to determine further antibiotic treatment based on reassessed PCT levels.

# Sepsis Follow PCT Antibiotic Use Algorithm

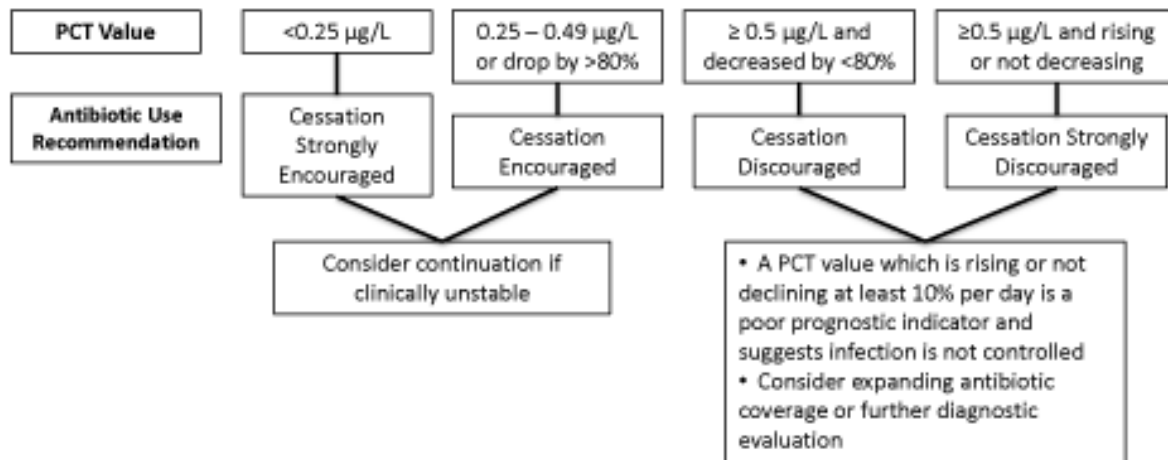


Figure 7. Sepsis PCT Follow Up Algorithm.<sup>20</sup>

These examples of PCT-guided algorithms may have differing PCT cut-off levels, they follow the same structure. Do PCT levels indicate bacterial infection, y/n? If yes, then begin antibiotics. Although the

decision to use antibiotics ultimately falls on the physician, experience with the use of a PCT-guided algorithm can aid in proper antimicrobial stewardship.

Monitoring PCT levels with repeated measurements over time would be helpful for estimating recovery from bacterial infection and prognosis and results in appropriate antibiotic therapies. PCT decreases once the bacterial infection is controlled and thus provides information about resolution of the illness. PCT-guided algorithms can be helpful to guide antibiotic therapy. PCT-guided therapy results in fewer antibiotic prescriptions and shorter antibiotic durations without an increase in adverse outcomes. One commonality amongst the various algorithms is the concentration at which antibiotics should be prescribed which is 0.25ng/ml. A successful POCD should be sensitive enough to provide a positive test at this concentration.

### 2.3 Point-of-care Testing and Devices

Traditionally, specimens (blood, urine, tissue etc.) were collected in one location, in a clinic or a doctor's office, and sent away for evaluation. Testing would then be almost entirely undertaken in centralized labs with sophisticated equipment and highly trained personnel. Results would then be presented hours or days later. PCT levels were also diagnosed this way. Blood samples would likely be collected in a clinic, hospital or physician's office and sent to a laboratory for prep and analysis.

A push toward developing technology that could be conducted at the point of care (POC) would be beneficial to both clinician and patient. Point-of-care testing (POCT) would be convenient and results would be achieved rapidly and, in turn, would allow for improved and more immediate clinical management decisions. Point-of-care diagnostics (POCD), metaphorically, removes the middleman. POCD would remove the need for centralized lab equipment and trained laboratory staff. Samples would be collected at the POC and results easily and rapidly obtained from a small, handheld device or small benchtop analyzer. Some familiar POC devices include blood glucose meters; pregnancy tests; and urinalysis dipsticks.

Not only are POCD efficient, increasing the speed of diagnosis and treatment, but their portability expands testing capabilities. Non-traditional testing locations can be accessed with portable POCD. These may include underserved populations, rural areas and locations with limited infrastructure or personnel like an accident or disaster site.

Table 1. The differences in needs for resource-limited point-of-care (POC) diagnosis and conventional diagnosis based on World Health Organization (WHO) standards<sup>1</sup>.

	Resource-limited POC diagnosis	Conventional diagnosis
<b>Cost</b>	Inexpensive, disposable	Expensive and costly to maintain
<b>Functionality</b>	Single diagnosis readout per unit	Multiple readouts possible with one unit
<b>Personnel</b>	Minimally trained personnel can operate, user-friendly operation	Requires highly trained personnel
<b>Environmental conditions</b>	Functional at high temperature and high humidity environments	Not suitable for high temperature and high humidity environments
<b>Infrastructure</b>	Does not require an infrastructure and a constant electrical supply	Requires advanced infrastructure and vulnerable to blackouts
<b>Flexibility of operation</b>	Can perform multiple diagnosis of pathogens and strains with minimal alteration	Requires different platforms for different diagnostic applications
<b>Accessibility</b>	Deliverable to end users without a need for centralized hospitals or clinics	Generally performed at established hospitals and clinics
<b>Accuracy and precision</b>	Moderate-high (based on application)	High
<b>Throughput</b>	High	High

The WHO has developed a set of criteria for an ideal POCD and suggest the ASSURED criteria should be the benchmark for diagnostic tests for resource-constrained settings<sup>1</sup>.

The ASSURED criteria stands for:

- Affordable (low cost)
- Sensitive (few false negatives)
- Specific (few false positives)
- User-friendly (simple to use with minimal training)
- Rapid and robust (time from sample collection to diagnosis and without the need for refrigeration)
- Equipment-free
- Deliverable to end-users

The advantages of POCT are driving the global market. The POCT market is expected to grow from US\$23.16 million in 2016 to US\$36.96 million in 2021<sup>21</sup>.

The Federal Drug Administration initially granted approval for PCT POCT to aid in risk assessment of critically ill patients and patients with severe sepsis or septic shock to be used in conjunction with laboratory tests. In 2017, the FDA expanded PCT assay indicators to include antibiotic management decisions<sup>16</sup>. Current POC PCT assays utilize immunofluorescence to determine PCT levels in human serum and plasma and can deliver results in roughly 20 minutes depending on the availability of in-house benchtop equipment. Table 2 (below) notes the time-to-result for benchtop assays, but it is also

important to note the sensitivities. A procalcitonin POCT would need to achieve these sensitivities to be considered a replacement for benchtop assays or conventional centralized testing.

Table 2. A compilation of time-to-result and sensitivities of commercially available benchtop procalcitonin assays.

<b>Product</b>	<b>Range of sensitivity, ng/ml</b>	<b>Time-to-result, min</b>
ADVIA Centaur BRAHMS PCT assay (Siemens Healthcare Diagnostics, Berlin, Germany) <a href="#">8</a>	0.02–75	26–29
BRAHMS PCT Sensitive Kryptor Assay (Thermo Fisher Scientific, Waltham, MA, USA) <a href="#">8</a>	0.02–5000	19
Elecsys BRAHMS PCT assay (Roche Diagnostics, Indianapolis, IN, USA) <a href="#">8</a>	0.02–100	18
LIAISON BRAHMS PCT assay (DiaSorin, Saluggia, Italy) <a href="#">8</a>	0.1–500	NA
VIDAS BRAHMS PCT assay (bioMérieux, Marcy-l'Étoile, France) <a href="#">8</a>	0.05–200	20

The goal of this research is to develop a qualitative, nano-scale thin film diagnostic device that uses the optical properties of incident light, protein and the thin film oxide/metal interfaces.

## 2.4 Thin Film Diagnostics

Thin film diagnostics take advantage of the optical phenomena produced by the optical properties between two different materials. Thin film interference produces the array of colours generated from gasoline on wet tarmac (Figure 8).



*Figure 8. Interference colours generated by changing optical path length of light passing through oil on wet tarmac. The oil is thicker in the center of the slick and thins as gravity pulls it outward<sup>22</sup>.*

Light is split, with some light reflected off the air/gasoline interface, and some reflected off the gasoline/water interface. These reflected rays of light recombine and interfere with each other to produce a different colour. The different colours are indicative of changing gasoline thickness as the spill is pulled out by the effects of gravity, that is thicker in the middle and thinner at the edges.

### 2.4.1 Substrate

Silicon substrates are ideal for thin films. They can be polished and have incredibly low surface roughness which minimizes background signal. Additionally, cleaving the wafers into desired sizes is straightforward and simple.

Silicon wafers were purchased from University Wafer, Inc. with the following parameters:

- 100mm diameter
- N-type phosphorous doped
- <100> orientation
- (0-100 Ohm/cm) resistivity
- 500  $\mu\text{m}$  thickness
- Single-sided polish
- Test grade

These are standard wafers used in industry and easily procurable. A N-type semiconductor is created by adding an impurity into the silicon. The impurity is phosphorous which is called a donor atom and can donate a free electron to a semiconductor. Single-sided polished wafers are chemically and mechanically polished on one side to achieve a super-flat, mirrored surface with an atomic level roughness. This is crucial for thin film diagnostics. Greater flatness produces less signal noise than generated by a rough surface. Silicon wafers can be cleaved with a diamond pen into desirable pieces. A piece of silicon wafer will serve as the base/substrate layer for the aluminum/tantalum/silicon complex.

### 2.4.2 Tantalum and Tantalum Oxide

Tantalum is a sixth period refractory metal—commonly referred to as one of the valve metals. It is easily sputtered and can generate interference colours when oxidized. Interference colours change based on oxide thickness. This oxide is called tantalum pentoxide, also known as tantalum (V) oxide ( $\text{Ta}_2\text{O}_5$ ). Tantalum pentoxide has been widely studied for its properties that include chemical resistance, conductivity, and mechanical strength<sup>23</sup>.

Sputter deposition is a physical vapour deposition (PVD) method used to deposit thin films onto a substrate. Using an established deposition rate, a controlled layer of tantalum will be sputtered onto a silicon wafer. Tantalum is readily deposited onto the silicon substrate and is the first layer of the thin film device.

The growth or thickness of the tantalum oxide layer is voltage dependent. It grows at a rate of  $16\text{\AA}/\text{V}^{24}$ . An Ångstrom is a tenth of a nanometer, so if a wafer is anodized at 6V, the thickness of the tantalum oxide layer will be 9.6nm. The tantalum oxide is also a dielectric which acts as an electric barrier to the passing current. In the example above, once the tantalum oxide reaches 9.6nm thick, no further current is passed through the films—effectively shutting down the electrochemical cell.

The reflectivity of tantalum oxide is an important feature of this device. The reflectivity of  $\text{Ta}_2\text{O}_5$  is around 50%<sup>25</sup>. Should the reflectivity be higher, like that of Aluminum—roughly 90%, the signal generated from the reflection of the metal layer would overwhelm the reflected signal from the air/protein interface<sup>26</sup>.

Tantalum oxide interference colours and its optical properties have been studied since the late 1950's<sup>27,28</sup>. The wide range of interference colours have also been investigated for its appeal to the visual arts<sup>29</sup>. Unlike dyes or pigments that operate on the absorption of certain wavelengths of light, the colours produced by an oxide film are dependent on interference of reflective light between layers. Light being reflected from the air/oxide interface undergoes constructive and destructive interference with the light reflected off the underlying oxide/metal interface<sup>30</sup>.

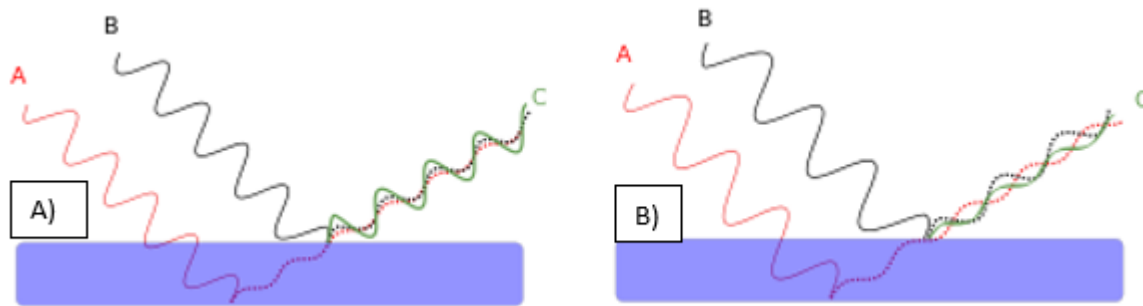


Figure 9. This figure shows two types of thin film interference. A) is an example of constructive interference where the rays A and B recombine in phase and the resultant ray is superposed. B) demonstrates two rays A and B recombining destructively<sup>31</sup>. [Figure Credit By Jhbdel, <https://commons.wikimedia.org/w/index.php?curid=25234684> Accessed: April 1, 2021]

Consider the blue layer above to be the aluminum oxide layer. Light ray A travels through the oxide and is reflected off the aluminum oxide/tantalum oxide interface. Meanwhile, light ray B is reflected off the air/alumina surface. In constructive interference, the two beams of light combine in phase—the peaks are additive—to form light ray C.

Destructive interference occurs when the recombinant light rays (Rays A and B) are not in phase. When A recombines with B after reflecting off the oxide/metal layer the resultant light C will have a different

colour. By varying the thickness of the oxide layer (blue) you can increase or decrease the path travelled by light ray B.

For very thin films, the difference in path lengths of rays A and B is negligible, but a phase change may occur. Reflected light will experience a  $180^\circ$  or  $\pi$  radian phase change when it encounters an interface and reflects from a medium of higher index of refraction, but not when it reflects from a medium with a smaller index. Figure 12, below, demonstrates that phase change occurs when rays are reflected at boundary interfaces where mediums are higher than the ones light is propagating through.

#### 2.4.3 Aluminum and Aluminum Oxide

Aluminum is the device's next deposited layer. Aluminum is an abundant metal largely found in the Earth's crust. It is very versatile and is found in the transportation, packaging, construction and electrical industries; however, bulk aluminum has different properties than nano-scale or thin film aluminum<sup>32,33</sup>.

Thin film aluminum is used in a variety of applications that include electrical, microelectronics, optical applications<sup>34</sup>. Aluminum thin films are deposited on polymers as a protective coating on the inside of food packages. This coating forms a barrier preventing diffusion of gases. The polymer bag is inflated with nitrogen that replaces the oxygen and sealed. This step prevents food from oxidizing.

A thin film of aluminum will be sputtered onto the layer of tantalum. This system will be anodized to form oxide layers. This is a crucial part of the diagnostic. Aluminum oxide is amorphous and colourless, but creates a platform for the protein to be adsorbed to. As the anodization occurs and the aluminum is transformed into oxide, small pores are created normal to the surface.

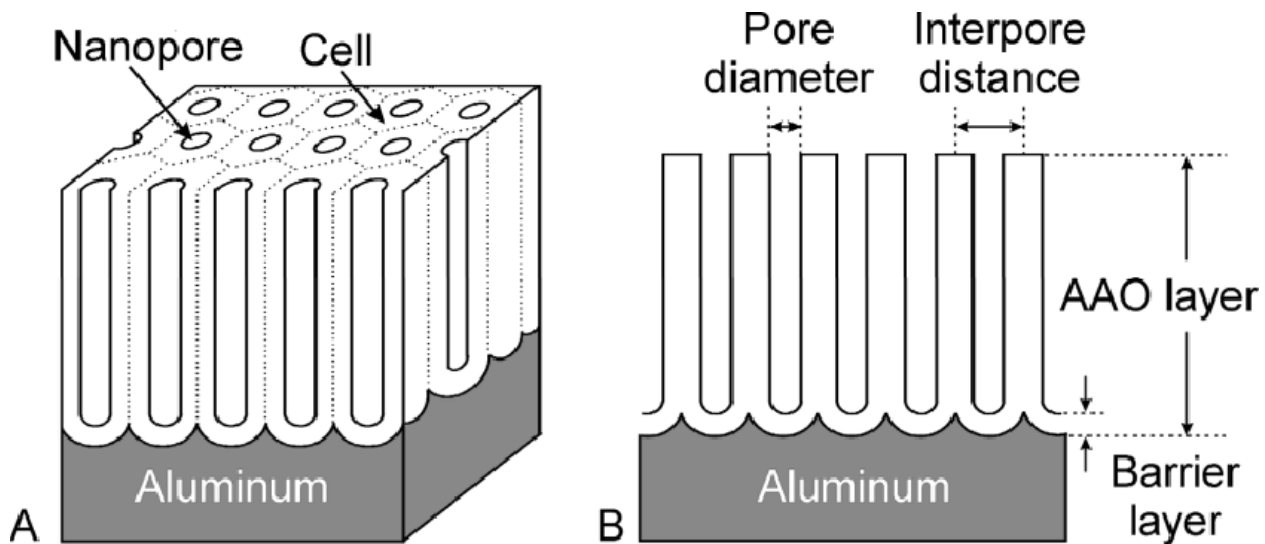


Figure 10. An illustration of the highly ordered porous nanostructure that develops during the anodization of aluminum. The introduction of pores introduces air into the channels that lowers the system's effective refractive index.<sup>35</sup>

The interpore distance is smaller than the proteins being applied. The pores also introduce air into the complex which effectively reduces the effective refractive index of the system. The refractive index of alumina is 1.7, but the addition of air, whose refractive index is 1, lowers the system's effective refractive index.

## 2.5 Anodization

When exposed to air, pure aluminum self-passivates by forming a surface layer of amorphous aluminum oxide 2 to 3 nm thick spontaneously within picoseconds<sup>36</sup>. The oxide layer protects the aluminum from corrosion. Aluminum (III) oxide has a chemical formula  $\text{Al}_2\text{O}_3$  and is commonly referred to as alumina. The oxide originates from the aluminum and integrates with the pure substrate. Anodization is an electrochemical process used to increase the thickness of the natural metal oxide layer to capitalize on the oxide's properties. The oxide grows by immersing the Al/Ta/Si complex into an acid electrolyte bath and passing electric current through it. The wafer is oriented opposite an aluminum foil cathode. The complex acts as the anode that passes electrons to the foil; as the electrons are lost the oxide layer grows. The growth of aluminum oxide is not voltage dependent like tantalum oxide and will continue until all aluminum is converted to oxide. Previous work by Nickel, demonstrates the utility of anodizing in a 0.4/0.1M phosphoric/oxalic acid bath as the electrolyte<sup>37</sup>. The addition of the 0.1M oxalic acid acts as a corrosion inhibitor and minimizes surface roughness for subsequent protein application.

## 2.6 Optical Path Length

Optical Path length (OPL) is an integral principle of this diagnostic device. It determines the interference and diffraction of light as it propagates and recombines through mediums. There are two variables that effect OPL, the refractive index ( $\eta$ ) of the medium and the physical distance the light travels ( $d$ ) within the object or medium.

$$OPL = \eta d$$

Consequently, a user can manipulate the OPL by altering the refractive index or by changing the physical path length traveled by light. Figure 11 illustrates how the adsorption of a protein layer to the alumina layer increases optical path length by increasing the distance of the protein/oxide layer. It is important that the refractive indices of the protein and oxide layer match to reduce noise and maximize signal strength.

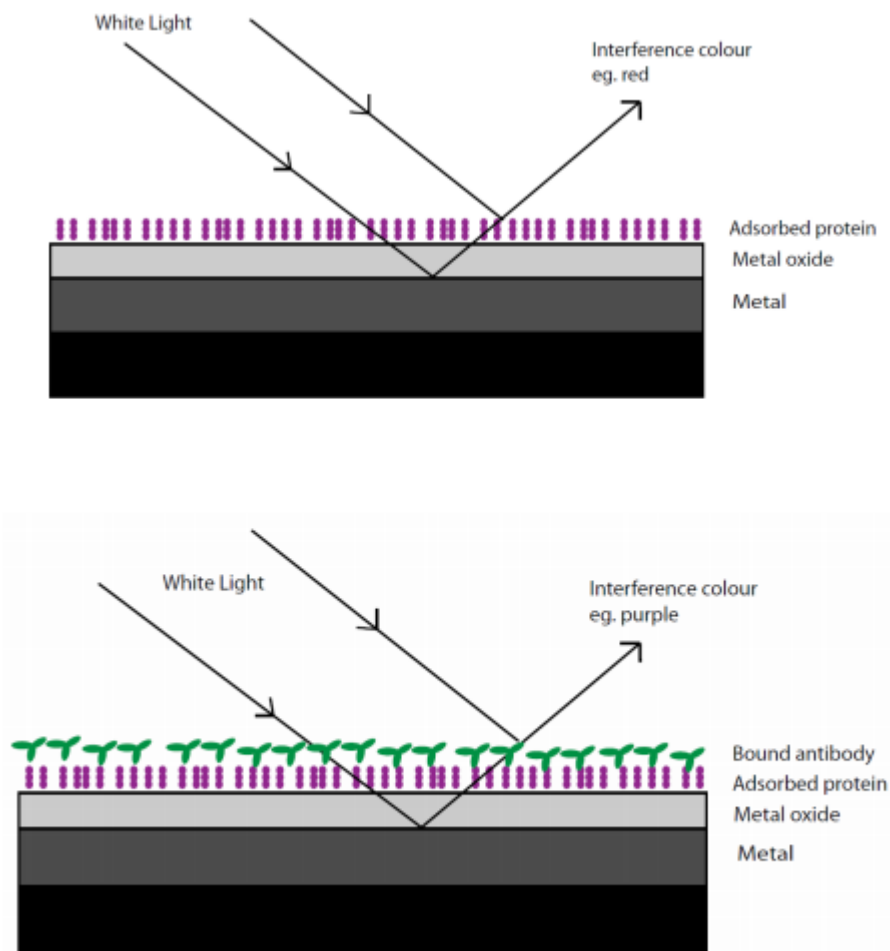


Figure 11. Demonstrates how an antigen/antibody pair produces different interference colours by increasing the distance light travels in between layers before recombining.<sup>37</sup>

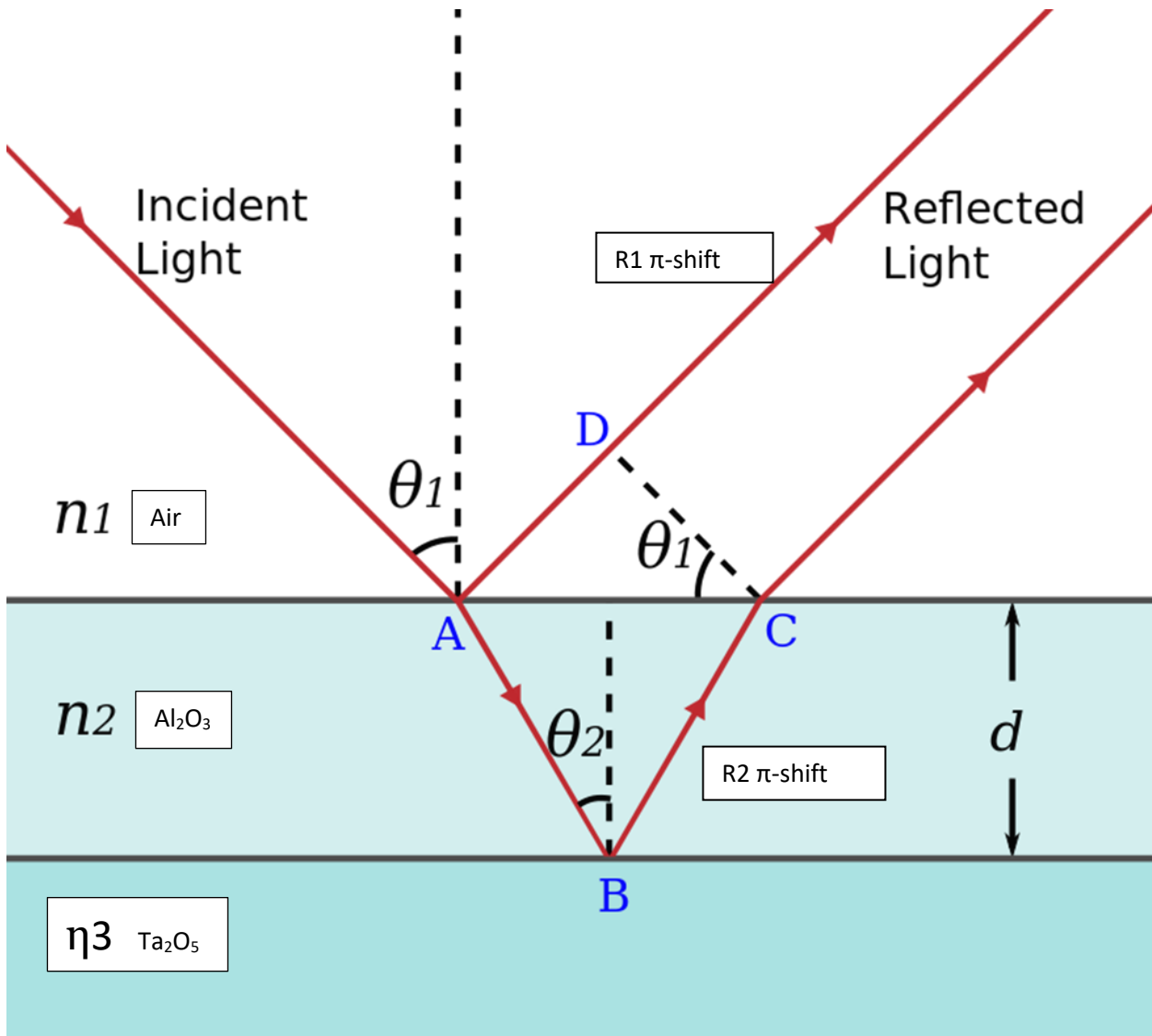


Figure 12. Light striking a thin film is partially reflected and partially refracted at the top surface. The refracted ray is partially reflected at the bottom surface and emerges as ray 2. These rays interfere in a way that depends on the thickness of the film and the indices of refraction of the various media. In this case,  $n_1 < n_2 < n_3$ . Rays A and B both experience a  $180^\circ$ , so there is no colour change due to phase shift. Image taken by work from Nicoguardo.<sup>38</sup>

### 2.6.1 Film Thickness

For thin film diagnostics, a colour change will be detectable by increasing  $d$ , the thickness of the protein/aluminum layer. This can be achieved by increasing the thickness of the alumina or, since the indices of the alumina and protein match, by adsorbing proteins to the surface of the oxide layer. Physical Vapour Deposition (PVD) is a technique that can deposit thin films at deposition rates in several Angstroms/s.

### 2.6.2 Refractive Index

Light refracts whenever it travels at an angle into a substance with a different refractive index. This change of direction is caused by a change in speed. For example, when light travels from air into water, it slows down, causing it to continue to travel at a different angle or direction. Similarly, whenever there is a change in refractive index there is a reflection. When this light recombines it will interfere and will produce a colour change that it is hopefully detectable

As noted previously, the collection of refractive indices is crucial for the thin film diagnostic. The refractive index ( $\eta$ ) is a ratio describes how fast light travels through the medium. It is described in the equation:

$$\eta = \frac{c}{v}$$

where  $c$  is the speed of light in a vacuum and  $v$  is the phase velocity of the light in that medium. Air in a vacuum has a refractive index of 1.00; comparatively, the refractive index of glass is 1.33. This number indicates that light travels 33% slower in glass. Diamond has a refractive index of 2.419<sup>39</sup>.

When light passes from one medium to another there is a reflection at the interface. In Section 2.5, we described the process of growing the aluminum oxide layer. Aluminum oxide is amorphous meaning it lacks clear structure. It has a refractive index of 1.768–1.772. The creation of pores during anodization introduces air ( $\eta = 1.00029$ ) into the alumina that effectively lowers its refractive index, this can be tailored to match that of the adsorbed protein. We match the refractive indices of the porous aluminum oxide and the adsorbed protein so that light is fooled. When matched properly, light does not recognize different materials and does not experience an index change at the protein/alumina interface that would reflect light causing noise in the system.

### 2.6.3 Amplification

To detect procalcitonin using a thin film diagnostic, the aluminum oxide layer needs to be saturated with antiprocalcitonin. This would produce a base colour—for example, straw yellow. An anticoagulated blood sample would be collected from the patient at the point of care and applied to the diagnostic. Should the patient have a bacterial infection, utilizing the procalcitonin/antiprocalcitonin binding specificity, the procalcitonin in the blood would bind to the protein layer. This immunocomplex increases the OPL by increasing layer thickness. A drawback of an antigen test is the size discrepancy of the antigen and antibody. Sigma-Aldrich, a renowned life-science technology company, lists the molecular weight of procalcitonin as 12.796 kDa. Comparatively, the procalcitonin IgG has a molecular weight of 150kDa—roughly twelve-fold difference<sup>40</sup>.

The interference colour generated from a positive procalcitonin test might shift from the device's base colour, straw-yellow to an amber yellow—not ideal for a visual confirmation test. A desirable colour shift may be straw yellow to purple or blue. To achieve this, an additional or secondary application of procalcitonin antibody could be applied to increase the light's physical path distance thus amplifying the colour shift. The secondary antibody would bind to the bound Procalcitonin IgG. This would create a stack or sandwich that would almost double the height of the protein layer. One problem that arises is that antibodies are generally quite large compared to their antigen counterparts. As noted in previous sections, the colour difference generated by a positive test is dependent on the change in thickness of the antigen/antibody/aluminum oxide layer compared to antibody/aluminum oxide layer. Consequently, a bound protein, because of its size, might not change the OPL sufficiently enough to make a noticeable colour change. The addition of a secondary antibody can drastically increase the optical path length and resultant colour shift.

Figure 13 (below) shows four different binding scenarios and their likelihood of success is discussed. Scenario 1 is the procalcitonin device, where the addition of the secondary antibody would produce a substantial colour change by drastically changing OPL. Scenario 2 is an antibody test where an immunocomplex is formed by the binding of antibodies in blood to adsorbed antigens on the device surface. This illustration should work because of the relative size similarity between the antigen and the antibody. Even if the adsorbed antigen were smaller, the size difference between antigen and antibody would still produce a significant colour shift. Scenario 3 is the device without the addition of the secondary antibody. As discussed, the difference in signal might not produce a discernable colour shift. Finally, scenario 4 is an antigen test where the antigen is of similar size to the adsorbed antibody. The difference in OPL would be approximately double and should produce a sufficient colour change.

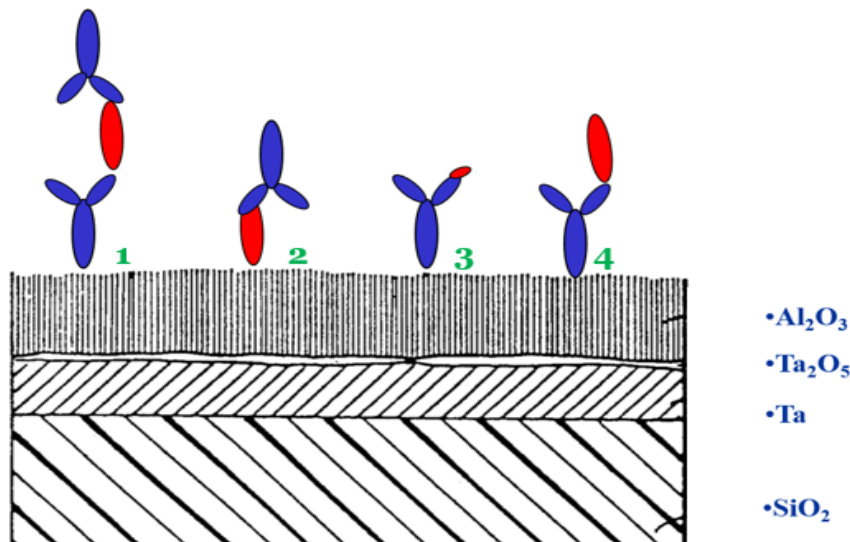


Figure 13. Four different binding scenarios and the likelihood of a significant colour shift from the base colour and the immunocomplex.

Scenario 3 might not produce a significant enough colour shift between the “base” colour and the shifted colour because the bound protein is not large enough to produce a significant change in layer thickness. Scenario 1 illustrates the application of a secondary antibody—thereby producing a significant increase in thickness and subsequent colour change. The procalcitonin POCD is an antigen test that would confirm the presence (or lack) of procalcitonin in a patient’s blood. To accomplish this, procalcitonin IgG is immobilized onto the aluminum oxide layer and oriented perpendicular to the alumina. This is accomplished with the addition of GLAs to the c-terminus of the antibody. Circulating procalcitonin from a patient’s blood, with a bacterial infection, would bind to the IgG and the optical path length (OPL) would increase.

#### 2.6.4 Tunability

An advantage of developing a point of care diagnostic using interference colours based on anodized aluminum/tantalum thin films is its versatility. Theoretically, the device could be used for any antibody/antigen pair. Additionally, the aluminum oxide layer can be increased or decreased, or the refractive index adjusted, thereby varying the OPL to achieve the desired interference colours. Depending on the size of the antigen or antibody, the deposited protein alumina layer  $d$  can be adjusted to optimize interference colours. The increased sensitivity achieved by tuning the refractive index allows for very sensitive colour shifts and picomolar ( $10^{-12}$ ) surface concentrations<sup>41</sup>.

#### 2.7 Colour Interference

The POC device design uses thin film interference to provide confirmation (positive or negative) of a bacterial infection evidenced by a colour change. Incident white light partially reflects off the protein layer while the remainder of the incident light refracts and travels through the aluminum oxide layer. That light encounters another change in refractive index at the alumina/tantalum oxide interface and reflects off the colour-generating tantalum oxide layer. The two reflections of light experience a corresponding phase changes, when encountering materials with a higher refractive index, and recombine in the observer’s eye. The waves recombine and interfere constructively or destructively to produce interference colours.

Interference colours progress in a natural progression from first order to second and third and so on. Sandstrom et. showed that the most sensitive colour shifts due to changes in film thickness are achieved in the first order colours<sup>42</sup>.



Figure 14. Order of interference colours generated with increasing thin film thickness from left to right. <sup>43</sup>

Once anodized, and the refractive index remains constant, the thickness of the protein/aluminum oxide layer is what determines the colour produced due to increasing or decreasing the optical path length. Increasing the aluminum oxide layer corresponds to increased thickness, in Figure 14. Colour interference repeats colours as you migrate into higher orders eventually only alternating between green and pinks due to the mixing of destructive and constructive interference of full and half wavelengths.

### 2.7.1 Colour Interference Charts

In 1931, a colour system was devised by the *Comission Internationale de l'Eclairage* (CIE) to produce an international standard model of human colour vision. The system provides a quantitative relationship between electromagnetic visible spectrum wavelengths and the physiologically perceived colours perceived in human vision. The human eye has three different colour sensors: red, green, and blue. Each type of colour sensor responds to different ranges of wavelengths of white light, but any perceived colour is a combination of the three wavelengths of light at varying intensities. Y corresponds to relative luminance; Y also carries color information related to the eye's "M" (yellow-green) cone response. X and Z carry additional information about how the cones in the human eye respond to light waves of varying frequencies.

## C.I.E. 1931 Chromaticity Diagram

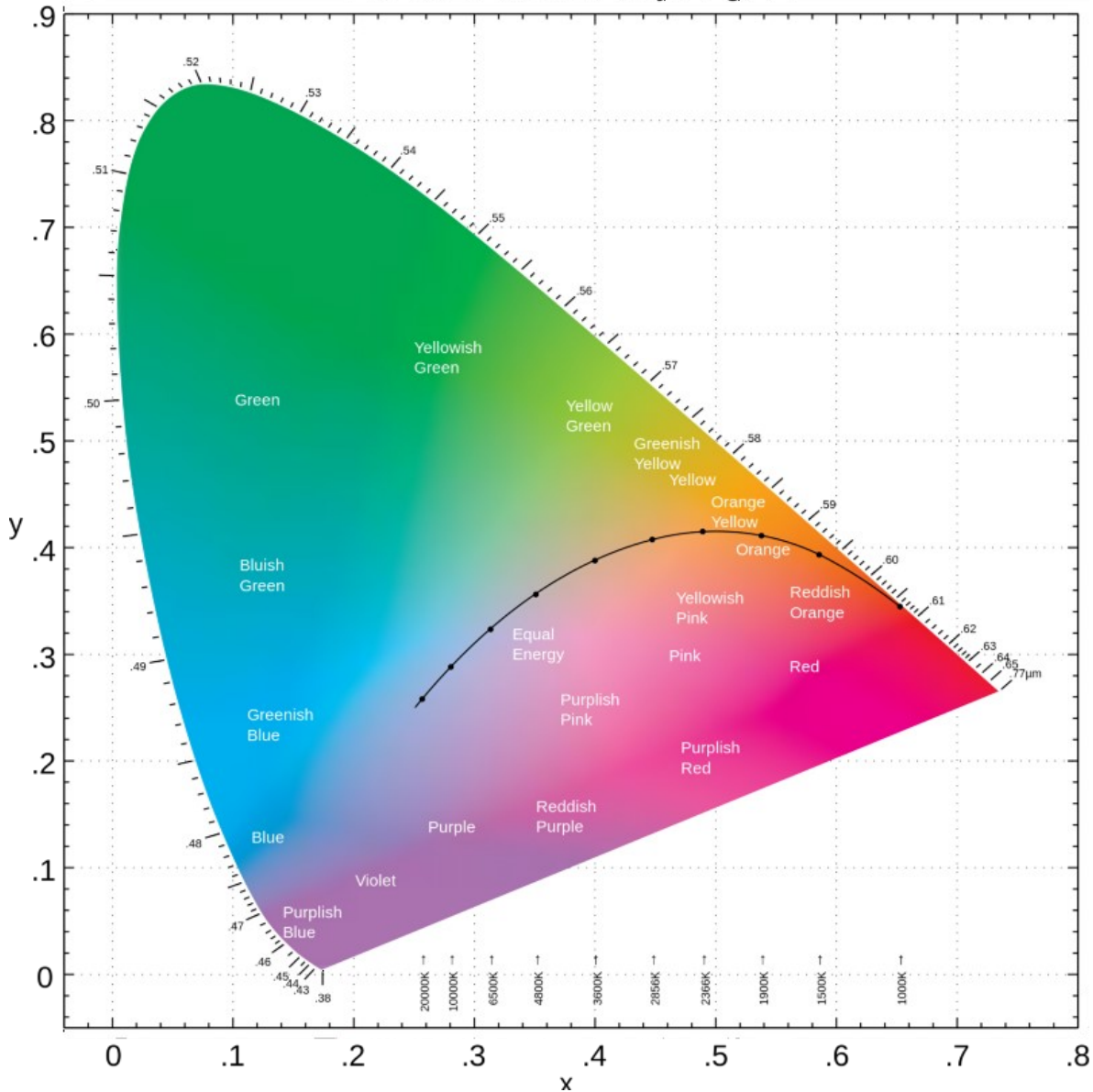


Figure 15. CIE 1931 Colour Chart. The CIE XYZ color space encompasses all color sensations that are visible to a person with average eyesight. The chart is a 2D representation of a 3D model. <sup>44</sup>

The perimeter of the chart indicates the wavelengths of the visible spectrum from violet light, with a wavelength beginning at 380nm, to red light with a wavelength of 740 nm. Every point inside the curve refers to a RGB Chromaticity Coordinate.

### 2.7.2 MacAdam Ellipse

MacAdam Ellipses are areas within the CIE colour chart where the colours within the ellipse are humanly indistinguishable from each other<sup>45</sup>. It is particularly important to optimize and control the aluminum oxide layer thickness so that a discernible colour change can be visualized by a positive test.



antibody contains two main parts, the extended arms of the Y is called the Fab Region, which stands for antigen binding fragment, and the trunk of the Y, known as the Fc or crystallized fragment (see Figure 17, below).

## IMMUNOGLOBULIN MOLECULE STRUCTURE

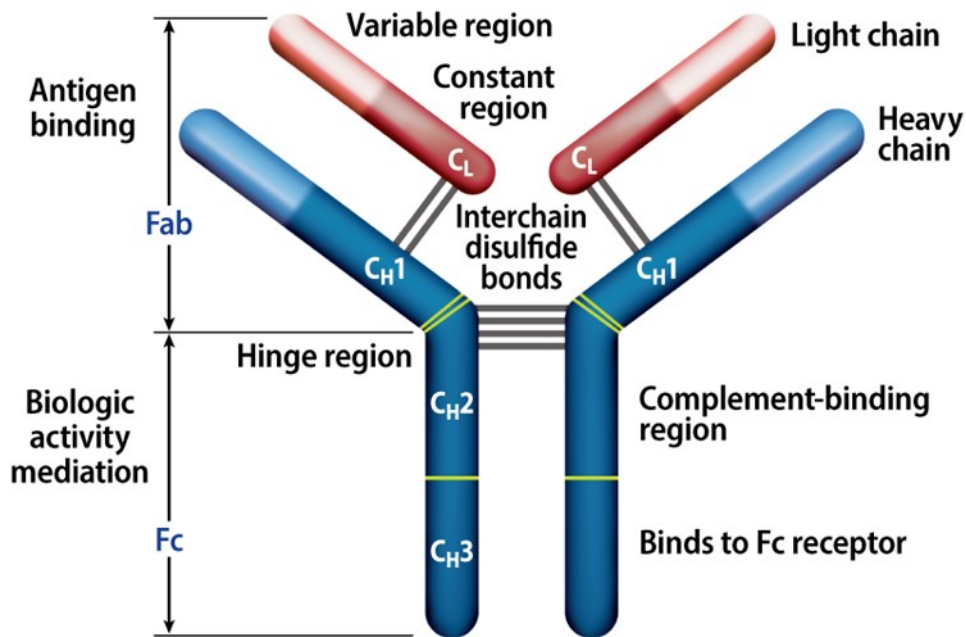


Figure 17. Antibody structure Human antibodies are composed of four polypeptide chains: two heavy chains (dark blue) and two light chains (light red). Antigen binding sites are each formed by the variable regions of a light chain and a heavy chain (Fab regions). The constant regions of the heavy chains form the trunk of the Y (Fc region). The two Fab regions and Fc region are linked by a flexible hinge region that improves the ability of the Ab to bind antigen. <https://www.myeloma.org/types-of-myeloma> Accessed: Mar 19, 2021<sup>47</sup>

A common metaphor to describe antibody/antigen pairs is the complementarity of a lock and key<sup>48</sup>. Consider the antigen to be the key and if it were to fit the antibody lock an immune response ensues. Each tip of the Y of an antibody contains a paratope, or antigen-binding site, that is specific to a particular epitope on the antigen that allows the two structures to bind together with precision.

They are heavy proteins that have a molecular weight of ~150kDa of about 10nm in size<sup>49</sup>. Conversely, procalcitonin is a 116 amino acids peptide with a molecular weight of 14.5 kDa.

### 2.8.2 Procalcitonin IgG/GLA Fusions

Procalcitonin is a biomarker found in response to pro-inflammatory stimulus—particularly of bacterial origin. Consequently, it is classified as an acute phase reactant because its plasma concentrations increase or decrease in response to inflammation. As previously noted, procalcitonin concentrations do not significantly rise with viral or non-infectious inflammations. Viral infections produce interferon that

inhibits the initial formation of procalcitonin<sup>50</sup>. Thus, it is possible to identify bacterial infections by confirming the presence of procalcitonin with procalcitonin antibodies.

Antiprocalcitonin belongs to a class of antibodies called Immunoglobulin G (IgG). IgG's are the most common antibody found in circulating human blood and make up to 10-20% of plasma protein<sup>51</sup>. As mentioned in the previous section, each IgG antibody has two paratopes or antigen binding sites.

To maximize signal strength and binding capability, antibodies should be oriented perpendicularly from the surface. Antibody applied to the surface may have unordered orientation and binding sites might not be exposed. This would compromise Procalcitonin's ability to recognize and bind to the adsorbed antibody, thus reducing the efficacy of the POCT. A potential solution is to engineer Procalcitonin antibodies with GLA proteins. Vitamin K-dependent carboxylation/gamma-carboxyglutamic (GLA), attached to the c-terminus, orient the antibodies normal to the surface of the aluminum oxide.

Four different procalcitonin antibody (APCT) fusions, listed in Table 2, were designed in Dr. Sachdev Sidhu's Toronto Recombinant Antibody Centre (TRAC) affiliated with the University of Toronto. These are Procalcitonin IgG/GLA fusions. Three of the antibodies, Antibodies A through C, have a GLA attached to each c-terminus of both polypeptides that make up the heavy chain as seen in figure 18. Antibody D differs in its composition with the GLA's attached to each section of the light chain. The GLA proteins orient the antibody perpendicular to the surface.

Table 2. List of the IgG/GLA fusions produced by Dr. Sidhu's Toronto Recombinant Antibody Centre.

Sample	Name	Approx. MW (KDa)	Lot	Format	Antigen
Antibody A	10773 IgG Hc F7.1	150	11/27/2019	IgG with Gla on Heavy Chain (2 Gla/full IgG)	Procalcitonin
Antibody B	10771 IgG Hc F7.1	150	11/27/2019	IgG with Gla on Heavy Chain (2 Gla/full IgG)	Procalcitonin
Antibody C	11643 IgG Hc F7.1	150	11/27/2019	IgG with Gla on Heavy Chain (2 Gla/full IgG)	Procalcitonin
Antibody D	10773 IgG hk F7.1	150	11/27/2019	IgG with Gla domain on light chain (2 Gla/full IgG)	Procalcitonin

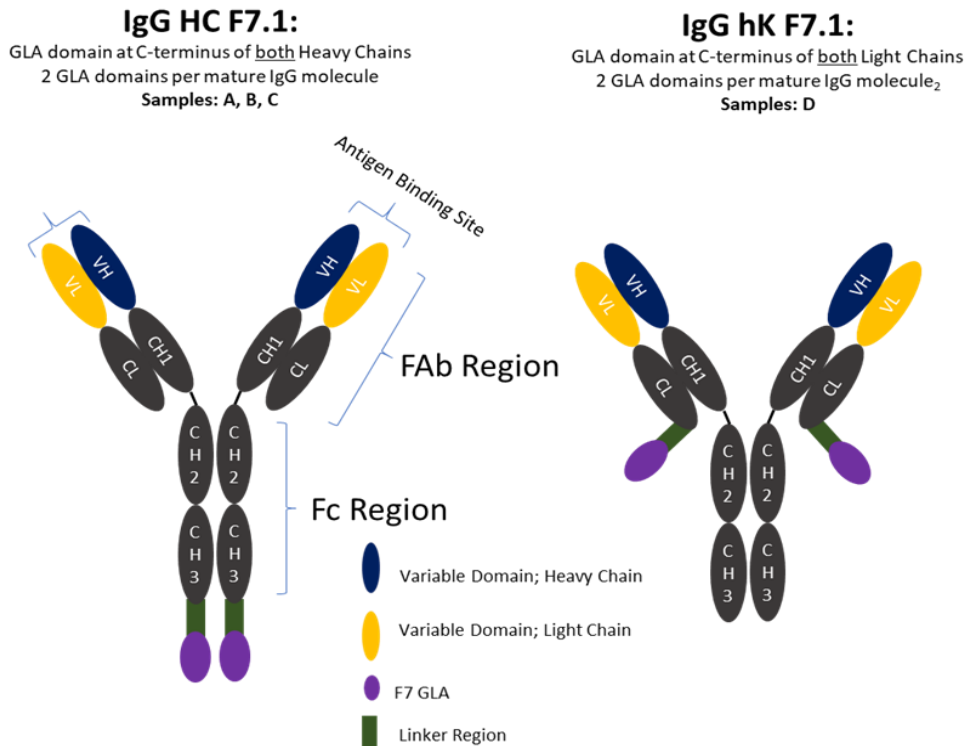


Figure 18. Graphical Representations of the IgG/GLA Fusions. Antibodies A, B, C have the GLA linked to the C-terminus of both heavy chain polypeptides. Sample D links the GLA to the C-terminus of both light chains. Credit to Blazer, L. TRAC

A matrix was designed to test the efficacy of the different APCTs as surface binding proteins and as secondary antibodies in combination with anodization and thickness parameters. Figure 18 demonstrates how a GLA domain orients the protein normal to the surface.

## Chapter 3 Methodology

### 3.1 Introduction

This chapter describes the methods and techniques used in the preparation and analysis of silicon slides used as the platform for the device. This includes: the process for depositing thin films; how deposition rates are established; how the thin films are prepared and characterized and, finally, how proteins will be applied.

### 3.2 Sputter Deposition

Sputtering is a form of physical vapour deposition. It is used in the deposition of thin films in the manufacture of optical coatings, semiconductor devices and nanotechnology products. Surface particles

of a solid target material are ejected onto a substrate due to the bombardment of the target by high energy argon plasma ions. Thin films were deposited onto unprocessed test-grade silicon wafers 100mm in diameter with <100> crystal plane configuration (University Wafer, South Boston, MA).

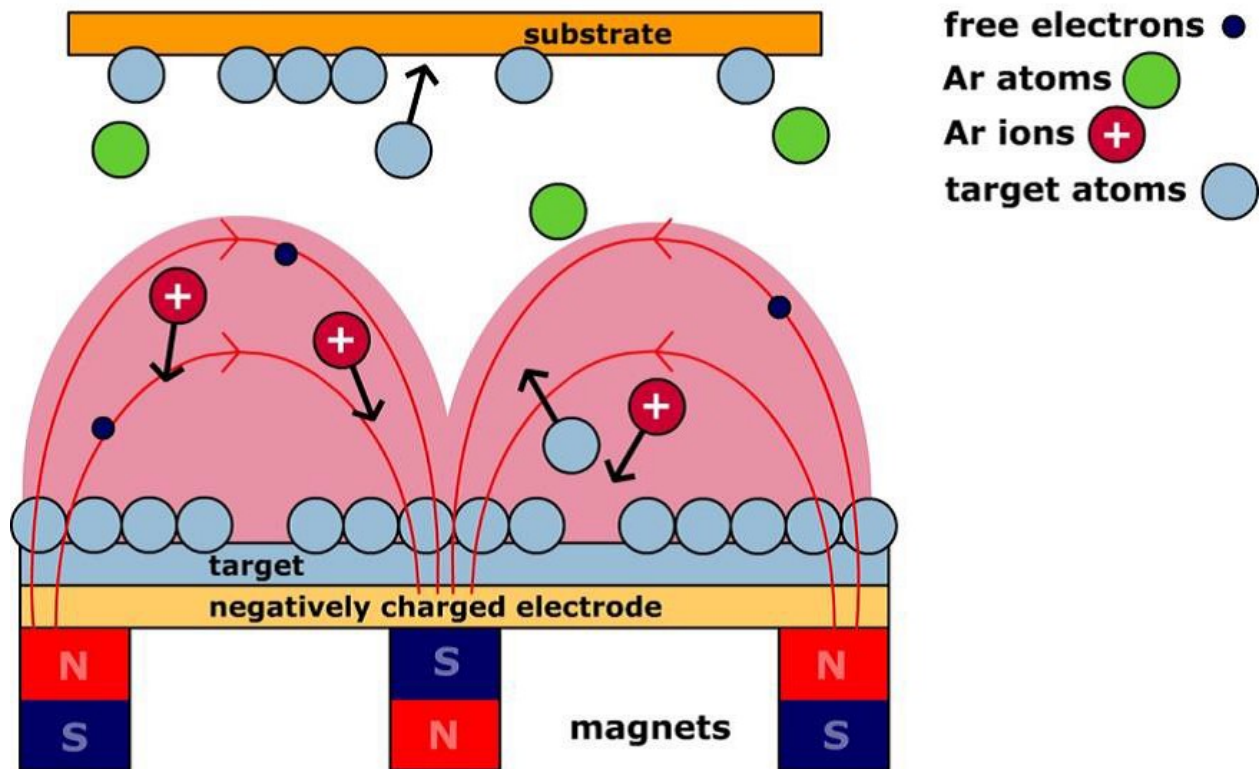


Figure 19. Graphical representation of a magnetron sputtering system. The magnetic field generated behind the target increases plasma density by confining charged plasma particles close to the target surface. <https://www.polifab.polimi.it/equipments/orion-8/> accessed: Mar22, 2021.<sup>52</sup>

The thin films for this device were sputtered at the University of Alberta’s nanoFab facility using two different magnetron sputtering systems. Magnetron sputtering uses magnetic fields to trap high-energy atoms close to a target material (Figure 19). The surface of the target is eroded and liberated target ions are deposited onto the substrate surface.

Tantalum thin films were deposited using the “Bob” sputter system—a manually operated planar magnetron sputter system, while aluminum thin films were deposited using the “Floyd” sputter system. Floyd differs from Bob in that it is a load-locked, computer-controlled, planar magnetron sputter system with dedicated targets. Once the deposition rate was established, deposition times were adjusted to achieve the desired thicknesses.

### 3.2.1 Tantalum Deposition

The planar magnetron system Bob (Kurt J. Lesker Company, Jefferson Hills, PA) was used to deposit an optically thick film ( $>200\text{nm}$ ) on the silicon wafers. A 7.62cm (3") tantalum target of 99.95% purity (Kurt J. Lesker, Jefferson Hills, PA) was always installed into Gun 2 for consistency.

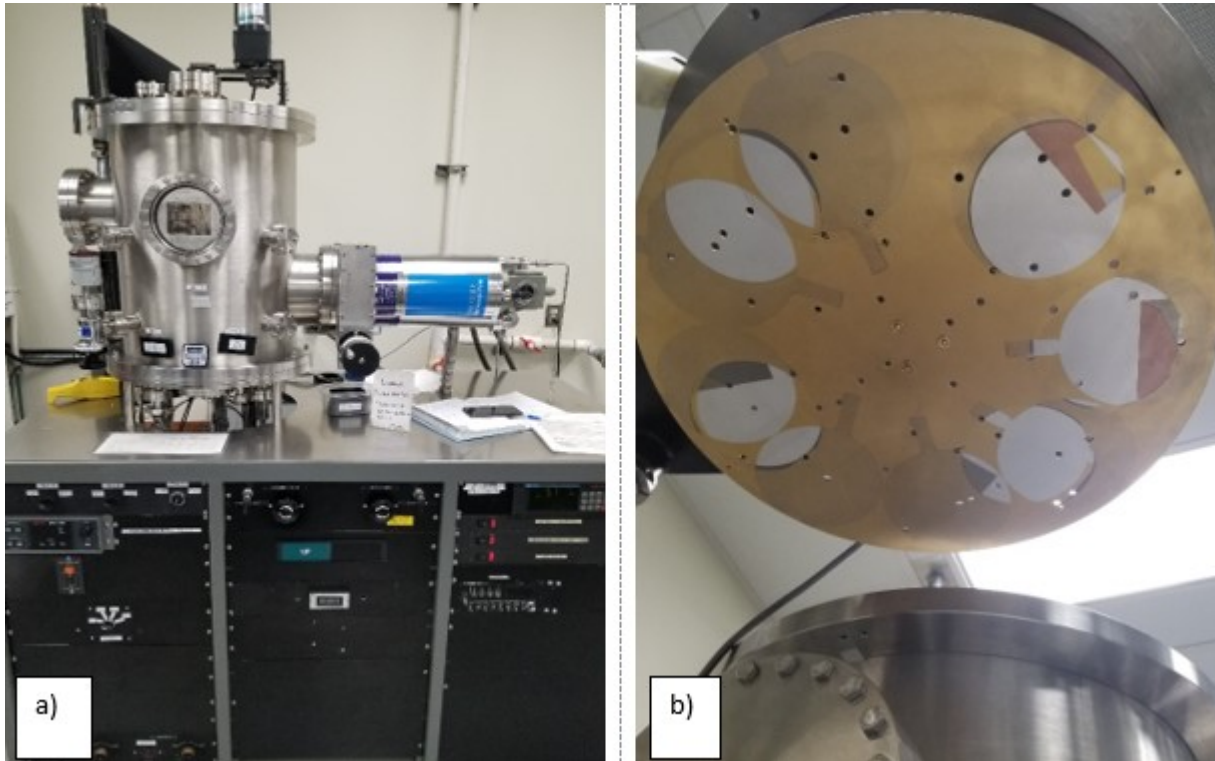


Figure 20. a) The University of Alberta nanoFAB's manually operated planar sputter system Bob used for tantalum deposition. b) Wafers are affixed to the underside of the platen with spring hooks with the side to be deposited on facing toward the target.

Bob is manually operated system that rotates a 40cm in diameter platen at 20rpm at a working distance of 12cm above three different target guns. The polished side of the silicon wafers are secured to the underside of the platen perpendicularly to Gun 2 with spring loaded clips. Bob's platen is large enough to accommodate 6 wafers at a time. Operation protocols are included in the Appendix (Bob Sputtering System SOP). A low base pressure below the vapour pressure of water ( $<2.0 \times 10^{-6}$  Torr) was achieved through roughing and cryogenic vacuum pumps. Once reached, argon gas is introduced with a flow rate of 10.1 sccm into the chamber to attain a working gas pressure of 7 mTorr. A constant power of 300W is applied to generate a plasma. The wafers undergo a 27-minute deposition to achieve a tantalum thickness of  $\sim 225\text{nm}$  at a dep rate of  $\sim 8.3\text{nm}/\text{min}$ . The thickness of the tantalum is not critical to the device provided it is optically thick, so tantalum target dep rate drift is of no real concern.

### 3.2.2 Aluminum Deposition

A different planar magnetron system, Floyd, was used to deposit a thin film of aluminum on top of the tantalum layer. Floyd is a load-locked, computer-controlled, planar magnetron sputter system with dedicated targets. Floyd's Gun 4 has a dedicated 7.62cm (3") aluminum sputtering target with a 99.9995% purity (Kurt J. Lesker Company, Jefferson Hills, PA). The system uses eKLipse software (Kurt J. Lesker, Jefferson Hills, PA) for semi-automated operation. Floyd's SOP will be included in the Appendix.

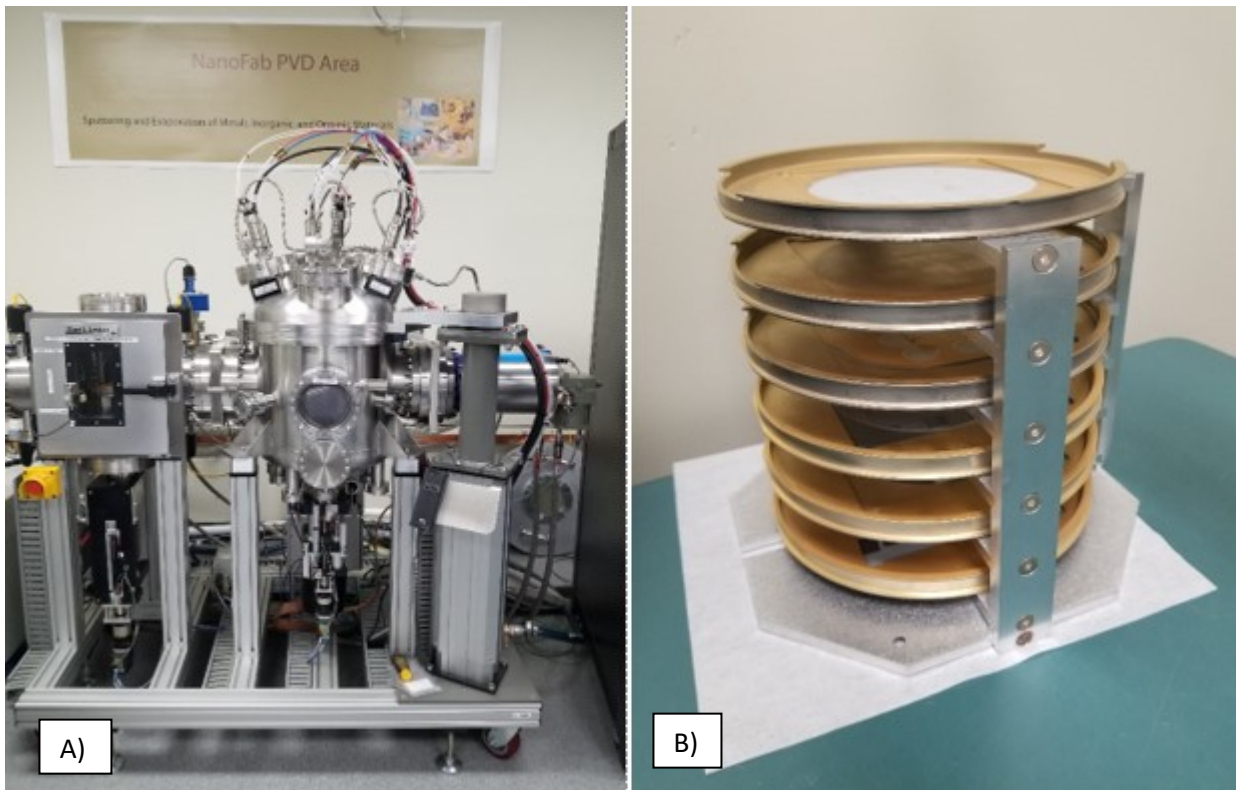


Figure 21. a) University of Alberta's nanoFAB Floyd Sputter system is a load-locked, computer-controlled, planar magnetron sputter system. b) Floyd's wafer holder with six wafer capacity

Depositions occur on individually loaded wafers at the time, but the load lock and its holder can store six wafers at a time on its shelves without breaking load lock pressure. Once base chamber pressures ranging from low  $10^{-7}$  to high  $10^{-8}$  Torr were achieved, argon gas is introduced to the system at a flow rate of 55sccm to establish a deposition pressure of 7mTorr. The wafer plate is rotated at 20rpm at a working distance of 12.5cm with the Gun 4 positioned at a  $15^\circ$  angle to the platen. Film thicknesses for Matrix 1 were varied from 80nm–130nm with a lower tolerance for error.

### 3.2.3 Establishing Deposition Rate

As previously noted in section 3.2.1, tantalum thickness is not critical to the device's optimization. Consequently, establishing the tantalum deposition rate is not as important provided the tantalum film

is optically thick. We use the nanoFAB's established deposition rate of 8.3nm/min to achieve film thicknesses ~225nm. Conversion of tantalum to tantala is voltage dependent occurring at 1.6nm/V. Matrix 1 anodization voltages range from 2V to 10V, so the colour-generating tantalum oxide layer will never be thicker than 16nm.

Establishing a deposition rate is more important for the aluminum layer because, once anodized, the aluminum oxide thickness impacts the OPL of light. Sweet found Floyd's deposition rates ranged between ~9 and 12 nm/min<sup>53</sup>. Deposition rates fluctuate depending on the life of the target and temperature of the target. It was crucial to establish a current deposition rate prior to depositing aluminum on a batch of wafers (10–12 in a session).

A single wafer would be coated with a predetermined deposition time—usually 550s. That wafer would be anodized and the oxide thickness measured by ellipsometry. The thickness per time ratio would be established and deposition times calculated for desired thicknesses.

#### *3.2.3.1 Ellipsometry*

The optical constants (refractive index,  $n$ , and extinction coefficient,  $k$ ) as well as the final oxide thicknesses were determined using a J.A. Woollam M-2000V spectroscopic ellipsometer (J.A. Woollam Co., Lincoln, NE). A model was built to represent aluminum oxide porous film and collected data was fit into this model developed by Nickel<sup>37</sup>. This model is an effective medium approximation (EMA) which combines alumina and void (i.e. air) that uses an anisotropic Bruggeman EMA model.  $\Psi$  and  $\Delta$  values were recorded for wavelengths 370 nm to 1000 nm at angles of 55°, 65°, and 75° from normal. CompleteEASE® software for Windows (J.A. Woollam Co., Lincoln, NE) was used to develop the ellipsometry model and tabulate refractive index and oxide thickness values.

Aluminum deposition rates were established by anodizing an aluminum/tantalum wafer and using the ellipsometer to determine the aluminum oxide thickness. The oxide thickness was compared with the time taken to deposit aluminum. This ratio was used to determine sputter times for desired thicknesses.

### 3.3 Anodization

Under normal atmospheric conditions, aluminum has a native aluminum oxide layer that is roughly 2-3nm. Buff, in 1857, demonstrated that aluminum could be electrochemically oxidized to grow the thickness of the oxide layer<sup>35</sup>. Anodizing is accomplished by immersing the wafer, acting as the anode, into an acid electrolyte bath and passing an electric current through the medium to a cathode. In Figure 22, the Princeton Applied Research Model 273A Potentiostat/Galvanostat (Ametek® Scientific Instruments, Berwyn, PE) is the power supply used for all anodizations performed in Dr. Burrell's lab in

University of Alberta's Research Transition Facility.



Figure 22. The Princeton Applied Research Potentiostat used for all anodizations.

A cathode of an aluminum foil wrapped disc is mounted on a bracket adjacent to the aluminum covered wafer. The bracket is lowered into an anodization bath. Once voltage is applied, the multilayered wafer acts as an anode, so that oxygen ions are released from the electrolyte to combine with the aluminum atoms at the surface of the substrate wafer. Anodizing is, therefore, a matter of highly controlled oxidation—the enhancement of a naturally occurring phenomenon. Wafers were placed in a 3D-printed holder opposite the 10cm aluminum foil-wrapped cathode at a distance of 4cm.

All wafers were anodized in a 0.4/0.1M Phosphoric/Oxalic acid bath. Work performed by Nickel<sup>37</sup>, demonstrated that the addition of 0.1M oxalic acid to the 0.4M phosphoric acid bath promotes even anodization, minimizes surface roughness and smaller standard deviation of pore size and visible grain boundaries. Additionally, using a strong inhibitor in the electrolyte bath can help achieve several important goals including, the high porosity needed for low refractive index films, a small pore size required to keep protein from adsorbing inside the pores and thus changing the refractive index, as well as an optically smooth surface to provide a uniform light reflecting substrate for the adsorption of protein.

The potentiostat supplied constant voltage to anodizations of 2, 4, 6, 8, and 10V. Current was measured over time and plotted using PowerSuite software (Ametek® Scientific Instruments, Berwyn, PE) in combination with an accumet™ saturated potassium chloride calomel reference electrode (Thermo Fisher, Waltham, MA)

Full wafers were anodized at room temperature ( $21\pm 2^\circ\text{C}$ ) in  $\sim 1.75\text{L}$  of a 0.4/0.1M Phosphoric ( $\text{H}_3\text{PO}_4$ )/Oxalic ( $\text{C}_2\text{H}_2\text{O}_4$ ) acid electrolyte solution contained in a 2500ml beaker. Experiments were carried out with a 200rpm magnetic stir bar, fast enough to homogenize the solution while minimizing solution turbulence. The anode and cathode, positioned in the 3D-printed holder and clipped with the corresponding electrode, are lowered into the electrolyte bath equidistant to the reference electrode. Electric potential is enabled on the potentiostat and the PowerSuite data logger engaged immediately upon lowering the cell into the bath. PowerSuite graphs current (A) over time (s) and produces a recognizable pattern. There are two different type of oxide layers that can be electrolytically grown on aluminum: a uniformly thick barrier layer on the surface; and ordered porous aluminum oxide films. Figure 23 demonstrates current/time graphs for the two different type of films.

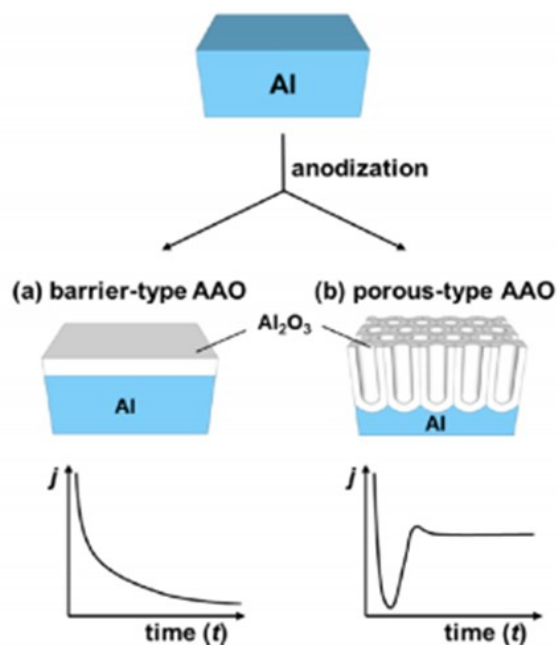


Figure 23. An illustration of the different current/time plot features based on type of oxide film being generated by anodization.<sup>35</sup>

Current density plots for the wafers anodized for this study exhibit common features. Figure 24 demonstrates several common zones: Zone A exhibits an initial drop in current due to an aluminum oxide barrier layer forming; Zone B, a steady-state plateaued region where pore formation in the alumina occurs under constant current; and Zone C, an area of linearly descending current where

tantalum oxide is being generated followed by another plateau that indicates that the tantalum oxide has finished growing acting as an electric barrier blocking current.

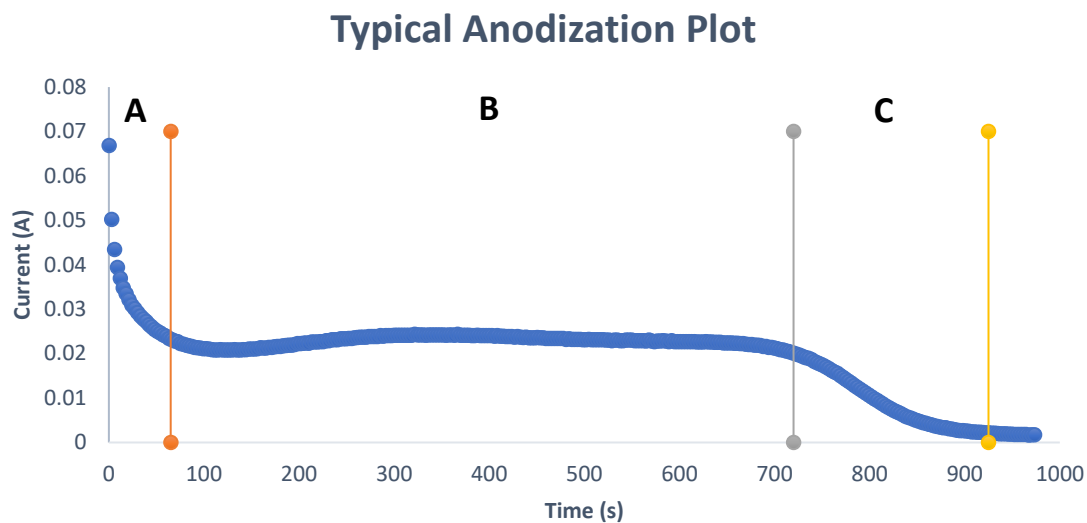


Figure 24. A typical anodization plot that demonstrates three distinct zones. An aluminum oxide barrier layer forming in Zone A, pore formation in the alumina layer in Zone B and a tantalum barrier layer forming in Zone C.

The length of time for an anodization was variable dependent on voltage and room temperature, so anodization runs were manually shut off once the graph reached the second plateau. Upon completion, samples are removed from the bath and rinsed thoroughly with deionized water. Wafers are left to dry on their edge resting against on top of paper towel. Once dry, the wafer is labelled and returned to a wafer container until needed.

### 3.4 Scanning Electron Microscopy

SEM was used to observe microstructural and topographical differences in pore size by changing anodization potential from 2V and 10V. Anodized wafers were cleaved into pieces and a  $\sim 1\text{cm}^2$  square affixed onto a 1cm diameter aluminum stubs (Ted Pella Inc., Redding, CA) by double-sided carbon tape (PELCO Tabs™, Ted Pella Inc., Redding, CA). Samples were examined using a Zeiss Sigma Field Emission Scanning Electron Microscope (FESEM) (Carl Zeiss Canada Ltd., Toronto, ON) at the nanoFAB – Fabrication and Characterization Center at the University of Alberta. Specimens were characterized under an ultra-high vacuum conditions  $< 10^{-8}$  Torr, viewed with an accelerating voltage of 3.00 and 5.00 keV, an aperture size of  $30\mu\text{m}$ , and a working distance of 5.5mm.

#### 3.4.1 Results

Figures 25 and 26 images generated from two samples and a rough estimate of pore size measured. As voltage increases pore size correspondingly increases. Conversely, and perhaps counterintuitively, as voltage increases, pore density decreases. Fewer pores introduce less air into the alumina layer and increases the system's effective refractive index. Consequently, refractive index increases with an increase of voltage.

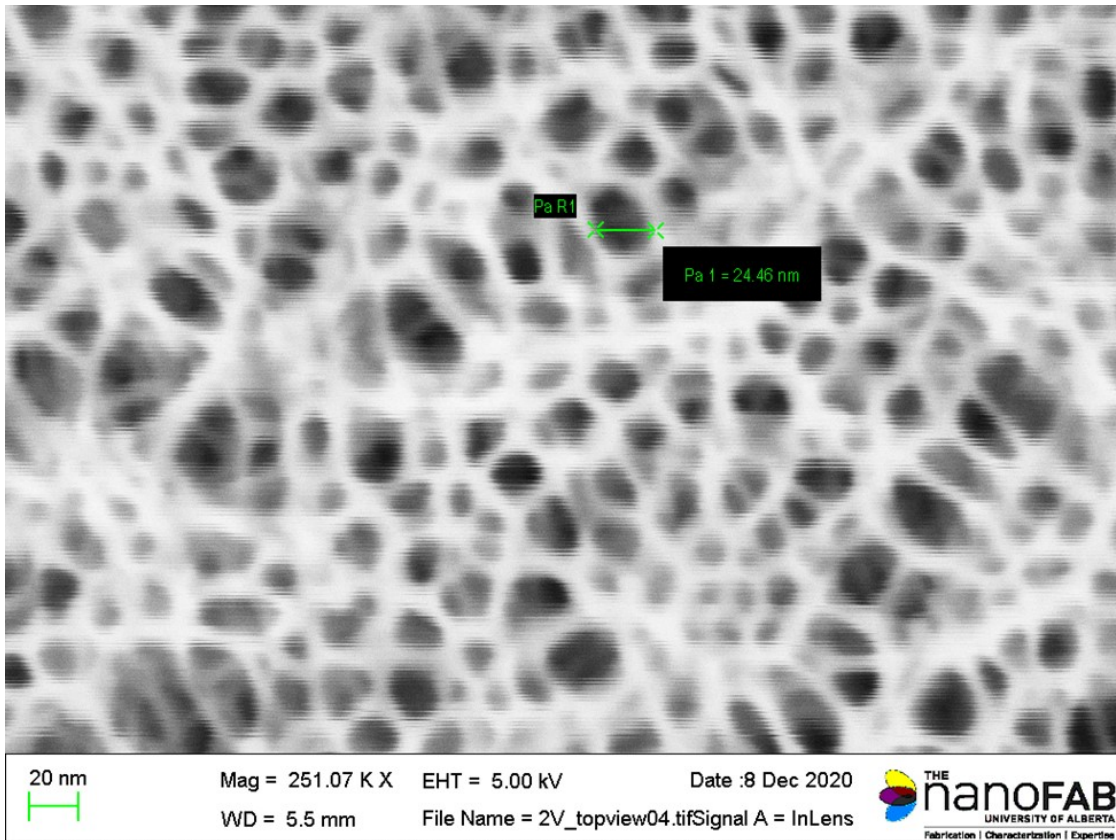


Figure 25. A topographic image of the porous nanostructure generated at 2V.

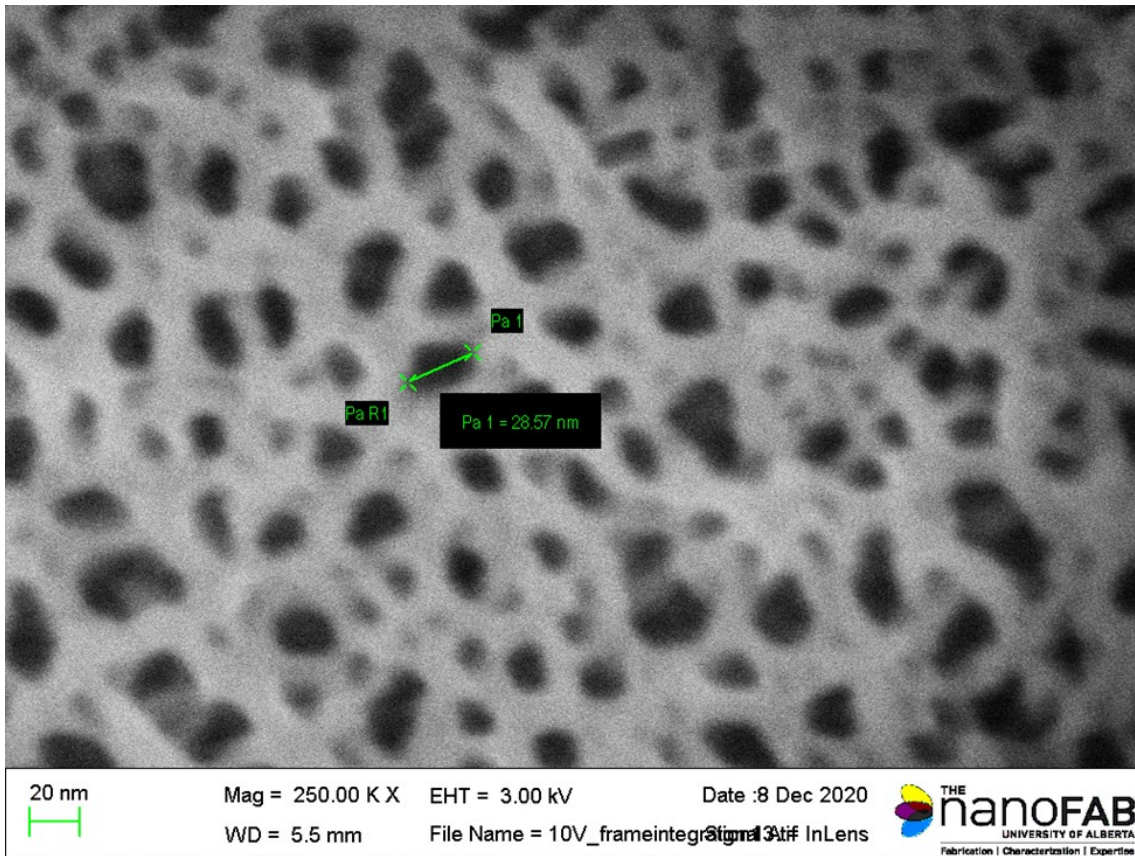


Figure 26. A topographic image of aluminum oxide pores anodized at 10V.

Measurements of the cross-sectional thin film thicknesses were also visualized. Figures 27 and 28 show the film thickness of the aluminum oxide and tantalum layers, respectively. Not visualized, nor measured was a 16nm Ta<sub>2</sub>O<sub>5</sub> layer.

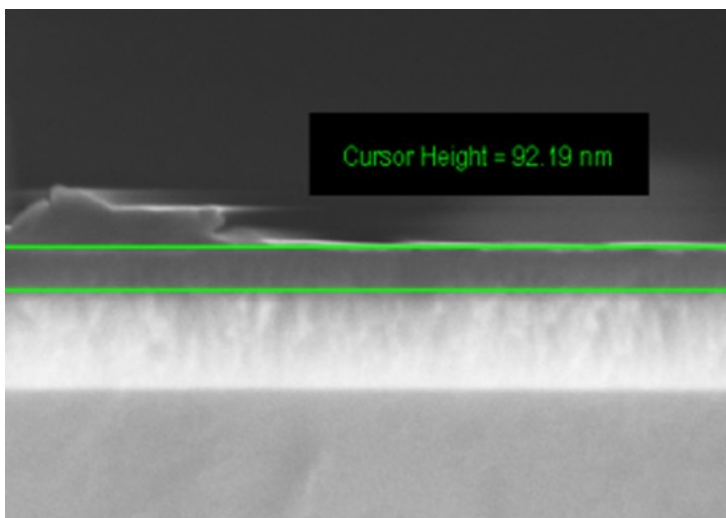


Figure 27. A cross-sectional image and measurement of the aluminum oxide layer. Target thickness was 90nm.

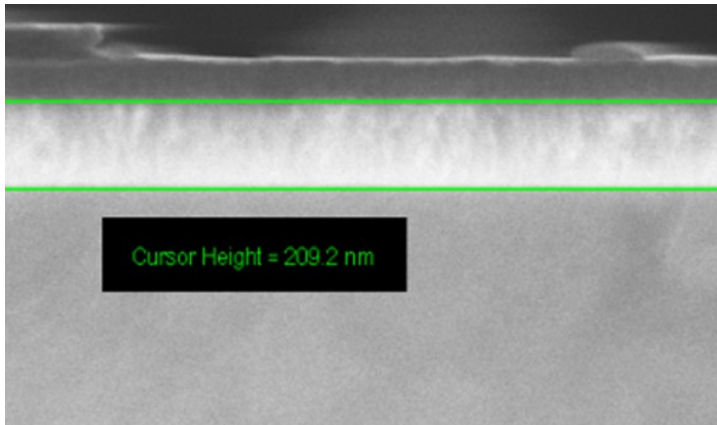


Figure 28. A cross-sectional image of the tantalum layer. Target thickness was 225nm.

### 3.5 X-ray Powder Diffraction

XRD was used to confirm the complete consumption anodization of aluminum into aluminum oxide. Any remaining aluminum would act as a light reflector in thin film system thus creating noise. An absence of an aluminum peak in the data would confirm that all aluminum had been converted to alumina. An Ultimate IV (Cu-source) diffraction system (Rigaku, Scottsdale, AZ) was used with the thin film stage. Data was collected between 10 and 80° 2 $\theta$  at 8°/min using a DHL slit of 15mm and a glancing angle of  $\omega=0.5^\circ$ . Jade 9™ software (Materials Data Inc., Livermore, CA) was used to analyze collected scans with established chemical composition peaks in the database.

#### 3.5.1 Results

Figure 29 demonstrates the alpha and beta tantalum peaks present in the XRD scan, there was no intensity peak corresponding to aluminum, thus confirming the complete consumption anodization of metallic aluminum. Aluminum oxide is amorphous and does not demonstrate a peak with x-ray diffraction.

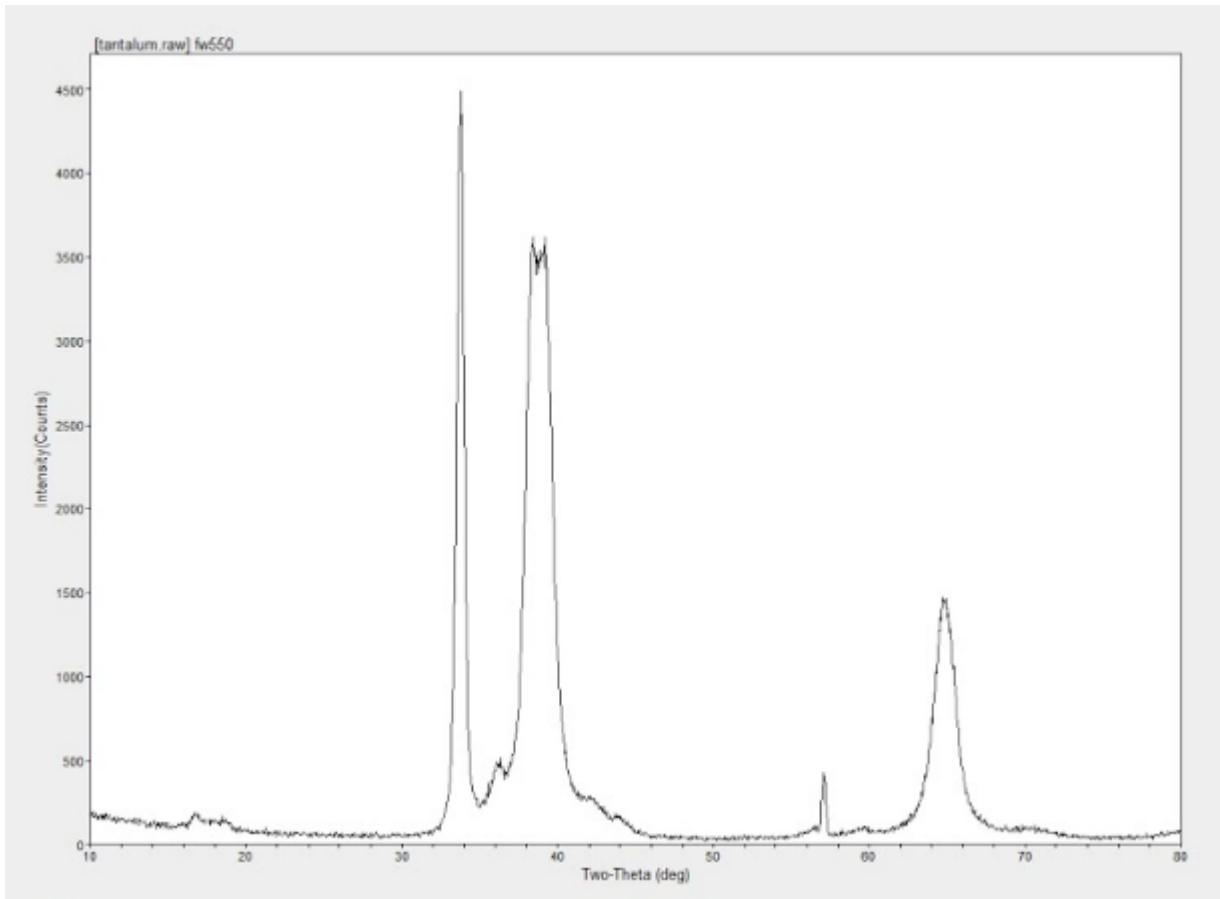


Figure 29. XRD scan of wafer segment demonstrates tantalum peaks for alpha and beta tantalum. The absence of an aluminum peak confirms the complete anodic consumption of aluminum.

### 3.6 Matrix 1: Anodization Voltage and Aluminum Oxide Thickness Combinations

There are two variables that can alter optical path length (OPL), aluminum oxide thickness and refractive index. Anodization converts aluminum to aluminum oxide and changing a metal with near 90% reflectance to a near invisible oxide with a refractive index of 1.7 [ref]. Figure 30 illustrates the reflectivity of several metals, but aluminum has over 90% reflectance within the visible spectrum.

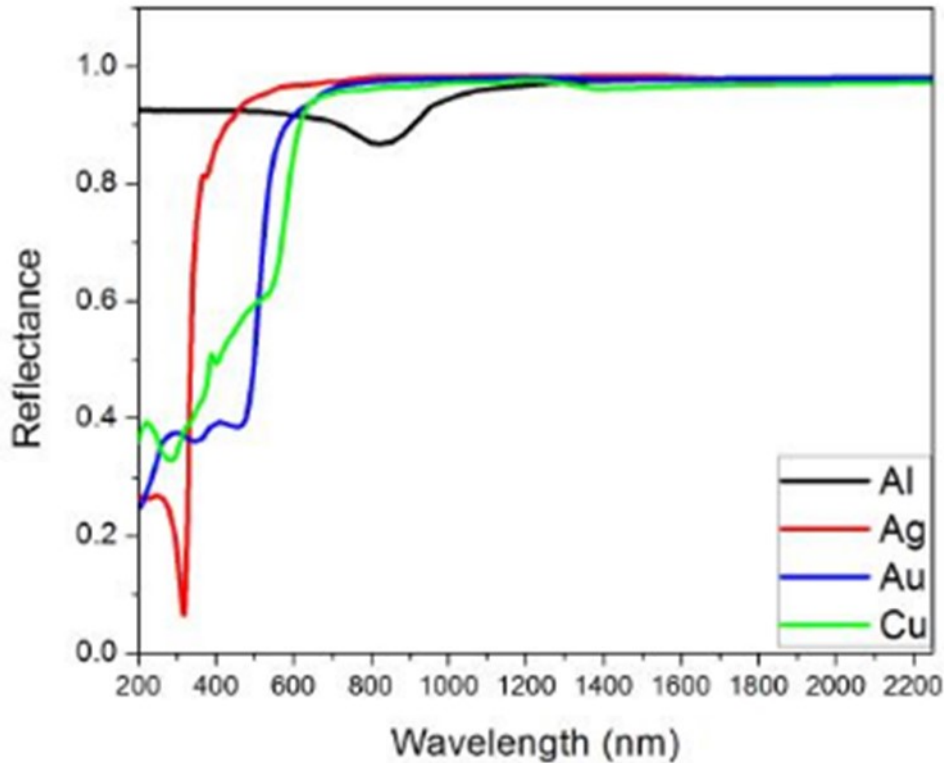


Figure 30. The reflectance spectra of silver, gold, copper and aluminum is represented. Aluminum has over 90% reflectance within the visible spectrum.<sup>26</sup>

The phosphoric acid encourages pore formation within the oxide layer. These pores introduce air into channels of the aluminum oxide thereby lowering the effective (air + oxide) refractive index. If the effective refractive matches the refractive index of protein, then light will propagate through both materials without an additional reflection. By increasing the thickness of the oxide—the distance light travels within the oxide lengthens.

Increasing voltage speeds up the conversion of aluminum to alumina, but the most important aspect of increased voltage is its effect of the tantalum layer. The conversion of tantalum to tantala is voltage dependent. The final thickness of the tantalum oxide layer grows at a constant rate of 1.6 nm/V (ref needed). A 2V anodization could have any size thickness of aluminum oxide on the surface, but only a 3.2nm thick tantalum oxide layer. Similarly, an 8V anodization, a 12.8nm thick layer. Tantalum oxide is the colour generating layer for the complex, so increasing its thickness results in a different “base” colour of the system.

Matrix 1 was designed to visually determine the optimal combinations of aluminum oxide thickness and anodization voltage. Slides that visually produced the most drastic colour changes with the addition of Procalcitonin antibodies and antigen were considered optimal.

In a medium of homogenous refractive index, the optical path length can be described as:

$$OPL = \eta d$$

where OPL is the optical path length,  $\eta$  is refractive index of the medium, and  $d$  is the physical length through which the light travels [16]. Thus, if there is a small change in the thickness of the film a change in color can be seen due to the change in the optical path length. Aluminum thicknesses chosen to range from 80nm to 130nm with an increase of 10nm per wafer.

Similarly, the other variable that can be altered is  $\eta$ , the refractive index. While a bulk material's refractive index is inherent, the refractive indices of proteins ( $\eta \sim 1.4$ )<sup>54</sup> and the aluminum oxide ( $\eta = 1.77$ )<sup>55</sup>, when protein is applied onto the anodized aluminum oxide layer, we can alter its effective refractive index with the addition of air. As mentioned earlier, the technology works by matching refractive indices between proteins ( $\eta \sim 1.4$ ) and the aluminum oxide ( $\eta = 1.77$ ). We accomplish this by introducing air into the oxide. Pores introduce air ( $\eta = 1$ ) into the aluminum oxide layer and the combination of these two indices result in an effective refractive index that matches that of proteins. By matching refractive indices, light does not have any secondary reflections that would introduce noise to the system affecting the resultant colour change. We can vary the anodization voltage to change pore size and refractive index<sup>56</sup>. Voltages chosen are: 2V, 4V, 6V, 8V, 10V. Matrix 1 will also determine if there are any difference in the engineered APCT fusions as base proteins or secondary antibodies.

Following anodization, each wafer will be cleaved into six long, rectangular slides. We standardize the rectangular slides by using a 3D printed template, shown in Figure 31, and a diamond pen. A tiny imperfection is scratched into the wafer with the diamond scribe. A small amount of flexion on either side of the flaw will cause the wafer to break along the crystal plane.

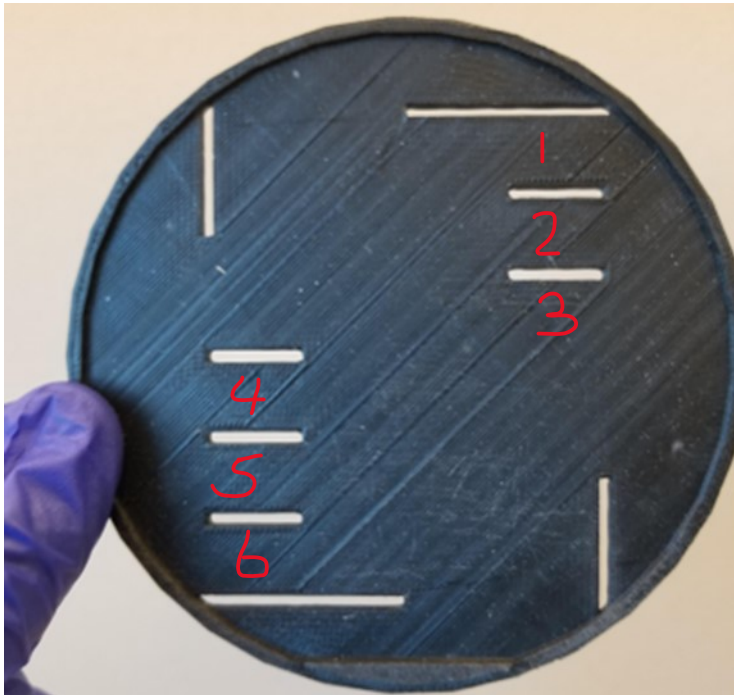


Figure 31. The 3D printed wafer template that was used to cleave the wafer into six long rectangles.

Each slide will have six 1cm diameter circles drawn onto them with an ultra fine tip marker as shown in Fig 32. The ink is thick enough to serve as a hydrophobic barrier for 20 $\mu$ l of solution.

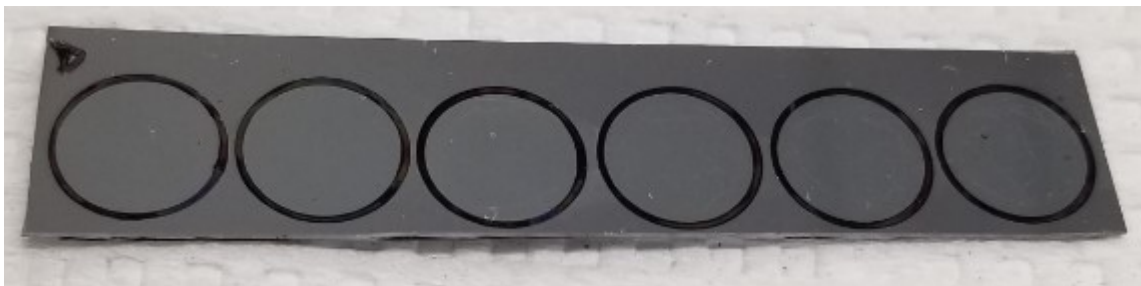


Figure 32. Wafer segment with six 1cm circles drawn with an ultra fine tip marker.

The various anti-procalcitonin with the different GLA's will be labelled: A; B; C; and D—recall Table 2 in section 2.8.2. The area outside the six circles serves as the control—natural colour generated by the oxide without IgG or antigen.

Step 1 involves the application of 20 $\mu$ l of one of the procalcitonin antibodies (A, B, C or D) will be applied on spots 1 through 6 and allowed to rest in a humid environment for 30 minutes; the antibody will be pipetted off and the slide will be rinsed and dried.

Once dry, Step 2 involves 20µl of 0.39mg/ml of procalcitonin applied to spots 2-6. The slide will again be allowed to sit in a humid environment for 30 minutes, at which point the PCT will be pipetted off and the slide rinsed with milliQ water and air dried.

Finally, spots 3 through 6 will be amplified. Spot 3 will receive 20µl of APCT A; spot 4 20µl of APCT B; spot 5 20µl APCT C; and spot 6 20µl of APCT D—the slide will rest for 30mins, rinsed and dried.

Pictures will be taken with a Logitech Brio 4K PRO (software: Logitech capture 2.06.8) with the addition of a sheet polarizer—following each step and stored in a folder on Google Drive. Each slide follows the naming structure of:

voltage\_thickness\_antiprocalcitonin antibody\_procalcitonin\_antiprocalcitonin antibody.

To maintain consistency, a naming convention was used. Following Step 2, the picture of the anodized slide at 6V, sputtered with 100nm of aluminum and APCTA used as the base protein will be named 6V\_100nm\_APCTA\_PCT. Pictures of the same slide taken following Step 3 will be named 6V\_100nm\_APCTA\_PCT\_APCT.

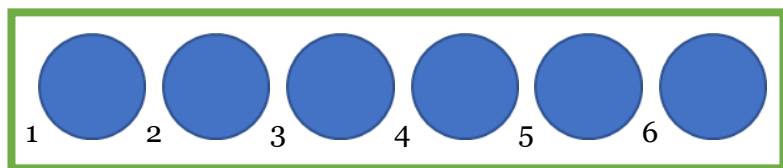


Figure 32. Visual Representation of the Six Spots on Each Slide

Table 3. Spot breakdown of a particular slide of voltage/thickness combination.

Ex 6V/100nm	Step1	Step 2	Step 3
Spot 1	Antibody A	Antibody A	Antibody A
Spot 2	Antibody A	Antibody A + Procalcitonin	Antibody A + Procalcitonin
Spot 3	Antibody A	Antibody A + Procalcitonin	Antibody A + Procalcitonin + Antibody A
Spot 4	Antibody A	Antibody A + Procalcitonin	Antibody A + Procalcitonin + Antibody B
Spot 5	Antibody A	Antibody A + Procalcitonin	Antibody A + Procalcitonin + Antibody C
Spot 6	Antibody A	Antibody A + Procalcitonin	Antibody A + Procalcitonin + Antibody D

After each step, visual comparison and pictures will be taken of each slide of each combination of thickness and voltage. Each slide will be compared twice: once by eye and repeated with the addition of a light polarizer placed in front of the eye and the camera lens. A polarizer is an optical filter that lets light waves of a specific polarization pass through while blocking light waves of other polarizations<sup>57</sup>. By using a polarizer, the signal is strengthened by filtering background light.

Matrix 1 is designed as follows in Table 4:

Table 4. Matrix 1: Voltage/Thickness Combinations

Table		Voltage									
		2V		4V		6V		8V		10V	
Thickness		A	B	A	B	A	B	A	B	A	B
	80nm		A	B	A	B	A	B	A	B	A
		C	D	C	D	C	D	C	D	C	D
90nm		A	B	A	B	A	B	A	B	A	B
		C	D	C	D	C	D	C	D	C	D
100nm		A	B	A	B	A	B	A	B	A	B
		C	D	C	D	C	D	C	D	C	D
110nm		A	B	A	B	A	B	A	B	A	B
		C	D	C	D	C	D	C	D	C	D
120nm		A	B	A	B	A	B	A	B	A	B
		C	D	C	D	C	D	C	D	C	D
130nm		A	B	A	B	A	B	A	B	A	B
		C	D	C	D	C	D	C	D	C	D

Optimal conditions will be performed in triplicate. The letters A, B, C, and D indicate which antibody fusion will be adsorbed to the aluminum oxide layer surface.

Table 5. The four different procalcitonin IgG's and their concentrations

Legend	Name	Concentration (mg/ml)
Antibody A	10773 IgG Hc F7.1	0.8
Antibody B	10771 IgG Hc F7.1	0.461
Antibody C	11643 IgG Hc F7.1	0.268
Antibody D	10773 IgG Hk F7.1	0.56

Despite the concentration differences between the four IgG's as shown in Table 5, 20µl of IgG was applied to the surface for 30mins in Step 1 and Step 3 to ensure surface saturation.

### 3.6.1 Results

Each slide was observed at a 15° angle from the surface and given a rating based on colour change to the naked eye. Ratings ranged from: (-) for no visible colour change; (+) for little colour change, but not significant; (++) for decent colour shift; (+++) for significant colour shift. Pictures were taken and ratings recorded in the matrix.

Following Table 3, Spot 1 only receives an application of antiprolactin and would be considered the “base” colour. Spot 2–6 would receive the addition of PCT in the second step. Finally, Spots 3 through 6 receives the addition of 20µl of secondary antibody and then compared.

The ideal combination of voltage and thickness would exhibit a substantial colour shift between Spots 1 and 2 so that a secondary antibody would not be required. However, a successful test would occur if any of Spots 3 through 6 were significantly shifted from Spot 1.

Table 6. Completed Matrix 2 with ratings

Table

Thickness	Voltage									
	2V	4V	6V	8V	10V					
80nm	+	-	-	+	+	+	+	+++	+	
	+	+	-	-	+++	+	+	+	+++	++
90nm	+	+	+	+	++	++	+	+	+	+
	++	-	+	+	+++	+	+	+	+++	+
100nm	-	-	+	+	++	++	+	+	+	+
	+	-	+	+	++	+	+	+	+++	+
110nm	+	+	+	+	++	++	+	+	+	+
	++	+	++	+	++	+	+	+	++	+
120nm	++	++	+	+	+	+	-	-	-	-
	+++	++	++	+	+	+	-	-	+	-
130nm	++	++	-	-	-	-	-	-	-	-
	+++	++	+	+	-	-	-	-	-	-

There is a trend that begins in the lowest voltage/thickest films and continues to highest voltage/thinnest films. It should be noted that these are subjective ratings and while a combination might not have received a (+++) rating, it does not mean that the colour shift is insignificant altogether. Smartphone software and camera can take RAW image pictures. It might be possible to read RGB coordinates to provide confirmation of a positive prolactin test. Although there is a trend, it cannot be assumed to be a linear relationship. A (+++) rating appears to occur when the light interference from the change in optical path length creates a substantial shift.

Examples of the visual colour ratings are demonstrated in Figure 33. There is no discernible colour shift between any of the 6 spots in the 10V/120nm/B slide, so it received a (-) rating. 2V/80nm/D received a rating of (+) because of a slight change in signal, particularly between spot 1 and 3, but not substantial enough to give a visual cue as a POCD. A (++) rating was given to the 6V/100nm/A. There is a decent colour shift between spot 1 and spot 3, but to my subjective eye, the colour shift moves from a burgundy to deep mauve. While the shift is discernible, it is not considered drastic enough for a visual POCD.

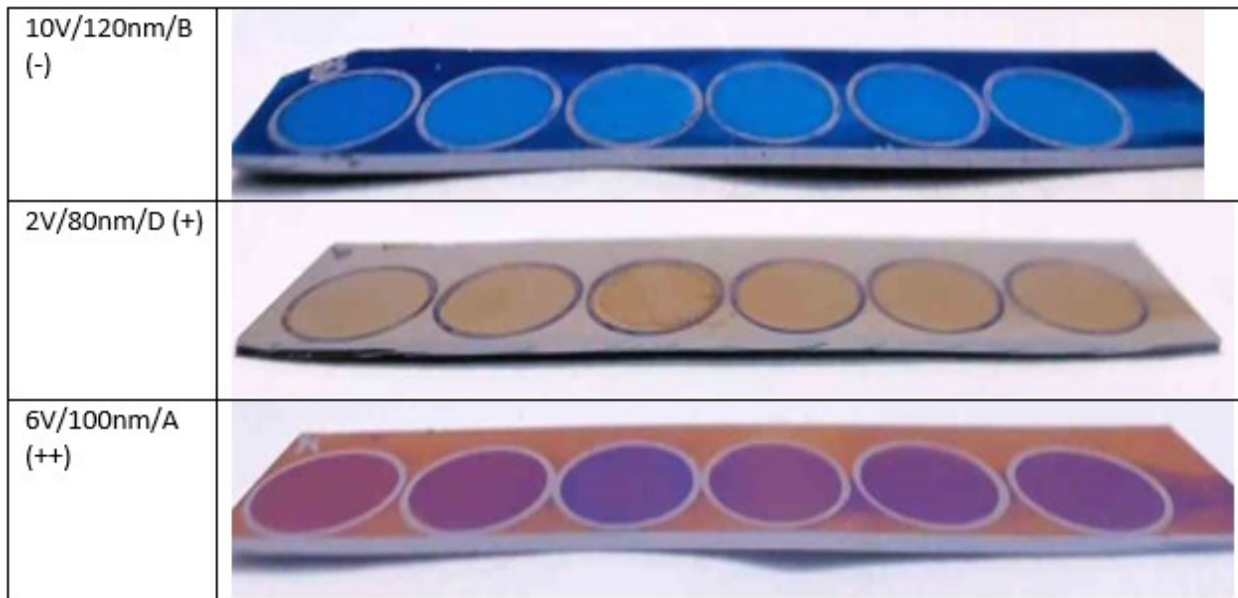


Figure 33. Examples of Voltage/Thickness Combinations and their ratings.

Again, it is important to note that although not visually optimal these colour shifts do provide information. Appropriate camera software installed on a smartphone might be able to evaluate RGB coordinates better than a human eye can observe a colour shift. Ultimately, Figure 34 demonstrates the two combinations that were deemed visually optimal with the naked eye.

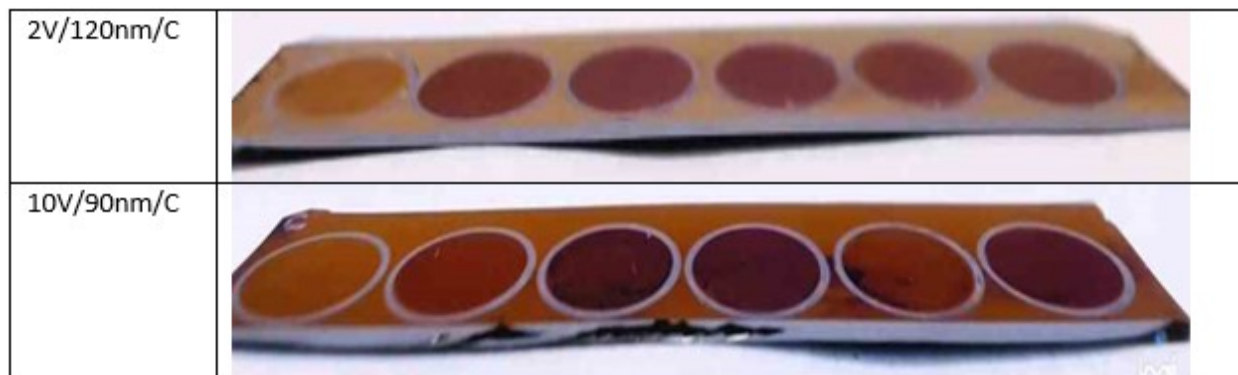


Figure 34. Optimal Combinations of Voltage/Thickness.

The 2V/120nm/C slide demonstrated the best colour shift between spots 1 and 2. Subjectively, the colour goes from a dark amber to dark russet or reddish brown. For a visual POCD, this would be ideal because a positive test would not require an amplification step. Results would be determined in the fastest time possible. The 10V/90nm/C presented the most significant colour shift following the amplification step. The colour shift went from a dark amber in spot 1 to a plum in spot 3. Antiprocalcitonin C, 11643 IgG Hc7.1, seemed to produce the starkest colour shifts from spot 1 to the other spots. Pictures of all other Voltage/Thickness combinations are available in Appendix 1.

### 3.7 Matrix 2: Procalcitonin Sensitivity of Optimal Condition Slides

The visually optimal combinations were then used for matrix 2. Matrix 2, shown in Table 7, tests the sensitivity of each optimal combination by varying the concentrations of PCT.

Table 7. Procalcitonin Sensitivity of Optimal Condition Slides

PCT Sensitivity	Procalcitonin Conc (ng/ml)						
Voltage/Thickness Combination	0	0.1	0.25	0.5	1	10	100
Ex 10V/90nm C							
Ex 2V/120nm C							

The concentrations of PCT will range through clinically significant concentrations—like those used in PCT algorithms found in section 2.2, Fig 5—and orders of magnitude higher. Seven 1cm circles were drawn on a wafer piece of each combination. Enough volume of each concentration was made for each concentration by diluting stock procalcitonin with PBS. 20µl of standard concentration APCTC was applied to spots 2–7 and allowed to sit for 30mins in a humid environment. The APCTC was pipetted off and the wafer segments rinsed and dried. The various concentrations were pipetted onto the appropriate spots and left in a humid environment for 24hours. Following 24hours, PCT was pipetted off and the wafers rinsed and dried. Photos were taken and then full concentration APCTC was applied to spots 2–7 for 1hour. Following the amplification stage, pictures were taken and the wafers were checked for a change in signal.

#### 3.7.1 Results

Photos were taken following a 24hr application of PCT concentrations and prior to the secondary application and are exhibited in Figure 35. A colour change is visible for both wafers at 0.1 ng/ml in spot 2.

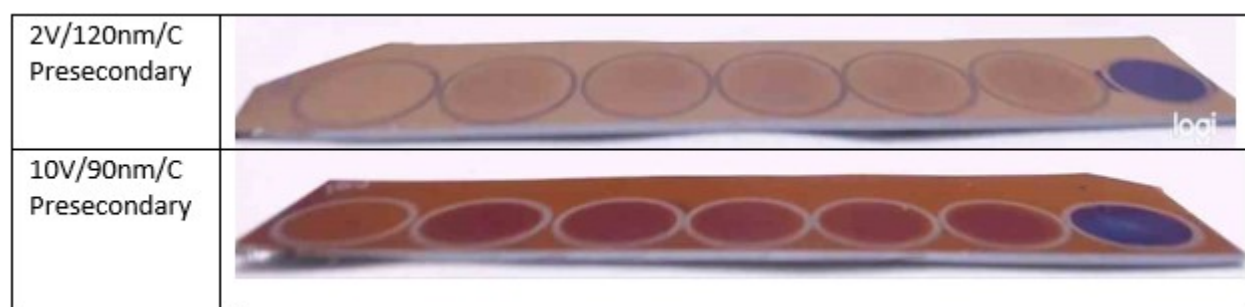


Figure 35. PCT sensitivity assay prior to amplification.

A secondary antibody was applied for 1hr and then the wafers were rinsed and dried. Once dry, photos were taken following the secondary antibody. Figure 36 shows the wafer segments following the amplification step.

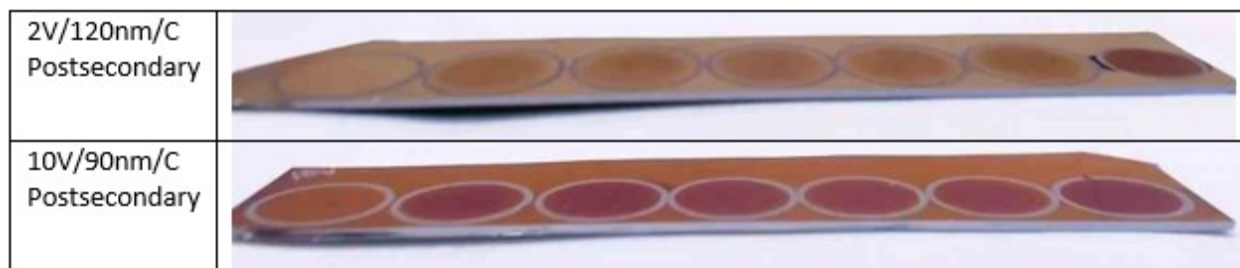


Figure 36. PCT sensitivity assay post amplification.

Again, we see a colour shift even down at 0.1 ng/ml. We can determine that the thin film device is sensitive enough to detect clinically relevant concentrations of procalcitonin in buffer.

### 3.8 Procalcitonin Specificity

An experiment was designed to test the procalcitonin immunocomplex specificity and serve as a negative control. A different protein, in this case, bovine serum albumin would be applied to a slide with antiprocalcitonin on the surface to see if any binding would occur. BSA lacks the proper epitopes to bind to procalcitonin IgG, so a signal is not expected. If a signal could be seen with BSA, then the PCT immunocomplex would not be specific and therefore not ideal for the determination of bacterial infection.

A slide was chosen with one of the optimal combinations. A 2V/120nm wafer piece with APCTC as the surface protein was prepared and 5 1cm circles drawn on the surface. Table 8 has the slide's spot breakdown. Spots 2—5 had 20µl of APCTC applied to the circle for 30mins in a humid environment. The procalcitonin IgG was pipetted off and the wafer was rinsed and dried. The standard procalcitonin concentration used in the lab is 0.39mg/ml, so a BSA solution of equal concentration was prepared in buffer. 20µl of procalcitonin was applied to spots 2 and 3, while 20µl of BSA was applied to spots 4 and 5. Following 30mins in a humid environment, both proteins were removed and the wafer rinsed and dried. Lastly, a 20µl secondary application of APCTC was applied to spots 3 and 5 for 30mins in a humid environment. This amplification step is used to see if signal could be improved.

Table 8. PCT Immunocomplex specificity spot breakdown

2V/120nm APCTC	Step1	Step 2	Step 3
Spot 1	Blank	Blank	Blank
Spot 2	APCTC	APCTC + PCT	APCTC + PCT
Spot 3	APCTC	APCTC + PCT	APCTC + PCT + APCTC

Spot 4	APCTC	APCTC + BSA	APCTC + BSA
Spot 5	APCTC	APCTC + BSA	APCTC + BSA + APCTC

### 3.8.1 Results

Figure 37 shows the slide used to test the procalcitonin immunocomplex specificity. Spot 2 shows the strongest signal. The amplification of spot 3 seems to weaken the signal, possibly because the OPL is changed by the added film thickness pushing the colour into the second order.



Figure 37. 2V/120nm APCTC slide used to test PCT immunocomplex specificity.

No signal can be seen in spots 4 and 5 indicating that no BSA bound to the surface. This would confirm the procalcitonin immunocomplex specificity in buffer.

## Chapter 4 ProvLab

### 4.1 Blinded Validation of Optimal Conditions

Having determined optimal Voltage/Thickness combinations along with procalcitonin's sensitivity and specificity, the next step was to test the same parameters with blood samples from Alberta Health Services Public Health Laboratory (ProvLab). An experiment was designed to test varying concentrations of procalcitonin-spiked blood and then be read by an independent viewer to observe and record any colour shifts.

Ethylenediaminetetraacetic acid (EDTA) is an additive used to collect anticoagulated blood samples. EDTA is a chemical that binds and holds on to (chelates) minerals and metals. For blood collection, EDTA binds to calcium and prevents the coagulation cascade<sup>58</sup>. 5ml of anticoagulated blood was collected for the assay and prepared two ways: normal anticoagulated blood and procalcitonin-spiked blood. Four different concentrations of procalcitonin were chosen: 0.1mg/ml; 0.1µg/ml; 20ng/ml; and 0.5ng/ml and would be tested on the two optimal slide combinations. Each concentration and Voltage/Thickness would be tested in triplicate see Figure 34. Each wafer piece would be prepared with

two 1cm circles drawn on them and 20µl of APCTC applied for 30mins. A randomizer was used to decide which circle, left or right, would receive the PCT-spiked blood while the other circle would receive the regular blood. This is illustrated in Figure 38.

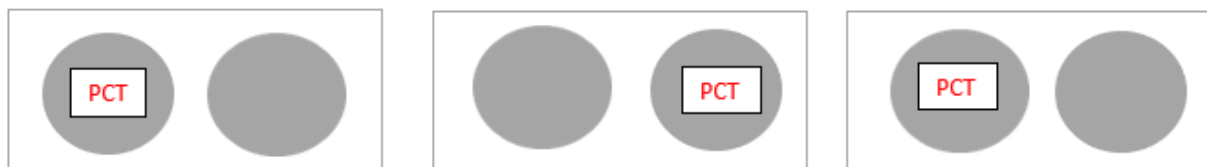


Figure 38. An example of the randomized series for a Voltage/Thickness combination Ex: 2V/120nm/C and 0.5ng/ml.

Figures 39 and 40 illustrate the total assay and PCT-spiked locations for the 2V/120nm/C and 10V/90nm/C combinations, respectively.

2V/120nm/C	PCT Concentration									
Solution A	0.1mg/ml	A		*	B		*	C		*
Solution B	0.1µg/ml	D	*		E	*		F	*	
Solution C	20ng/ml	G		*	H	*		I	*	
Solution D	0.5ng/ml	J	*		K		*	L	*	

Figure 39. Randomized PCT-spiked blood for 2V/120nm/C. \* denotes PCT-spiked sample.

10V/90nm/C	PCT Concentration									
Solution A	0.1mg/ml	M		*	N	*		O		*
Solution B	0.1µg/ml	P		*	Q		*	R		*
Solution C	20ng/ml	S	*		T		*	U	*	
Solution D	0.5ng/ml	V	*		W	*		X		*

Figure 40. Randomized PCT-spiked blood for 10V/90nm/C. \* denotes PCT-spiked sample.

Blood was applied to the surface for 30mins rinsed off and the wafer pieces dried. An amplification step would be carried out on all the circles that received the PCT-spiked blood.

#### 4.1.1 Results

Blood is full of clotting proteins that make it very sticky and ready to clot. It was hoped that by collecting the blood in EDTA, the stickiness would be minimized. No clear signal was generated by any of the blood samples. Despite vigorous rinsing with deionized water, there was too much non-specific binding

to the surface. Figure 41 illustrates the non-specific binding that makes seeing a colour change due to a procalcitonin immunocomplex impossible.

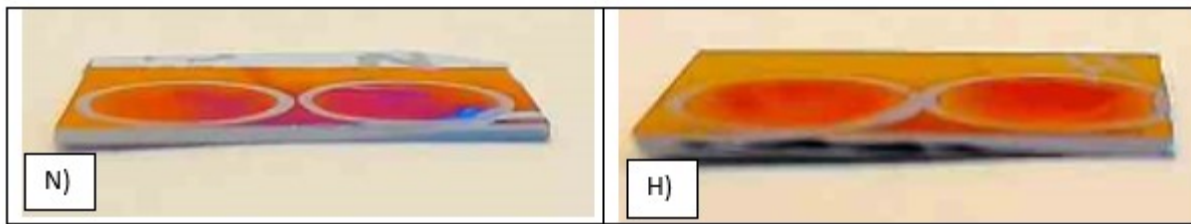


Figure 41. Non-specific binding onto two different wafer combination surfaces.

Photos were taken of all wafer segments, but the independent observation and sample collection from ProvLabs was abandoned due to the difficulty of recognizing a procalcitonin colour shift due to the non-specific binding properties of blood.

## Chapter 5 Device Manufacturing

### 5.1 Procalcitonin Point of Care Device Benefits

Point of care testing (POCT) enables rapid clinical decision-making, confirmation of bacterial infection, treatment choice, monitoring and evaluating the conclusion of infection. Point-of-care devices improve specimen stability. Unprocessed samples can be used to deliver accurate results without the need for centrifugation. Additionally, the volume of blood drawn is similar to a blood sugar test (~20µl) rather than a typical blood vial which generally holds between 3 to 10ml. A portable procalcitonin point-of-care device (POCD) may also promote positive antimicrobial stewardship through tailored therapy—not just type, but duration. A full course of antibiotics might not be necessary, provided a 2<sup>nd</sup> procalcitonin test showed no further infection.

### 5.2 Device Requirements

The WHO's ASSURED (Affordable, Sensitive, Specific, User-friendly, Rapid and robust, Equipment-free, and Deliverable) criteria was used as a framework in the development of the procalcitonin diagnostic. A procalcitonin kit was developed to help guide a physician's or pharmacist's decision making. The kit has the capacity to collect blood, apply it to an APCT-treated substrate and a white reflective background for observation. The kit is stackable and robust and could be stored in a cabinet.

The kit includes: a 23-gauge lancet for pricking a finger; an EDTA collection tube and small strip of treated wafer. EDTA is an anticoagulant that makes for easier blood application to the test piece. All

materials are contained in a 3D printed box whose lid also serves as part of the reader. The kit is shown in Figure 42.

The estimated cost to build the kit in its current iteration is approximately \$10. The lancet and collection tube were sourced for \$0.20 and \$1.35, respectively. Jacob Damant and Khally Bhan, summer student designers of the 3D box, estimated that \$2 worth of polylactic acid was used in its printing. The box's dimensions are 9cm (l) x 6cm (w) x 2.5cm (h). The reader's testing area measures 1.5cm x 5.3cm—although the wafer piece can be much smaller than that. The estimated cost of small wafer piece, sputtered and anodized, is \$3 while a small 1cm treated with ~20 $\mu$ l of APCT is estimated to cost another \$3. Naturally, price could come down with purchasing in bulk and molded plastic instead of 3Dprinting.

Comparatively, I asked three different healthcare providers—a urologist, an endocrine surgeon and an obstetrician—how much a procalcitonin test and phlebotomy would cost in a hospital setting and their estimates averaged out to \$91.67. Efforts were made to determine the cost on Alberta Health Care Insurance Plan's Schedule of Fees, but could not be found.

### 5.3 Device Design

The design of the device was meant to house everything necessary to complete the test while also being portable and deliverable to the end user. The kit is designed as a box with a tight-fitting lid. The top side of the lid has a thin channel that can rest securely on the side of the box. The underside of the box has a flat surface that the APCT treated wafer segment will be affixed to as shown by the X in Figure 42. Immediately behind the wafer strip is a white reflective surface angled at 15° towards the user. This white background eliminates signal noise and improves the readability of the diagnostic. The box has three designed holders. One holder for a lancet, one for the collection tube and a third hole for the collection tube to be held vertically after opening the lid. This kit would come with two options. A base model as described above and a second option that would include a small polarizing film sheet and a small aliquot of APCT for secondary amplification.

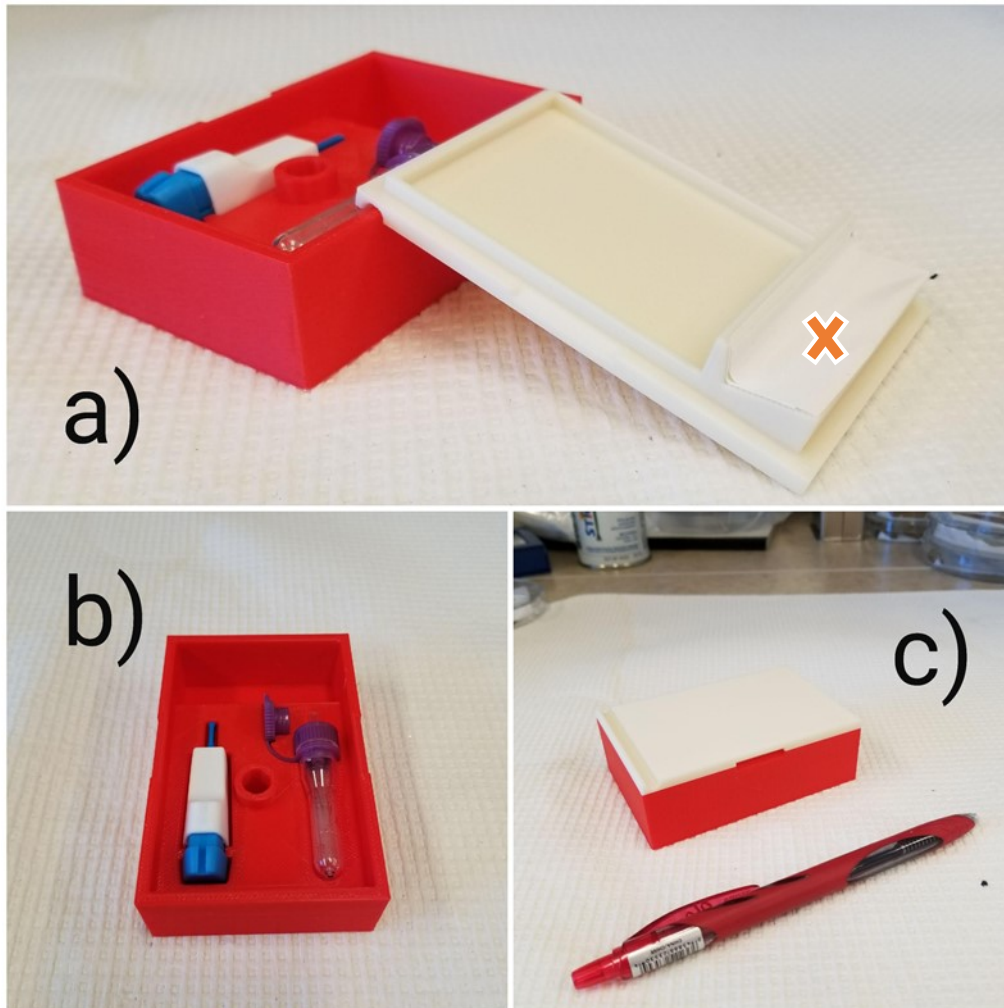


Figure 42. The 3D printed PCT blood testing kit. A) The lid removed and placed on box edge. The X denotes the testing area. B) The interior of the box with compartments for a 23-gauge lancet, an EDTA blood collection tube and a collection tube holder. C) The size of the box in relation to a pen.

The easy-to-use, robust kit can be easily delivered to a physician’s office or pharmacist. They are the gatekeepers of antibiotic therapies. By aiding them to differentiate between viral and bacterial infections at the point of care, improved patient outcomes and improved antimicrobial stewardship follow. The kit can be used in lieu of expensive, bulky benchtop analyzers or centralized lab tests at a fraction of the cost.

## Chapter 6 Conclusions

This work has expanded the knowledge of thin film diagnostics based on anodized aluminum-tantalum films and how they might be used as a procalcitonin point of care diagnostic to improve patient outcome and promote antimicrobial stewardship. The following is a list of key conclusions resulting from this study:

- 1) Optimal Voltage/Thickness combinations were established based on the colour shift generated by the difference in optical path length of the procalcitonin immunocomplex and type of antibody used. These were 2V/120nm/C for unamplified samples and 10V/90nm/C for samples that required a secondary antibody.
- 2) Clinically relevant sensitivities were achieved using the optimal Voltage/Thickness combinations.
- 3) Antibody C, 11643 IgG Hc 7.1, proved to be the ideal antibody applied to the surface. Although similar in design to two of the other three antibodies, it produced the most striking colour shifts compared to the other three.
- 4) A prototype procalcitonin kit was developed that could be delivered to point of care end users to improve patient outcomes and antimicrobial stewardship.
- 5) Procalcitonin-spiked blood samples do not generate clear signals due to non-specific binding at the thin film surface.

## 6.1 Future Directions

Future work on the diagnostic can be divided into two main foci, 1) materials and 2) improved protein testing. Further anodization and tuning of the thin film device would be recommended. Matrix 1 increased voltages by a step of 2V and aluminum oxide thicknesses by 10nm. Smaller increments of each parameter around the optimal condition might produce better colour shifts due to small changes in optical path length. Similarly, the procalcitonin kit design and materials could be improved and cost reduced.

Finding a solution to the problem of non-specific binding at the surface of the device is paramount. In buffer, colour shifts generated by the procalcitonin immunocomplex can be visualized, but blood samples cause non-specific binding that makes viewing procalcitonin detection near impossible. Studies could be performed with serum instead of blood to see if that improves signal. Likewise, a series of washing steps with a 3% hypertonic sodium chloride solution might remove unwanted proteins adsorbed to the surface and could improve the procalcitonin signal. These future works should be addressed so that the procalcitonin kit can be commercialized and sent to end users.

Lastly, it was mentioned that there was value to be gleaned from tests that were not visually optimal. Development of smartphone camera software could be used to measure RGB coordinates which could give the end user quantified data used in diagnosis.

## References

1. Kosack CS, Page AL, Klatser PR. A guide to aid the selection of diagnostic tests. *Bull World Health Organ.* 2017;95(9):639-645. doi:10.2471/BLT.16.187468
2. Koczula KM, Gallotta A. Lateral flow assays. *Essays Biochem.* 2016;60(1):111-120. doi:10.1042/EBC20150012
3. About Antibiotic Resistance | Antibiotic/Antimicrobial Resistance | CDC. <https://www.cdc.gov/drugresistance/about.html>. Accessed March 11, 2020.
4. *TACKLING DRUG-RESISTANT INFECTIONS GLOBALLY: FINAL REPORT AND RECOMMENDATIONS THE REVIEW ON ANTIMICROBIAL RESISTANCE CHAIRED BY JIM O'NEILL.*; 2016.
5. Ventola CL. The Antibiotic Resistance: part 1: causes and threats. *P T.* 2015;40(4):277-283. <http://www.ncbi.nlm.nih.gov/pubmed/25859123>. Accessed September 5, 2019.
6. No Title. <https://www.nobelprize.org/uploads/2018/06/fleming-lecture.pdf>. Published 2018. Accessed April 1, 2021.
7. Singer RS, Finch R, Wegener HC, Bywater R, Walters J, Lipsitch M. Antibiotic resistance--the interplay between antibiotic use in animals and human beings. *Lancet Infect Dis.* 2003;3(1):47-51. <http://www.ncbi.nlm.nih.gov/pubmed/12505035>. Accessed September 3, 2019.
8. Pardo J, Klinker KP, Borgert SJ, Trikha G, Rand KH, Ramphal R. Time to positivity of blood cultures supports antibiotic de-escalation at 48 hours. *Ann Pharmacother.* 2014;48(1):33-40. doi:10.1177/1060028013511229
9. Imanpour S, Nwaiwu O, McMaughan DK, DeSalvo B, Bashir A. Factors associated with antibiotic prescriptions for the viral origin diseases in office-based practices, 2006-2012. doi:10.1177/2054270417717668
10. Fontela PS, O'Donnell S, Papenburg J. Can biomarkers improve the rational use of antibiotics? *Curr Opin Infect Dis.* 2018;31(4):347-352. doi:10.1097/QCO.0000000000000467
11. Jin M, Khan AI. Procalcitonin: Uses in the Clinical Laboratory for the Diagnosis of Sepsis. *Lab Med.* 2010;41(3):173-177. doi:10.1309/lmq2grr4qlfkch9
12. Riedel S, Melendez JH, An AT, Rosenbaum JE, Zenilman JM. Procalcitonin as a marker for the detection of bacteremia and sepsis in the emergency department. *Am J Clin Pathol.* 2011;135(2):182-189. doi:10.1309/AJCP1MFYINQLECV2
13. Thompson D, Pepys MB, Wood SP. The physiological structure of human C-reactive protein and its complex with phosphocholine. *Structure.* 1999;7(2):169-177. doi:10.1016/S0969-2126(99)80023-9
14. Nakamura A, Wada H, Ikejiri M, et al. EFFICACY OF PROCALCITONIN IN THE EARLY DIAGNOSIS OF BACTERIAL INFECTIONS IN A CRITICAL CARE UNIT. *Shock.* 2009;31(6):587-592. doi:10.1097/SHK.0b013e31819716fa

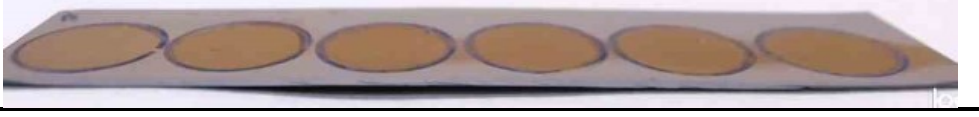
15. Meisner M. *Procalcitonin Biochemistry and Clinical Diagnosis*. UNI-MED-Verl; 2010.
16. Covington EW, Roberts MZ, Dong J. Procalcitonin Monitoring as a Guide for Antimicrobial Therapy: A Review of Current Literature. *Pharmacotherapy*. 2018;38(5):569-581. doi:10.1002/phar.2112
17. Maruna P, Nedelníková K, Gürlich R. Physiology and genetics of procalcitonin. *Physiol Res*. 2000;49 Suppl 1:S57-61. <http://www.ncbi.nlm.nih.gov/pubmed/10984072>. Accessed September 12, 2019.
18. Corti C, Fally M, Fabricius-Bjerre A, et al. Point-of-care procalcitonin test to reduce antibiotic exposure in patients hospitalized with acute exacerbation of COPD. *Int J COPD*. 2016;11(1):1381-1389. doi:10.2147/COPD.S104051
19. Shaddock EJ. How and when to use common biomarkers in community-acquired pneumonia. *Pneumonia*. 2016;8(1). doi:10.1186/s41479-016-0017-7
20. (No Title). <https://www.unmc.edu/intmed/divisions/id/asp/news/docs/procalcitonin-guidance.pdf>. Accessed April 1, 2021.
21. Vashist SK, Luppá PB, Yeo LY, Ozcan A, Luong JHT. Emerging Technologies for Next-Generation Point-of-Care Testing. *Trends Biotechnol*. 2015;33(11):692-705. doi:10.1016/j.tibtech.2015.09.001
22. Thin Film Reflection and Interference. <http://hyperphysics.phy-astr.gsu.edu/hbase/phyopt/oilfilm.html>. Accessed April 1, 2021.
23. Silva RA, Silva IP, Rondot B. Effect of surface treatments on anodic oxide film growth and electrochemical properties of tantalum used for biomedical applications. *J Biomater Appl*. 2006;21(1):93-103. doi:10.1177/0885328206056378
24. Wu CT, Ko FH, Hwang HY. Self-aligned tantalum oxide nanodot arrays through anodic alumina template. *Microelectron Eng*. 2006;83(4-9 SPEC. ISS.):1567-1570. doi:10.1016/j.mee.2006.01.092
25. Rodríguez-de Marcos L V., Larruquert JI, Méndez JA, Aznárez JA. Self-consistent optical constants of SiO<sub>2</sub> and Ta<sub>2</sub>O<sub>5</sub> films. *Opt Mater Express*. 2016;6(11):3622. doi:10.1364/ome.6.003622
26. Metallic Reflection - Engineering LibreTexts. [https://eng.libretexts.org/Bookshelves/Materials\\_Science/Supplemental\\_Modules\\_\(Materials\\_Science\)/Optical\\_Properties/Metallic\\_Reflection](https://eng.libretexts.org/Bookshelves/Materials_Science/Supplemental_Modules_(Materials_Science)/Optical_Properties/Metallic_Reflection). Accessed March 28, 2021.
27. Polling JJ, Charlesby A. The influence of anodic oxide films on the thermal oxidation of zirconium. *Acta Metall*. 1954;2(5):667-674. doi:10.1016/0001-6160(54)90113-3
28. Smith DJ, Young L. Comparison of spectrophotometric and ellipsometric methods of measuring the thickness of anodic oxide films on tantalum. *Thin Solid Films*. 1983;101(1):11-19. doi:10.1016/0040-6090(83)90489-3
29. Gaul E. Coloring titanium and related metals by electrochemical oxidation. *J Chem Educ*. 1993;70(3):176. doi:10.1021/ed070p176
30. Sheng CC, Cai YY, Dai EM, Liang CH. Tunable structural color of anodic tantalum oxide films. *Chinese Phys B*. 2012;21(8). doi:10.1088/1674-1056/21/8/088101
31. Knittl Z. *Optics of Thin Films; An Optical Multilayer Theory*. Wiley; 1976.

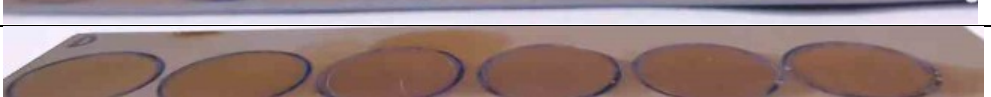
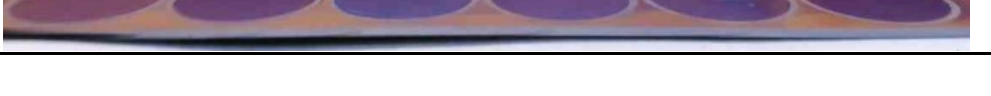
32. Puri P, Yang V. Effect of particle size on melting of aluminum at nano scales. *J Phys Chem C*. 2007;111(32):11776-11783. doi:10.1021/jp0724774
33. Vera-Londono L, Ruiz-Clavijo A, Caballero-Calero O, Martín-González M. Understanding the thermal conductivity variations in nanoporous anodic aluminum oxide. *Nanoscale Adv*. 2020;2(10):4591-4603. doi:10.1039/d0na00578a
34. Aluminum facts. <https://www.nrcan.gc.ca/our-natural-resources/minerals-mining/minerals-metals-facts/aluminum-facts/20510>. Accessed April 1, 2021.
35. Lee W, Park SJ. Porous anodic aluminum oxide: Anodization and templated synthesis of functional nanostructures. *Chem Rev*. 2014;114(15):7487-7556. doi:10.1021/cr500002z
36. Sheasby PG, Pinner R, Pdf RP. *THE SURFACE TREATMENT AND FINISHING OF ALUMINUM AND ITS ALLOYS (VOLUME 1) (V. 1 AND 2) BY DOWNLOAD EBOOK : THE SURFACE TREATMENT AND FINISHING OF ALUMINUM AND ITS ALLOYS (VOLUME 1) (V. 1 AND 2) BY*.
37. Nickel MR. Physical and Optical Characterization of Anodized Aluminum-Tantalum Thin Films for use in Thin Film Diagnostics. 2018. doi:10.7939/R30PoX670
38. Thin-film interference - Wikipedia. [https://en.wikipedia.org/wiki/Thin-film\\_interference](https://en.wikipedia.org/wiki/Thin-film_interference). Accessed April 1, 2021.
39. Index of Refraction. <http://hyperphysics.phy-astr.gsu.edu/hbase/Tables/indrf.html>. Accessed April 1, 2021.
40. Procalcitonin Escherichia coli, Sigma-Aldrich. <https://www.sigmaaldrich.com/catalog/product/sigma/srp6003?lang=en&region=CA>. Accessed April 1, 2021.
41. Burrell RE, Naylor AG, Rosenfeld AM, Ontario K. *United States Patent to Date of Patent: 54) THIN FILM DIAGNOSTIC DEVICE*. Vol 124.
42. Sandström T, Stenberg M, Nygren H. Visual detection of organic monomolecular films by interference colors. *Appl Opt*. 1985;24(4):472. doi:10.1364/ao.24.000472
43. Why Is Asbestos Fibrous. [http://academic.brooklyn.cuny.edu/geology/powell/core\\_asbestos/analyze/interfer/interfer\\_to\\_ol.htm](http://academic.brooklyn.cuny.edu/geology/powell/core_asbestos/analyze/interfer/interfer_to_ol.htm). Accessed June 7, 2020.
44. A Beginner's Guide to (CIE) Colorimetry - Color and Imaging - Medium. <https://medium.com/hipster-color-science/a-beginners-guide-to-colorimetry-401f1830b65a>. Accessed June 6, 2020.
45. Chevallier E, Farup I. *Interpolation of the MacAdam Ellipses.*; 2018. <https://hal.archives-ouvertes.fr/hal-01625921v2>. Accessed June 7, 2020.
46. File:CIExy1931 MacAdam.png - Wikimedia Commons. [https://commons.wikimedia.org/wiki/File:CIExy1931\\_MacAdam.png](https://commons.wikimedia.org/wiki/File:CIExy1931_MacAdam.png). Accessed April 1, 2021.
47. Types of Multiple Myeloma | International Myeloma Foundation. <https://www.myeloma.org/types-of-myeloma>. Accessed April 1, 2021.
48. Braden BC, Dall'Acqua W, Eisenstein E, et al. Protein motion and lock and key complementarity in antigen-antibody reactions. *Pharm Acta Helv*. 1995;69(4):225-230. doi:10.1016/0031-6865(94)00046-X

49. Reth M. *Matching Cellular Dimensions with Molecular Sizes.*; 2013. doi:10.1038/ni.2621
50. Sandkovsky U, Kalil AC, Florescu DF. The use and value of procalcitonin in solid organ transplantation. *Clin Transplant.* 2015;29(8):689-696. doi:10.1111/ctr.12568
51. Vidarsson G, Dekkers G, Rispens T. IgG subclasses and allotypes: From structure to effector functions. *Front Immunol.* 2014;5(OCT):520. doi:10.3389/fimmu.2014.00520
52. Sputtering System – AJA ATC Orion 8 | PoliFAB. <https://www.polifab.polimi.it/equipments/orion-8/>. Accessed April 1, 2021.
53. Sweet HM. *Development of a Nanostructured Thin Film Device and Optics System for Protein Detection.*
54. Vörös J. The Density and Refractive Index of Adsorbing Protein Layers. *Biophys J.* 87:553-561. doi:10.1529/biophysj.103.030072
55. Refractive Index of Al<sub>2</sub>O<sub>3</sub> for Thin Film Thickness Measurement. <https://www.filmetrics.com/refractive-index-database/Al2O3>. Accessed April 1, 2021.
56. Rahman MM, Garcia-Caurel E, Santos A, Marsal LF, Pallarès J, Ferré-Borrull J. *Effect of the Anodization Voltage on the Pore-Widening Rate of Nanoporous Anodic Alumina.* Vol 7.; 2012. doi:10.1186/1556-276X-7-474
57. *Dictionary of Pure and Applied Physics.* CRC Press; 2018. doi:10.1201/9781315219608
58. Palta S, Saroa R, Palta A. Overview of the coagulation system. *Indian J Anaesth.* 2014;58(5):515-523. doi:10.4103/0019-5049.144643

## Appendix 1 Pictures

Matrix 1 pictures

2V_80nm	A	
	B	
	C	
	D	
2V_90nm	A	

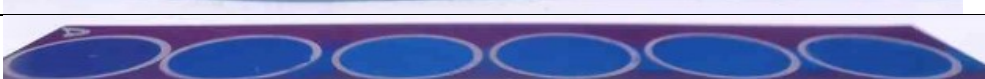
	B	
	C	
	D	
2V_100nm	A	
	B	
	C	
	D	
2V_110nm	A	
	B	
	C	
	D	
2V_120nm	A	
	B	
	C	
	D	
2V_130nm	A	

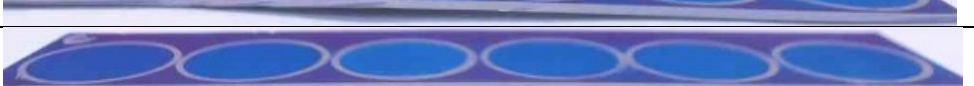
	B	
	C	
	D	

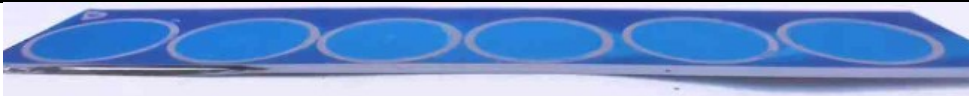
4V_80nm	A	
	B	
	C	
	D	
4V_90nm	A	
	B	
	C	
	D	
4V_100nm	A	
	B	
	C	
	D	
4V_110nm	A	
	B	

	C	
	D	
4V_120nm	A	
	B	
	C	
	D	
4V_130nm	A	
	B	
	C	
	D	

6V_80nm	A	
	B	
	C	
	D	
6V_90nm	A	
	B	
	C	

	D	
6V_100nm	A	
	B	
	C	
	D	
6V_110nm	A	
	B	
	C	
	D	
6V_120nm	A	
	B	
	C	
	D	
6V_130nm	A	
	B	
	C	
	D	
8V_80nm	A	

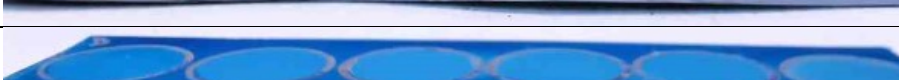
	B	
	C	
	D	
8V_90nm	A	
	B	
	C	
	D	
8V_100nm	A	
	B	
	C	
	D	
8V_110nm	A	
	B	
	C	
	D	
8V_120nm	A	
	B	
	C	

	D	
8V_130nm	A	
	B	
	C	
	D	

10V_80nm	A	
	B	
	C	
	D	

10V_90nm	A	
	B	
	C	
	D	

10V_100nm	A	
	B	
	C	
	D	

10V_110nm	A		
	B		
	C		
	D		
10V_120nm	A		
	B		
	C		
	D		
10V_130nm	A		
	B		
	C		
	D		

## Appendix 2 University of Alberta nanoFAB SOPs

The following three SOPs are from the University of Alberta's nanoFAB. They were accessed April 1, 2021. There were some formatting issues. Copies can be found here:

<https://www.nanofab.ualberta.ca/user-information/centre-access/photomask-information/documentation/>

### Bob Sputtering System SOP

Location: 10K PVD area

Primary Trainer: Les Schowalter (587-879-1516),  
les.schowalter@ualberta.ca) Secondary Trainer:

#### OVERVIEW

August 06 2014

### BOB SPUTTERING TOOL



A planar magnetron sputter system with three sources. The gun/substrate configuration is designed for sequential sputtering. The third source can be used for magnetic materials.

## SAFETY PRECAUTIONS

When using the hoist to close the system take care that your fingers are not between the chamber lid and body. Some materials are not compatible with a vacuum system; if you aren't sure of your material please see the primary trainer.

If you are bringing any new materials into the NanoFab for use in your process, it is necessary to fill out a chemical import form (available on our website, <http://www.nanofab.ualberta.ca>) and supply an MSDS data sheet to Stephanie Bozic.

## OPERATING INSTRUCTIONS

### Opening & Loading

1

1.0 Press “emis” on the multi gauge controller to turn off the ion gauge then press “channel” until TC1 is shown and nothing on the bottom right.

2.0 Turn the Baratron valve clockwise until closed.

3.0 Close the cryopump valve clockwise until closed; there should be a solid click sound when closed. Also note the cryopump temperature, if it's not below 20K please inform nanoFAB staff. 4.0 Flip the chamber vent switch up. When the pressure readout is at 760 Torr the chamber should be at atmosphere and the chamber vent switch must be closed.

5.0 Lift the lever on the back of the chamber lid.

6.0 Press the up button on the hoist and raise the top of the chamber until the substrate holder is clear of the main chamber, and then move the chamber top away.

7.0 Please put gloves on for the next steps.

8.0 Check the inside of the chamber for flaking and other debris; vacuum as required. 9.0 If the glass view port is coated with metal, pull out and replace glass. Please use IPA to clean all six sides of glass before installing.

10.0 Change targets as required, check to see if the proper target is in the chamber or in the correct container. Sputtering the wrong material may set your project back.

11.0 Make sure the dark space shield has adequate spacing. Most targets are ¼” thick and the dark space shield shouldn't be on any notch, Targets such as Au and Pt are thinner and should go onto the smallest notch. Check spacing with the voltmeter, you should have an open circuit.

12.0 Close the shutters. Remove any particles around the main o-ring using a cleanroom wipe and IPA. 13.0 Load your substrate(s) and move the top over the chamber; move the lever down and press the lower button on the hoist. Make sure you hold onto the top section as it wants to move to the right. When the top meets the chamber stop pressing the lower button, it can't lower any further!

### Pump down

1.0 Open the chamber roughing valve about one full turn and observe if the chamber pressure is dropping. If

the pressure doesn't change, check to see if the lid is properly seated onto the chamber. If pressure still doesn't drop close roughing valve and find nanoFAB staff to look into the issue.

2.0 Rough to about 350 Torr then open the roughing valve all the way then close about a half turn. Rough out to  $3.0 \times 10^{-1}$  (about five minutes depending on which roughing pump is used.) then close roughing valve. 3.0 Slowly open the cryo valve all the way by turning counterclockwise.

4.0 Open the Baratron valve by turning it counterclockwise.

5.0: Press "**channel**" on the multi gauge controller until BA1 is shown in the lower right of the display, then press "**emis**".

6.0 Pumpdown takes about one hour to reach the low -6 Torr.

7.0 Write your deposition parameters in the logbook, and put the sputter system in use sign up.

## Deposition

### 2

1. Press "**emis**" on the multi gauge to turn off the filament, then press "**channel**" until aux1 is shown in the lower section of the display.

2.0 Pull and lift the power switch on the MKS controller, then lift switch 1 for Ar gas, close the cryo gate valve about four turns until the Multi gauge controller reads  $7 \times 10^{-3}$  Torr.

3.0 Put target selector switch to the desired target. Switch on the power on the back of the MDX 500 power supply; adjust the power setting required for the material you are depositing. Remember the power supply should only be used in power mode.

4.0 Set substrate rotation to the desired speed, three to four is normal. Press the rotation switch. 5.0 Set a timer for the deposition time plus preconditioning. Target conditioning is usually three minutes except for Pt and Au which is one minute.

6.0 Press start on the power supply to condition the target. Look in the chamber to make sure the shutter is closed.

7.0 After the target conditioning step is over gently open the shutter and deposit for the desired time. Remember to write the voltage in the logbook. Press stop on the power supply when the desired time is reached.

8.0 Close the shutter and repeat steps three to six if another metal is required.

9.0 After the deposition is completed, turn off MDX 500 power supply (switch at the back).

10.0 Stop substrate rotation.

11.0 Turn target selector switch to off.

12.0 Turn off Argon switch, and MKS master power.

13.0 Press "**channel**" on the multi gauge controller until TC1 is shown and nothing else in the lower right

section of the display.

14.0 Close the Baratron valve.

15.0 Close the cryo gate valve.

16.0 Flick the chamber vent switch to put a few Torr of N<sub>2</sub> in the chamber then wait five minutes before venting.

17.0 After venting, open chamber using the same instructions as opening and loading starting at step #5. Put gloves on after moving the chamber top, remove substrate(s) and inspect chamber for flaking. If flaking is discovered please vacuum.

18.0 If you used a Pt target, please remove it from the system.

19.0 Follow steps from pumpdown section. Please note that you don't have to start with slow pump down.

## TROUBLESHOOTING

If you can't get a plasma do the following:

Close the cryo gate valve to the point of causing resistance.

Change power setting to 50 watts.

If you still can't get a plasma find the trainer for the tool or other **nanOFAB** staff to look into the issue.

3

If you encounter an unexpected error or require assistance please contact the primary or secondary trainer listed above. Should they not be available, please contact any staff member for assistance.

## APPROVAL

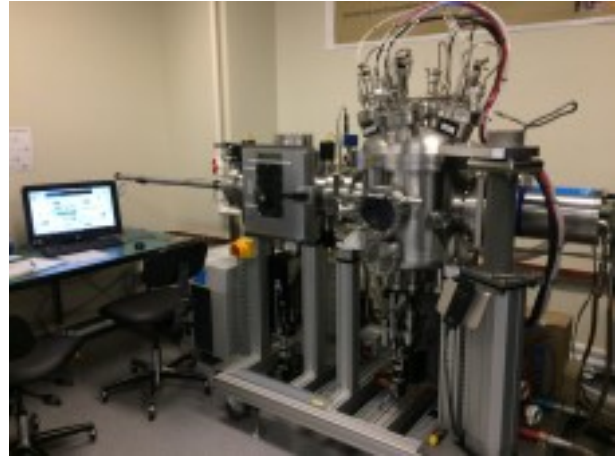
Qualified Trainer: Les Schowalter

Training Coordinator: Stephanie Bozic

## Floyd Sputtering System SOP

W1-60 ECERF Building Edmonton, AB, CANADA T6G 2V4

p: 780.492.0167 [www.nanofab.ualberta.ca](http://www.nanofab.ualberta.ca)



### **Sputtering System #3 (Floyd) 2016-11-11**

**Location:** 10k Deposition Area

**Primary Trainer:** Les Schowalter

587.879.1516

[les.schowalter@ualberta.ca](mailto:les.schowalter@ualberta.ca)

### **OVERVIEW**

**Secondary Trainer:** Aaron Hryciw

780.940.7938

[ahryciw@ualberta.ca](mailto:ahryciw@ualberta.ca)

Sputtering System #3 (Floyd) is an automated planar DC magnetron sputtering system with four sputter guns. The system load lock contains six shelves, each of which can accommodate substrates from small pieces up to 150 mm diameter wafers, in a sputter-down configuration. The transfer of shelves to/from the process chamber, as well as the deposition itself, is computer controlled. The system is also equipped with a power supply for RF etchback, primarily used for resist descum prior to deposition for lift-off.

## **SAFETY PRECAUTIONS**

Do not put any pressure on the load lock door: this can put it out of alignment, compromising the load lock chamber vacuum.

Before bringing any new materials into the nanoFAB for processing, it is necessary to fill out a new chemical import request on LMACS.

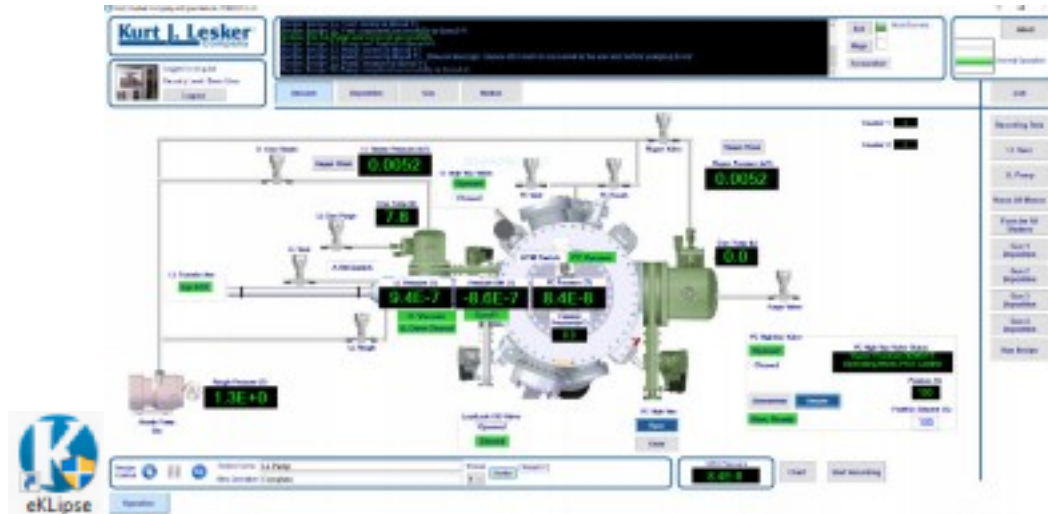
1 of 4 *An environment designed for success*

W1-60 ECERF Building Edmonton, AB, CANADA T6G 2V4

p: 780.492.0167 [www.nanofab.ualberta.ca](http://www.nanofab.ualberta.ca)

## **OPERATING PROCEDURE**

1. On LMACS, login to tool *Sputtering System #3 (Floyd)*; Location: *10k Deposition Area*.
2. The system control



software, eKlipse, should be running. If not, start it by clicking the eKlipse icon on the desktop.

3. Login to eKlipse: click the **Login** button in the upper-left corner and enter your username and password. All users receive their own unique login information once signed off on Floyd.
4. Click **LL Vent** on the right side of the screen. Wait for venting to finish: the Recipe Name field of the *RecipeMonitor* window should read **LL Vent Recipe Complete**, and the load lock atmosphere indicator should be green: **ATM Switch**.
5. Open the load lock door and load your specimens.
  - If you only require one shelf, place specimen(s) on the top shelf (Shelf 6); in this case, it is not necessary to remove the shelf or shelf stack from the load lock.
  - If you require more than one shelf, remove the six-shelf stack and place it on a cleanroom wipe on the table. Load each individual shelf with your samples. It is important that the top shelf has notches cut out of the left and right sides, and that all shelves have their flat edges aligned to the right side of the stack (see following image). Ensure each shelf is securely seated on its three pins: failure to do this will cause a loading failure and possible damage to the loading arm. Return the six-shelf stack to the load lock, fitting it

securely to the three pins in the load lock.

**N.B.** Ensure that the shelf stack is full (i.e., has six shelves loaded) and that the top shelf has the appropriate notches before continuing.

2 of 4 *An environment designed for success*

W1-60 ECERF Building Edmonton, AB, CANADA T6G 2V4

p: 780.492.0167 [www.nanofab.ualberta.ca](http://www.nanofab.ualberta.ca)

Notches in  
top shelf

Shelf stack  
alignment  
pins

Shelf flats aligned  
along this edge  
of stack

Shelf  
alignment  
pins

Divots for pins  
in shelf stack  
(on shelf bottom)

Shelf  
flat

6. Click **LL Pump**. Do not load any shelves into the process chamber until the load lock pressure drops below  $5 \times 10^{-6}$  Torr; this may be a few minutes after the recipe completes.
7. While waiting for the load lock to pump down, exercise the gun shutters: click **Exercise All Shutters**. It is recommended to do this twice to ensure all shutters open and close smoothly.
8. Load the desired shelf into the process chamber: click **Run Recipe** to open the *RecipeSelector* window, and select the appropriate "S[N] to PC" recipe, where [N] is the number of the shelf you wish to load. Remember that the shelves are numbered from 6 to 1, top to bottom. Click the **Run Recipe** button in the *RecipeSelector* window to start the shelf transfer.
9. After the shelf load recipe is finished, you may run a deposition or RF etchback process. To deposit a film, click the appropriate **Gun [N] Deposition**, where [N] is the gun containing the material you wish to deposit (e.g., **Gun 4 Deposition** to deposit Al); the current gun configuration is posted on the wall above the computer monitor. In the resulting *Parameter Passing Recipe* window, adjust the parameters in the *Value* column as required. The default parameters usually do not need to be changed, except for deposition time and possibly burn-in time. The default burn-in time of 30 s is generally sufficient unless a lot of material (different from the material you wish to sputter) has

3 of 4 *An environment designed for success*

W1-60 ECERF Building Edmonton, AB, CANADA T6G 2V4

p: 780.492.0167 [www.nanofab.ualberta.ca](http://www.nanofab.ualberta.ca)

been deposited immediately before (consult the logbook to verify); in this case, a burn-in time of 60 s is recommended. Next, enter your required deposition time in seconds; a table of deposition rates for different materials and powers is posted on the power supply rack. Click **Continue Load**.

**N.B.** It is also possible to run process recipes by clicking the **Run Recipe** button and choosing from the list in the *RecipeSelector* window. The four **Gun [N] Deposition** recipes can be run this way, as well as **Cr/Au Deposition** (a shortcut to deposit two common films back to back) and **RF Etchback**.

10. After the recipe is complete, repeat Step 9 to perform further deposition/etchback processes on the loaded shelf, if required.
11. Unload the shelf from the process chamber: click **Run Recipe** to open the *RecipeSelector* window, and select the appropriate "PC to S[N]" recipe. Click the **Run Recipe** button in the *RecipeSelector* window to start the shelf transfer back to the load lock.
12. After the shelf unload recipe is complete, repeat Steps 8–11 to process additional shelves, if required.
13. Vent the load lock by clicking the **LL Vent** button.
14. When the recipe is complete you can safely open the door and remove the shelf stack and/or

remove your specimens from the shelves. Return all shelves to the shelf stack (ensuring that each one is properly seated on its three pins in the shelf stack), and return the shelf stack to the load lock (properly seated on the three load lock pins).

15. Click **LL Pump**.

16. Logout from eKlipse: click the **Logout** button in the upper-left corner.

17. Logout from tool *Sputtering System #3 (Floyd)*; on LMACS.

## **TROUBLESHOOTING**

If there are any problems or questions regarding use of the tool, do not hesitate to contact the primary or secondary trainers.

## **APPROVAL**

**Qualified Trainer:** Les Schowalter

**Fabrication Group Manager:** Aaron Hryciw

### **Version history**

Les Schowalter, 2016-11-08 (*Floyd SOP.docx*)

4 of 4 *An environment designed for success*



### Rigaku Ultima IV XRD 2021-03-22

- 2 **Location:** Characterization Lab, ECERF W1-040A
- 3 **Primary Trainer:** Nancy Zhang **Secondary Trainer:**
- 4 780.289.1707
- 5 [nzhang@ualberta.ca](mailto:nzhang@ualberta.ca)

### 6 **OVERVIEW**

7 X-ray diffractometer is a technique primarily used for phase ID of a crystalline material, as well as phase composition. This tool comes with 3 sample stages, thin film (surface of sample), standard (for powder/bulk sample) and ASC-10 (powder samples only). For powder samples, particle size should be small (<1  $\mu\text{m}$  if possible). There are different scan axes, e.g. theta/2theta, 2theta, Theta, 2theta/Chi/phi, or phi scan depending on different applications.

### 8 **SAFETY CONSIDERATIONS**

9 Normal laboratory practices apply. Radiation certificate is renewed every 2 years. There is an interlock on the chamber door for x-ray. X-ray radiation is well shielded within the instrument chamber. **OPERATING INSTRUCTIONS**

11  
12

1. The system is interlocked with LMACS: ensure you login to *Rigaku XRD* before operation.

13

2. **Check X-ray condition before use the tool:**

40 kV/44 mA	Operational Steps 4 (standard stage), 5 (ASC-10), 6 (multi purpose)
20 kV/2 mA	Standby Step 3.4
0 kV/0 mA	OFF Step 3

14

15

16

3. **Power up/Warming up the X-Ray (everyday)**

17

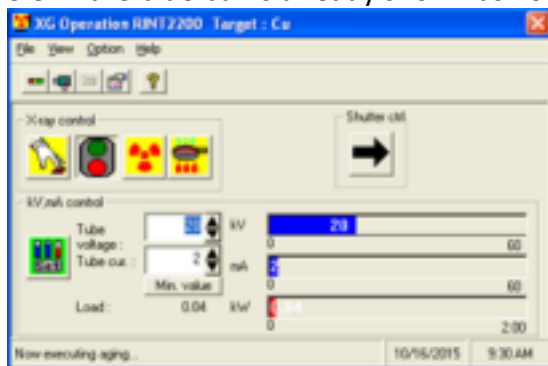
3.1.  On the window, click the return key on the right corner to normalize the window (XG Operation RINT 2200).

18

3.2. If there is no blue bar shown on the window (no voltage/current on X-ray tube), turn ON X-ray first by clicking on the **x-ray** icon . **The tube setting is always 20 kV and 2mA.** Wait till you see 20KV and 2mA blue bars shown on the screen.

19

3.3. If the blue bar is already shown as 20 KV/ 2mA, go to step 3.4.



20

21

3.4. Click on  “Execute Aging” (Aging is a program ramping the voltage from 20kV/2mA to 40kV//44mA) icon to power up X-ray, wait till “now executing aging...” message disappears (~16 min). X-ray now is stable to run samples.

22

3.5. Click on  “mini monitor” to minimize this window to prevent accidentally turning off the x-ray by clicking.

23

3.6. **DO NOT open the instrument chamber while the X-ray tube is aging.**

24

4. **Standard Stage or Powder/Bulk Sample Measurement**

25

4.1. On the “Standard Measurement” window change the XG Ending after to **“present condition”** before sample run (unless using step 7.5.2) . (“XG Ending after” means the X-ray tube voltage setting after the data is collected.)

26 4.2. Locate your folder line and change the column of “USE” to yes, and change any

other 2 of 9 *An environment designed for success*



W1-60 ECERF Building Edmonton, AB, CANADA T6G 2V4  
p: 780.492.0167 [www.nanofab.ualberta.ca](http://www.nanofab.ualberta.ca)

27  
28

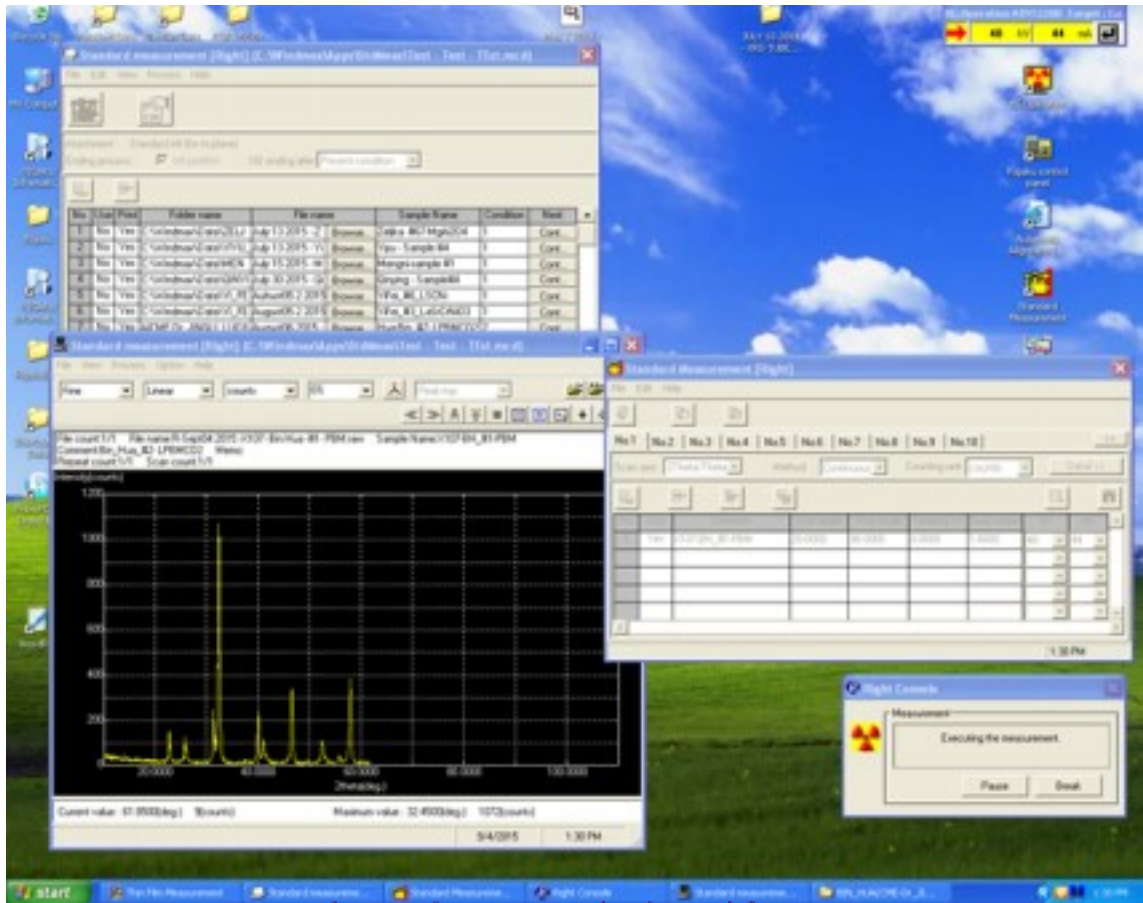
“yes” to “no” to prevent overwriting others’ data. Select Print (Yes/No). Update/change the file name, and change sample name if needed. If you couldn’t find your line, you can also copy a line, and use the “browse...” function.

29 4.3. **Double-click** the number in the “condition” column to modify scan parameters. Make sure in the “Condition” window, the TAB matches the number you selected. Make sure the condition selected has “Yes” under the “USE” column in the condition window.

Scan axis	Theta/2theta, or 2theta <b>Start angle &gt; 3°</b>
use	Yes End Angle 90° (commonly)
Method	continuous/FT/CT Sampling  width 0.01- <b>0.05</b>
Counting unit	counts Scan Speed 0.1~20 °/min (default=2)
kV	40 DivSLit 0.67deg
mA	44 SctSlit 0.67 deg
Offset angle	Step 4.5 RecSlit 0.3 mm
DivH.L. Slit	<b>10 mm. (Depend on size of sample, 2, 5, 10, or 15 mm)</b>

30  
31  
32

4.4. Leave the condition window open during data acquisition.



33

3 of 9 *An environment designed for success*



W1-60 ECERF Building Edmonton, AB, CANADA T6G 2V4  
p: 780.492.0167 [www.nanofab.ualberta.ca](http://www.nanofab.ualberta.ca)

34

35 **4.5. Parameters: 2theta range minimum angle is 3°, max is 150°.**

**Change**

36 **DHL slit according to your sample size.** For FT method, choose step  
37 size 0.02 degree, and count with 1 or 2 sec/step. For focus beam scan  
38 axis, option of 2theta/theta or 2theta. If 2theta scan is chosen, the  
39 offset angle is similar to glancing angle for thin film sample (graph  
40 showed a standard stage zero-background sample holder).

41 4.6. Load sample to holder. The smaller the particle size (1µm) the  
stronger the signal. Use a pestle and mortar to grind your sample if needed.  
Make sure the sample surface is flat and leveled to your holder frame.

42 4.7. Press the yellow door lock button. After hearing an audible sound, slide to  
open the doors gently. Insert the sample holder to standard stage.

43 4.8. Close the doors and push the door lock button again. The audible sound should  
stop.

44 4.9. Click "Execute measurement"  in the measurement window. Wait till answer  
all the questions and the yellow graph starts on black window indicating data is



collecting.

45 **5. Multi-Sample Holder (ASC-10) Stage (powder samples)**

46 5.1. ASC-10 sample stage is suitable for powder samples, and it automatically runs up to 10 samples without user attendance.

47 5.2. On the “Standard Measurement” window change the XG Ending after to

“**present**

48 4 of 9

49 **condition**” before running any sample (unless using step 7.5.2). (“XG Ending  
50 after” means the X-ray tube voltage after the data is collected.)

51 5.3. Locate your folder line and change the column of “USE” to yes, and change any  
other “yes” to “no” to prevent overwriting others’ data. Select Print (Yes/No).  
Update/change the file names, and change sample names if needed. Or click  
“Browse...” to find your folder and give a file name for your sample.

52 5.4. For operation of multi-samples, highlight your row number and click the “add  
condition” button (on top left). Copy as many lines as the number of samples.  
Update the file names and sample names. Make sure all the required lines are Yes  
under Use.

53 5.5. On the sample execution sequence table, “**sample**” means position on the 10-  
sample stage, “**attach**” means sample rotation option for that particular sample. Give

“attach” and “sample” the same number. In the “attach”, if you set to rotate sample holder, 10 rpm is a good rotation speed (make sure you have enough sample to cover the whole holder to prevent centrifugation effect).

54 5.6. Double click the number in the “condition” column to modify the scan parameters. Make sure in the “Condition” window, the TAB matches the number you selected. Make sure it is marked as “yes” in the “USE” column on the condition window. **Leave the condition window open during data acquisition.**

55 5.7. Parameters: **2theta range minimum angle is 3°, max is 150°. Change DHL slit according to your smallest sample’s size.**

Scan axis	Theta/2theta, or 2theta <b>Start angle</b>	<b>&gt; 3°</b>
use	Yes End Angle	90° (commonly)
Method	continuous/FT/CT Sampling width	0.01- <b>0.05</b>
Counting unit	counts Scan Speed	0.1~20 °/min (default=2)
kV	40 DivSLit	0.67deg
mA	44 SctSlit	0.67 deg
Offset angle	Step 5.9 RecSlit	0.3 mm
DivH.L. Slit	<b>10 mm. (Depend on size of sample 2, 5, 10 or 15mm)</b>	

56

57

58 5.8. For scan axis, option of 2theta/theta or 2theta. If 2theta scan is chosen, the offset angle is similar to glancing angle for thin film sample.

59 5.9. Suggest to use one condition for multi-samples. If you have to use multi-conditions, **make sure only one DHL is set during the entire automatic run.**

Otherwise, acquisition will be held till the required DHL is exchanged by the user.

60 5.10. Sample preparation. The smaller the particle size (1µm) the stronger the signal. Use pestle and mortar to grind your sample if needed. Make sure the sample surface is flat

61 5 of 9

62

and leveled to your holder rim.

63

64 5.11. Press the door lock button, after you hear an audible sound, slide to open the doors gently. Put the sample holder(s) to ASC-10 stage.

- 65 5.12. Close the doors and push the door lock button again. The audible sound should stop. 5.13. Click “Execute measurement” under measurement window. Wait till answered all the questions and a yellow graph shows in black window indicating data is collecting.
- 66 **6. Multi-Purpose Stage (Thin film, Coating Layer (<1 μm) or Bulk (sample height < 9mm) sample)** 6.1. This stage can perform in-plane or out-of-plane scan, phi or 2theta/Chi/Phi scan.
- 67 6.2. On the “Profile Measurement [right]” window, change the XG Ending after to “**present condition**” unless you want to turn off the x-ray after data collection.
- 68 6.3. Locate your folder line and change the column of “USE” to Yes, and change any other “yes” to “no” to prevent overwriting others’ data. Select Print (Yes/No). Update the file name, and sample name if needed. (You can use browse... function to find your folder).
- 70 6.4. Double click the number in the “Condition” column to modify the scan parameters. Make sure in the “Condition (another Profile Measurement)” window, the TAB matches the number you selected. **Leave the condition window open during data acquisition.**
- 71 6.5. **Specimen Alignment.** In the “Profile Measurement” **condition** window, check **only** “Specimen Alignment” and “Delete previous setting result” . In the “Specimen Alignment” table, give your sample height plus a glass slide (1 mm), and click set button.
- 72 6.6. Specimen Alignment settings:

73 6 of 9

74

Scan Sequence	Z to Omega		Origin
ATT	1/800	2theta	2.00 deg
DS	0.2 deg	Omega	0.5-7 deg
SS	open	2ThetaChi	2.00 deg
RS	0.20mm	Phi	0.00 deg

75

76

77

6.7. Press the door lock button, after you hear an audible sound, slide to open the doors gently. Put your sample on a glass slide, and leave them on the center of the crossair.

78

6.8. Insert correct DHL slit on primary arm to fit your sample size.

79

**6.9. Make sure, in the instrument 2theta arm, PSA is a vertical slit. (The slit is inserted in a way that the label “in-plane 0.5” is facing you.) Note: Expensive slit. Use gloves and Do not drop! Make sure not to touch the slit!**

80

6.10. Close the door and press the door lock again. The audible sound should stop.

6.11. Click “Execute measurement” under “Profile Measurement” window to perform sample height alignment.

81

6.12. Once specimen alignment is successful, rotate the PSA 90 degree so that the slit is horizontal and label “PB 0.5” is facing you.

82

6.13. For data collection, uncheck “Specimen Alignment”, and check “Profile Measurement”, “Exec” and “Origin”. Scan axis can be 2Theta, 2Theta/Omega, Omega, Phi and

83

2Theta/Chai/Phi. Choose the one according to your need.

Scan Axis	2Theta Scan Speed 0.1~10 °/min (default=2)
Scan Method	Continuous/FT/CT
Range setting	Absolute ATT open
Start angle	> 3° DS 0.1 deg
End Angle	90° (commonly) SS open
Sampling step	0.01- 0.05 RS open

84

85

86 6.14. In "Origin" condition, give the glancing angle as omega. **Omega is glancing angle.** 6.15. Click "Execute measurement" under "Profile Measurement" window, A yellow graph starts on the monitoring window indicating the data is collecting.

87 7 of 9

88

### 7. **Goniometer Standby and the X-ray Standby (after your sample run)**

89 7.1. The Goniometer should be always in initial position (Both arms at low positions). If you stopped sample collection half way, the goniometer stayed at the position it stopped. In this case, set the parameter to initial condition, such as  $2\theta$  start angle at 10, or set (TF stage) Origin section as per step 6.14, and execute the data collection, stop as soon as you see yellow line on data window or arms are at down position.

90 7.2. The x-ray tube is always set as "standby (20 kV/2mA)" when you finish your run before 4pm. The X-ray tube can be turned standby or OFF at the end of the day.

91 7.3. To set the X-ray Tube to "standby", click the button on "XG Operation RINT 2200 window" (graph in step 3.3). Double check the tube setting is 20 kV and 2 mA before clicking the button.

92 7.4. Turn OFF X-ray at the end of the day (after 4 pm, and nobody booked the tool

after). 7.4.1. If you already finished your last sample, go to "XG Operation RINT 2200

window,

93 click the “X-ray”  
tube power (Step  
tool should be

94 7.4.2. Or if the  
finished after 5  
your last batch,  
to “X-ray off”,  
The X-ray will be  
finished.

button to turn off x-ray  
3). The red light on the  
OFF after 2-3 min.  
data collection will be  
pm, before you execute  
change “XG ending after”  
and then click “execute”.  
off after the last sample is

95 8 of 9

96

## 97 **Data transfer**

98 **Use WinSCP to transfer data. No USB allowed.**

99 Data will be analyzed with Jade software located in nanoFAB computing area.

## 100 **AFTER-HOUR ACCESS Billing**

101 **Stay logging in while the instrument is collecting data.** If your data collection will be finished in the evening or after midnight, stay logged in till next morning you transfer your data, and send a request (Type-Administration) for tool usage correction by using the time data generated as ending time.

## 102 **TROUBLESHOOTING**

103 If you encounter an unexpected error or require assistance, please contact the primary or secondary trainer listed above. Should they not be available, please contact any staff member for assistance.

## 104 **APPROVAL**

105 **Qualified Trainer:** Nancy Zhang

106 **Characterization Group Manager:** Peng Li

107 **Version history**

108 Nancy Zhang, 2020-04-20 (*Rigaku XRD-1.gdoc*)

109 9 of 9